ERDC/CHL TR-15-8

US Army Corps
of Engineers®
Engineer Research and
Development Center

ERDC
INNOVATIVE SOLUTIONS
for a safer, better world

Old River Control Complex Sedimentation Investigation

Ronald E. Heath, Gary L. Brown, Charles D. Little,
Thad C. Pratt, Jay J. Ratcliff, David D. Abraham, David Perkey,
Naveen B. Ganesh, Keith Martin, and David P. May

June 2015

Coastal and Hydraulics Laboratory

The U.S. Army Engineer Research and Development Center (ERDC) solves the nation's toughest engineering and environmental challenges. ERDC develops innovative solutions in civil and military engineering, geospatial sciences, water resources, and environmental sciences for the Army, the Department of Defense, civilian agencies, and our nation's public good. Find out more at www.erdc.usace.army.mil.

To search for other technical reports published by ERDC, visit the ERDC online library at http://acwc.sdp.sirsi.net/client/default.

ERDC/CHL TR-15-8
June 2015

Old River Control Complex Sedimentation Investigation

Ronald E. Heath, Gary L. Brown, Charles D. Little, Thad C. Pratt, Jay J. Ratcliff, David D. Abraham, David Perkey, Naveen B. Ganesh, Keith Martin, and David P. May

Coastal and Hydraulics Laboratory
U.S. Army Engineer Research and Development Center
3909 Halls Ferry Road
Vicksburg, MS 39180-6199

Final report

Prepared for U.S. Army Corps of Engineers
Washington, DC 20314-1000

Abstract

This report documents an investigation of sediment diversions at the Old River Control Complex (ORCC) conducted for the U. S. Army Engineer District, New Orleans. The investigation was conducted via a combination of field data collection and laboratory analysis, geomorphic assessments, and numerical modeling. The objectives were to determine current rates of sediment diversion, evaluate potential impacts on the stability of the Mississippi River, and identify options to increase sediment diversion rates. As operated since the early 1990s, sediment diversion at the ORCC probably is less efficient than required to maintain channel stability in the Mississippi River downstream of the ORCC. While there is clear evidence of significant channel aggradation in the vicinity of the ORCC, the impacts of ORCC operations on regional sedimentation remain uncertain. Operational alternatives were analyzed that potentially could increase the long-term sediment diversion efficiency at the ORCC. In particular, the investigation found, via a synthesis of field investigations and numerical modeling, that while the auxiliary control structure is the most efficient at diverting bed material from the Mississippi River, the low sill structure is more efficient at delivering bed material to the outfall channel leading to the Atchafalaya River.

Contents

Figures and Tables

Figures

Tables

Preface

This report describes a sedimentation investigation of the Old River Control Complex (ORCC). The study was conducted between January 2010 and April 2012 by personnel of the U.S. Army Engineer Research and Development Center (ERDC), Coastal and Hydraulics Laboratory (CHL), Vicksburg, MS, in cooperation with the U.S. Army Engineer District, New Orleans (MVN). Project manager for the MVN was Don Rawson, Chief of Channel Stabilization.

The scopes of work for this investigation were prepared by Dr. Jay J. Ratcliff, Coastal Engineering Branch, and Ronald E. Heath, River Engineering Branch, and Thad C. Pratt, Field Data Collection and Analysis Branch, with assistance from Gary L. Brown and Keith Martin, Estuarine Engineering Branch; Charles D. Little, Jeremy A. Sharp, and Dr. David D. Abraham, River Engineering Branch; and Dr. Bernard Hsieh, Hydrologic Systems Branch.

Project coordinator for the CHL was Heath with Ratcliff assisting as an on-site liaison with the MVN. The field data collection and analysis program was managed by Pratt with technical assistance from Abraham and David P. May, River Engineering Branch. The geomorphic assessment was conducted by Little. Ratcliff conducted a companion analysis of vegetation changes and river channel capacity. Heath and Brown jointly managed the numerical model study with assistance from Ian Floyd, River Engineering Branch, and Martin and Dr. Phu V. Luong, Estuarine Engineering Branch. Terry Waller of the Field Data Collection and Analysis Branch made numerous contributions to the modeling effort through his insights into river behavior and by providing context to field measurements.

The numerous contributions of Will Veatch, Don Rawson, Russell Beauvais, and Nancy Powell (retired) to the understanding of ORCC operations and the historical behavior of the Mississippi River is gratefully acknowledged. The Old River Control Complex Sedimentation Investigation was conducted under the general supervision of Dr. William Martin (retired), Director CHL; Dr. Rose Kress (retired), Chief, Navigation Division; Bruce A. Ebersole (retired), Chief, Flood and Storm Protection Division; Lisa Hubbard (retired), Chief, River Engineering; Pat McKinney (retired), Chief, Field Data Collection and Analysis Branch; Dr. Robert

McAdory, Chief, Estuarine Engineering Branch; and Dr. Jeff Waters, Chief, Coastal Engineering Branch.

At the time of publication, LTC John T. Tucker III was Acting Commander of ERDC. Dr. Jeffery P. Holland was ERDC Director.

Unit Conversion Factors

Multiply	By	To Obtain
acres	4,046.873	square meters
acre-feet	1,233.5	cubic meters
cubic feet	0.02831685	cubic meters
cubic yards	0.7645549	cubic meters
degrees Fahrenheit	(F-32)/1.8	degrees Celsius
feet	0.3048	meters
inches	0.0254	meters
microns	1.0×10^{6}	meters
miles (U.S. statute)	1,609.347	meters
pounds (mass)	0.45359237	kilograms
pounds (mass) per cubic foot	16.01846	kilograms per cubic meter
pounds (mass) per square foot	4.882428	kilograms per square meter
slugs	14.59390	kilograms
square feet	0.09290304	square meters
square miles	2.589998 E+06	square meters
tons (2,000 pounds, mass)	907.1847	kilograms
yards	0.9144	meters

Executive Summary

Impact of ORCC operations on sediment diversions

In order to maintain a 30%–70% flow split between the Atchafalaya and Mississippi Rivers, the Old River Control Complex (ORCC) is operated to divert approximately 17% to 28% of the Mississippi River flow approaching the complex on a typical day. The long-term average water diversion through the ORCC is approximately 23% of the Mississippi River inflow.

The fraction of Mississippi River sediment diverted through the ORCC is a function of several factors, including the river discharge, the state of the river bed (e.g., bathymetry and bed material gradation), the shape of the hydrograph, and the distribution of flow allocated to each diversion structure: the hydropower structure, the low sill structure, and the auxiliary structure. This flow allocation among structures is of particular importance, since each structure passes a different amount of sediment for the same diverted flow. Hence, changes in operations at the ORCC can have a significant impact on the amount of sediment diverted for a given water diversion. Bed material sediments, primarily sand in the Mississippi River, strongly influence the morphology of the channel; therefore, the diversion of bed material is the primary focus of this study.

Sediment Diversion Coefficient. To characterize sediment diversions, the concept of a sediment diversion coefficient has been adopted from the HEC-6 one-dimensional (1D), sedimentation-modeling computer program (USACE 1993). This coefficient is defined as the ratio of the average sediment concentration in the diverted flow to the average sediment concentration in the approaching Mississippi River flow.[1] Thus, if the fraction of the river discharge diverted and the fraction of the sediment load diverted are equal, the sediment diversion coefficient would be 1. In an HEC-6 model, the sediment diversion coefficient is defined as a function of grain size and diversion discharge and is applied at each simulation time-step, typically one day or less, to compute the diverted sediment load.

[1] The sediment diversion coefficient and efficiency are described in detail in Chapter 5 of this report.

Sediment Diversion Efficiency. By accumulating flows and sediment loads over longer periods of time, a sediment diversion efficiency, based on the above ratio, may be computed that incorporates the impacts of structure operations, hydrograph shape, variability of sediment supply, and other factors for the entire complex or for individual diversions. Because sediment load is a nonlinear function of water discharge, the efficiency value may differ significantly from the sediment diversion coefficient defined above. The efficiency characterizes the average rate of sediment diversion for the complex or individual structures over longer periods of time (e.g., annually). It should be noted that due to the nonlinear nature of sediment transport phenomena, the efficiency required to maintain stability in an alluvial channel, initially at equilibrium with the bed material load, would be greater than 1.

Analytical Model. A theoretical analysis of bed material (i.e., sand and gravel), diversion from an equilibrium channel, considering observed bed material loads in the Mississippi River indicates that a sediment diversion efficiency of 1.8 would be required to maintain channel stability downstream of the diversion (Letter et al. 2008; Brown et al. 2013). Since the Mississippi River has been adjusting to both unregulated and regulated diversions in the vicinity of Old River for decades, this estimate represents the best available estimate for required bed material diversion efficiency. This analysis does not consider historical cutoffs, channel stabilization works, and other influences that may affect channel stability.

Physical Model. A review of a previous moveable-bed physical model investigation that considered only low sill and auxiliary structure operations indicates that the low sill structure is capable of sediment diversion efficiencies between 1.0 and 1.8 on an annual basis for diversion of bed material (i.e., coal particles in the model, moving as bed load) (USACE 1980). For Ratio 1, the selected operating plan for these structures, the model indicated an efficiency of 1.0 for the Low Sill Structure, 5.2 for the auxiliary structure, and a combined efficiency of 2.7 for both structures. Mississippi River bed material, typically fine to coarse sand with a d_{50} of approximately 0.3 millimeters (mm), is transported both as bed load and as suspended load. Since finer suspended materials, including suspended bed material, tend to be more uniformly distributed throughout the water column, efficiency for suspended sediment load diversion will tend toward a value of 1. Therefore, the annual efficiency values determined from the physical model represent an upper bound on the potential long-term efficiency of these structures.

AdH/SEDLIB Numerical Model. For the current study, the Adpative Hydraulics (AdH) multidimensional hydrodynamic model, coupled with the SEDLIB sediment transport library, was used to investigate sediment transport and morphologic change for the Mississippi River and the ORCC. The model results yielded the following efficiency values for the various structures at the ORCC for a simulation of historical operations from January through September of 2010 are shown in the following table.

AdH/SEDLIB results for the ORCC efficiency for diversion of total sand load.

ORCC structure inflow channel	Sediment Diversion Efficiency
	Jan–Sep 2010
Hydropower	0.5
Low Sill	1.3
Auxiliary	2.0
ORCC	1.0

The differences in the sediment diversion efficiency of each structure are due primarily to their relative locations in river bends. The hydropower channel diverts water from the outside of a river bend, where the sediment concentration is at a minimum (bed material load tends to be higher toward the inside of a bend). the low sill channel is located at the transition between bends, and the auxiliary channel is located at the inside of the next downstream bend.

The differences in the efficiency estimates between the numerical and physical model studies can be attributed primarily to the fact that the numerical model includes both bed load and suspended load transport. Both modes of transport are influenced by river bends, but bed load is influenced more significantly than suspended load, due to the proximity of bed load to the near-bed current. Hence, the influence of the river bend on the efficiency of the diversions is more pronounced in the physical model study, which only considered bed load transport.

Analysis of Actual Versus Target Bed Material Diversion Efficiency. In order to assess the potential impacts of the ORCC operations on sediment dynamics in the Mississippi River downstream of the ORCC, numerical results were compared against the analytical estimate of the equilibrium sediment diversion efficiency (i.e., 1.8).

The numerical model was run for the simulation period from January–September of 2010. The historical (observed) structure operations were

applied to the model. The total mass of bed material diverted at the ORCC for this simulation was 9.1 million tons. Based on the analytic estimate of the required ORCC sediment diversion efficiency, the amount of bed material that must be diverted to maintain downstream equilibrium is 16.6 million tons. Hence, the excess bed material passed downstream for this simulation period is 16.6 – 9.1 = 7.5 million tons.

Screening Tool. In order to allow water control personnel to apply the results of this study to practical operational decisions, a spreadsheet application has been developed whereby the results of the numerical analysis can be used to experiment with changes in the ORCC operations. Long-term estimates of the sediment diversion efficiency of individual ORCC structures for historical operations are shown in a table below. The sediment diversion coefficient estimates were derived from numerical, multidimensional sedimentation model simulations of the January through September 2010 hydrograph and represent the mean daily values for the time periods when individual structures were in operation. For each structure, the operational efficiency was determined by using the sediment diversion coefficient to estimate daily sand loads (Equation 1) for water years 1991 through 2010, a procedure that considers both historical structure operations and the nonlinear response of sediment transport rates to flow variations.

$$Q_S = k \cdot \delta_{SD} \cdot C_R \cdot Q_D \tag{1}$$

where:

Q_S = diverted sediment load, tons per day
k = conversion factor (0.0027)
δ_{SD} = sediment diversion coefficient
C_R = average inflowing bed material concentration in the Mississippi River, milligrams per liter
Q_D = diverted flow, cubic feet per second.

The accumulated flow and daily sand loads at the entrance to each inflow channel were compared to corresponding values in Mississippi River upstream of the ORCC to determine the sediment diversion efficiency for the entire 19 year (yr) period. See the following table.

Long-term estimates of ORCC efficiency for diversion of total sand load for water years 1991 through 2010.

ORCC structure inflow channel	Total Sand Load	
	Sediment Diversion Coefficient	Sediment Diversion Efficiency
Hydropower	0.5	0.5
Low Sill	1.3	1.9
Auxiliary	1.7	1.8
Old River Control Complex		0.9

Since hydropower production accounted for most of the ORCC diversion during low-flow periods when sediment loads were relatively low, its estimated efficiency was slightly, but not significantly, lower than its estimated sediment diversion coefficient. Since the largest flow diversions at the low sill and auxiliary structures were experienced when sediment loads were relatively high, their efficiency is higher. This procedure provides a relatively simple method for estimating how operational changes would affect the diversion of sand from the Mississippi River.

Using the screening tool, the potential impact of flow regulation on sediment diversion is demonstrated for a hypothetical scenario in the following table where all flow is diverted through the low sill and auxiliary control structures according to the Ratio 1 operation plan. This scenario results in the diversion of an additional 7 million tons of sand per year as compared to historical operations described in the previous table.

Long-term estimates of ORCC efficiency for diversion of total sand load for hypothetical Ratio 1 operations for water years 1991 through 2010.

ORCC structure inflow channel	Total Sand Load	
	Sediment Diversion Coefficient	Sediment Diversion Efficiency
Low Sill	1.3	1.2
Auxiliary	1.7	1.7
Old River Control Complex		1.5

Limited geomorphic assessment

A limited geomorphic assessment was conducted to identify long-term morphological changes on the Mississippi River that may influence the performance of the ORCC structures. The limited geomorphic assessment consisted of an update of selected specific gage records developed as part of the 1999 Lower Mississippi River Sediment Study and an analysis of channel geometry changes that have occurred in the study area since the

construction of the low sill structure. The objective of the assessment was to describe the morphologic trends of the Mississippi River in the study area to provide insight into the development and interpretation of the numerical models.

Selected specific gage records developed as part of the 1999 Lower Mississippi River Sediment Study were updated for the period 1999 to 2010 for this study. Selected locations on the Mississippi River include Vicksburg, Natchez, Red River Landing, Bayou Sara, and Baton Rouge. Locations on the Atchafalaya River include Simmesport and Krotz Springs. Trends indicated by the specific gage records were evaluated from both a visual assessment and a statistical analysis. An overall trend was determined based on the combination of both visual and statistical trend results.

The overall trend assessments for the Mississippi River specific gage records for the entire periods of record indicate a general increasing, or aggradation, trend over time. Approximately 3 to 5 feet (ft) of aggradation is noted from the specific gage records of Vicksburg (1950–2010) and Natchez (1936–2010), and approximately 5 to 7 ft of aggradation is noted from the specific gage record for Red River Landing (1935–2010), most of which has occurred fairly uniformly over the entire period of record. As much as 5 to 10 ft of stage increase was noted from the specific gage records for Bayou Sara (1951–2010) and Baton Rouge (1963–2010), although almost all of this occurred prior to 1973. For the post-1973 flood time period, an overall increasing trend was determined for Natchez, but no trend was observed for Vicksburg and Red River Landing. For Bayou Sara and Baton Rouge, analysis of the post-1973 flood period indicates no significant trends and a relatively stable reach.

For the Atchafalaya River gages for the pre-1980 time period, an overall decreasing, or degradation, trend was observed for the specific gage records at both Simmesport (1943–1980) and Krotz Springs (1943–1980). As much as 15 ft of degradation occurred in these reaches during this time period, with the changes occurring fairly uniformly with time. However, the specific gage records indicate a discernible shift occurred in the early 1980s, with a transition to very stable reaches with no significant trend observed in the specific gage records from that time to 2010.

The geometric data analysis incorporated comparative cross sections and contour maps developed from historic hydrographic surveys to assess channel geometry changes that have occurred since the construction of the

low sill structure. Analysis of the comparative cross sections indicates a generally shallower river channel in 2010 than existed in 1975 for the reach just upstream of the hydropower channel to just downstream of the auxiliary structure channel. The most notable changes were observed between the hydropower channel and the low sill structure channel, where approximately 25 to 30 ft of filling occurred between 1992 and 2008. Deposition in the range of 10 to 20 ft was also observed for the river channel in the vicinity of the low sill channel. Comparison of contour maps also indicates a reduction in river channel depths between the hydropower channel and the low sill structure channel from 1992 to 2004.

Discussion

It is uncertain whether or not the excess bed material load being passed down the Mississippi River has had any adverse effects on flood risk upstream or downstream of the ORCC. During the flood of 2011, higher-than-historical stages were observed at several locations, for a given flood discharge. This tends to indicate that the flow line for the river may be rising. However, specific gage analyses for discharges at or below bank full do not indicate a significant trend. If the changes in stage observed at flood flows were caused by the loss of channel capacity due to aggradation, the expectation would be to see the same trend for lower flows. An analysis of changes in land cover in the overbank region between the levees downstream of ORCC showed significant changes in the last several decades. These changes introduce uncertainty in the overbank drag during flood flows and could potentially contribute to the observed change in stage at flood flows.

Given these uncertainties, it is not possible to positively attribute changes in flood stage to aggradation in the Mississippi River. However, the modeling analysis indicates that excess sediment is being passed downriver, and therefore any mitigation of this excess sediment should either have a neutral or positive effect on flood stages.

Recommendations

Additional modeling analyses were used to identify several suggested changes to ORCC operations that would serve to divert more sediment through the complex. Note that these represent a limited set of suggested changes, and other options may be investigated with the screening tool. The recommendations are given as follows:

- In order to have any significant impact on sediment diversion at the ORCC, it is necessary to alter the operation of the Hydropower Structure.
- The sediment load in the river on the rising limb is much greater than on the falling limb. Therefore, sediment diversion should be focused on the rising limb of river hydrographs
- During the rising limb of the hydrograph, as much flow as possible should be diverted through the low sill structure. Field observations indicate that the low sill structure is very efficient at passing sediment from the river though the ORCC, when the structure is operated with sufficient flow to mobilize the sediment in the channel. Note that, in order for this to be effective, it is necessary to limit the flow to the hydropower structure to maximize the diversion volume at the low sill structure.
- During the peak flow and falling limb of the hydrograph, full flow capacity can be restored to the hydropower structure. The remaining flow diversion requirement should be passed through the auxiliary structure to the extent feasible. The auxiliary structure is the most efficient structure at removing sediment from the river, but when sediment concentrations are high, the auxiliary channel tends to shoal, and hence, sediment does not reach the downstream side of the complex. Confining the operation of the auxiliary structure to the falling limb of the hydrograph ensures that the structure is only operated when the concentration of sediment in the river is relatively low: hence, the auxiliary channel has less of a tendency to fill.

Operation of the auxiliary structure on the falling limb will also serve to scour the shoal formation located in the Mississippi River between the low sill and auxiliary channels. The drawdown of the river induced by the auxiliary structure serves to accelerate the flow over this shoal. This entrains sediment from the shoal and transports this sediment into the auxiliary channel.

It must be emphasized that, while the hydropower and low sill structures tend to pass nearly all of the sand diverted from the Mississippi River, the entrance channel to the auxiliary structure traps a significant portion of the diverted sediment load, particularly during Mississippi River floods. This behavior was documented in the physical model report which describes flushing operations in which flow was diverted exclusively through the auxiliary structure for up to 7 weeks at low-to-moderate Mississippi River stages to remove the deposits.

Consequently, the low sill structure is more efficient at delivering bed material to the Atchafalaya River side of the ORCC than the other structures as currently operated. This behavior was observed during field measurements of bed load transport in the combined outflow channel which consistently showed the largest transport rates occurring when the low sill structure was in operation.

1 Introduction

Study area and brief history

The Old River Control Complex (ORCC) (Figure 1.1) is located on the west bank of the Mississippi River approximately 48 miles northwest of Baton Rouge, LA, and 37 miles south-southwest of Natchez, MS. The complex regulates the diversion of flow and sediment from the Mississippi River to the Atchafalaya River and the Red River Backwater Area. The complex is operated to maintain a 30%–70% flow split between the Atchafalaya and Mississippi Rivers as estimated from rating curves at the Simmesport and Red River Landing gages downstream of the complex. Since 1977, the complex has been operated to maintain the 30%–70% flow split as closely as practical on a daily basis. On average, approximately 23% of the Mississippi River flow is diverted through the complex, but the daily diversion percentage can vary significantly in response to the variations in the relative contribution of the Red River to Atchafalaya River flow.

Figure.1.1. ORCC map.

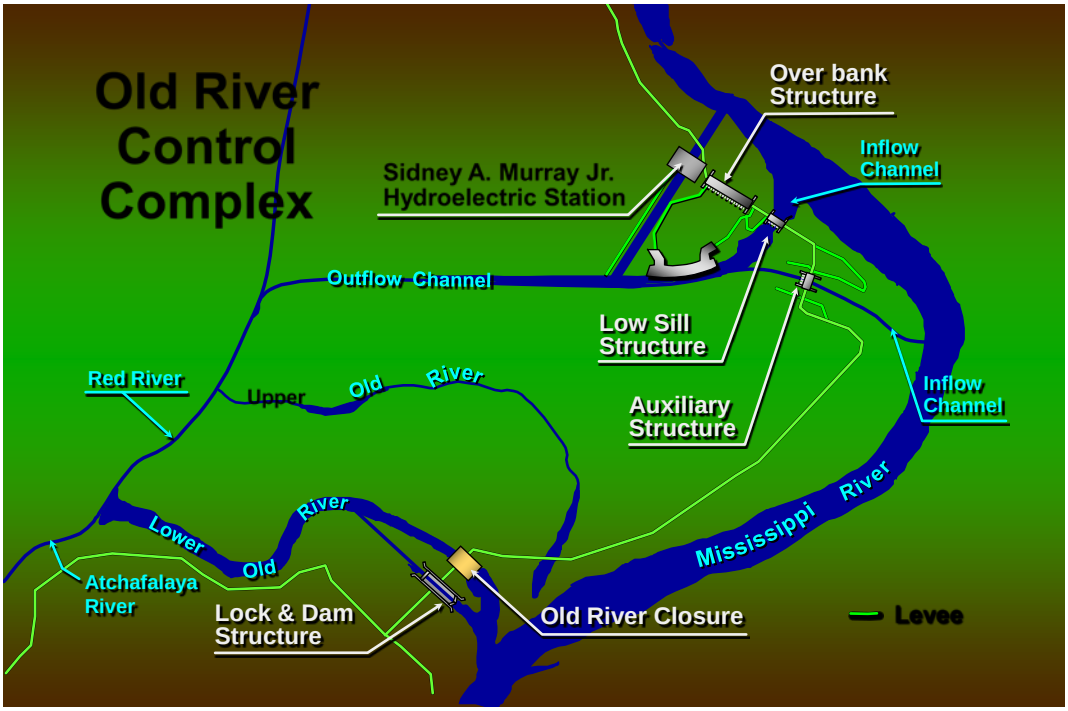

Prior to construction of the complex, an unregulated diversion through Old River permitted a steadily increasing portion of the Mississippi River

flow to pass into the Atchafalaya River. Construction on the complex began in 1955 and was intended to prevent capture of the Mississippi River by the Atchafalaya River. Originally, the complex consisted of a navigation lock and two flow-regulation structures, the low sill structure that was operated year round and the overbank or high sill structure that operated only during Mississippi River floods[1]. Construction was completed in 1962, and the unregulated diversion through Old River was closed.

Excessive scour in the low sill structure inflow channel resulted in the collapse of the left-descending, inflow wing wall during the 1973 flood. The auxiliary structure, completed in 1986, was intended to reduce inflow channel scour, to relieve pressure on the low sill structure by maintaining an acceptable head differential at the structure, and to divert more bed material into the Atchafalaya River, which had experienced significant bed degradation over a period of decades. Physical, moveable bed model studies conducted by Waterways Experiment Station's Hydraulics Laboratory (predecessor to the ERDC CHL) contributed to the adoption of the Ratio 1 operating scheme (Figure 1.2), which proportions diversion flows between the low sill and auxiliary structures based on observed stages at the Knox Landing gage located on the west bank of the Mississippi River between the structures. The model study indicated that Ratio 1 operations would divert "approximately 65% of the total Mississippi River bed load above Old River, as compared with 44%" for operation of only the low sill structure. The model study also indicated this operation would result in significant shoaling in the auxiliary structure inflow channel. A flushing scheme was successfully evaluated that required diverting all flow (72,000 and 60,000 cubic feet per second [cfs]) through the auxiliary structure for the final 46 days (i.e., the low flow portion) of the average annual hydrograph tested in the model (USACE 1980).

The Sidney A. Murray Jr. Hydroelectric Station entered operation in 1990. Since the fall of 1991, the Station has accounted for most of the flow diverted through the complex for Mississippi River inflows of less than 800,000 cfs (Figure 1.3). As Mississippi River inflows increase above 800,000 cfs, flow diversion through the Station (hydropower structure) approaches its maximum capacity of approximately 170,000 cfs and accounts for a progressively smaller fraction of the total flow diversion.

[1] The high sill structure is operated infrequently and was not incorporated into sediment diversion estimates made as part of this study.

Figure 1.2. Flow diversion curves for the auxiliary structure.

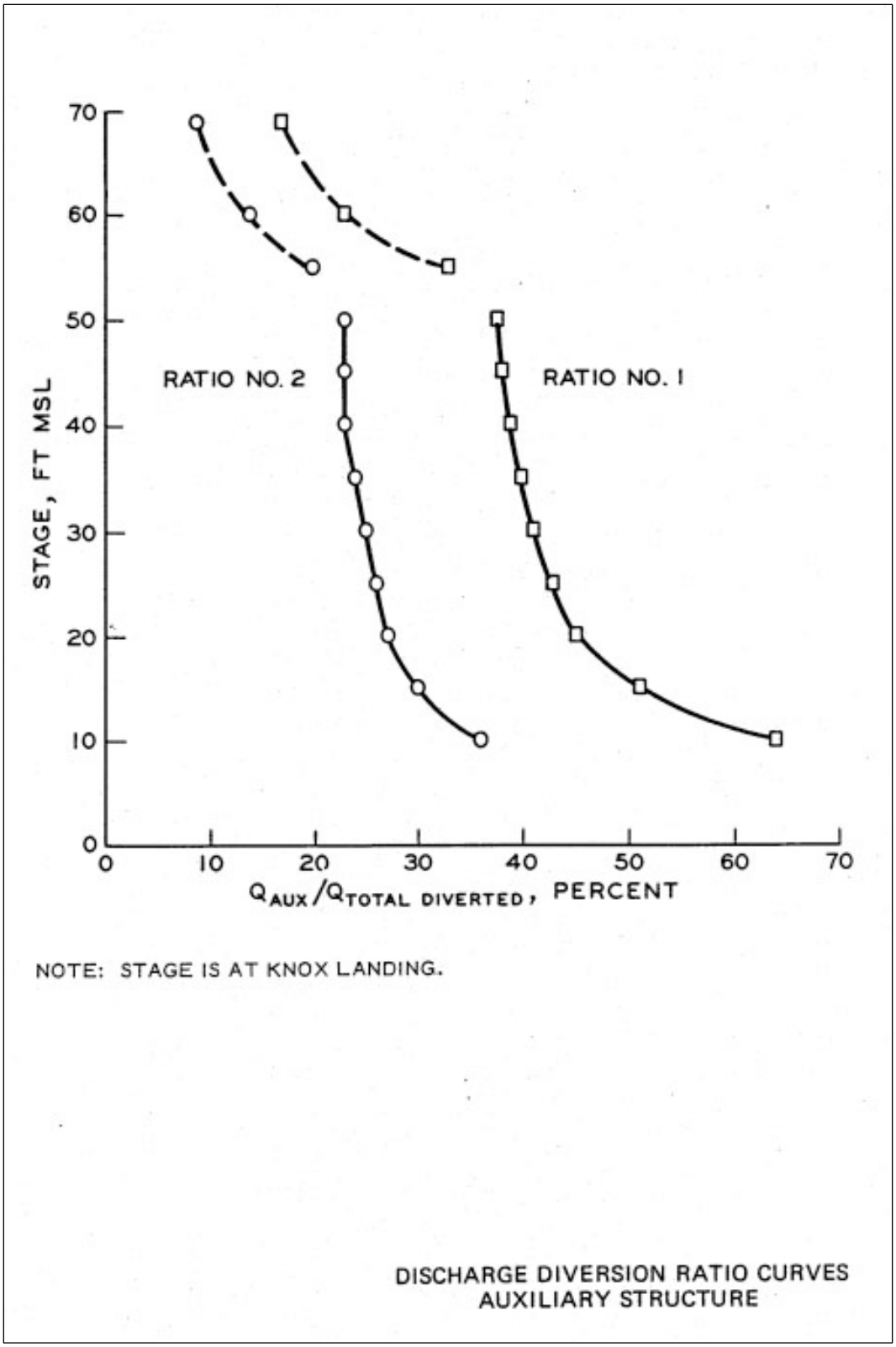

Figure 1.3. Daily hydropower flow diversions experienced during water years 1992–2010 as compared to total ORCC flow diversions.

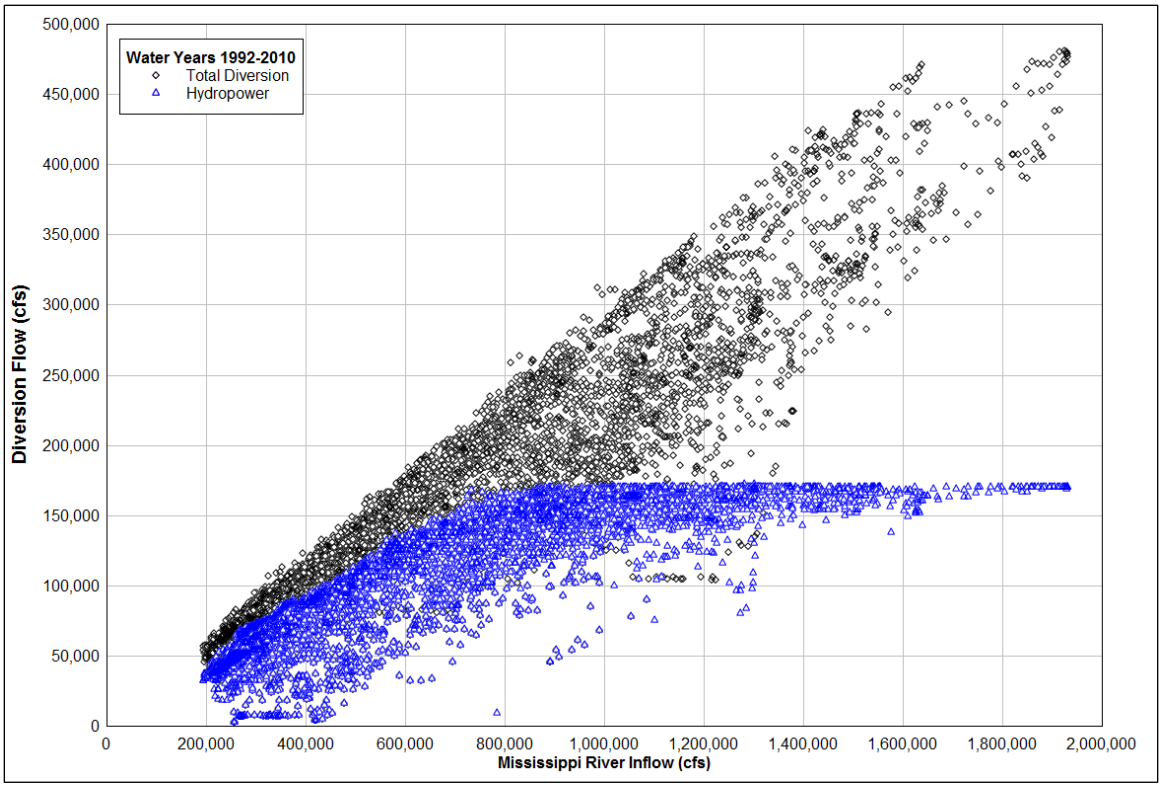

Issues

The 76th Meeting of the USACE Committee on Channel Stabilization reported the following:

> For many years, Corps personnel have noticed and documented an accumulation of coarser grained sediment in the vicinity of the Old River Complex (ORC), which consists of four federal hydraulic control structures and the privately constructed and operated Sydney A. Murray Jr. Hydroelectric Station (Hydroelectric Station)... Significant accretion is also occurring on the banks of the Mississippi River, contributing to bank instability and failures, as well as creating problems for facility operators and other users.
>
> Additionally, numerous bank failures are occurring on the lower 44 miles of the Red River and in some reaches of the Atchafalaya River. Bank failures in the Mississippi River occur less frequently, but are much more massive. Recently, there has been an increase in the number of reports by dock and facility operators of sediment

accumulation in wharf areas and municipal water intakes in the vicinity of New Orleans.

Hydraulic engineers from the Mississippi Valley Division (MVD) and the New Orleans District (District) believe that a continued accumulation of large-grain sediment in the Mississippi River may lead to a deterioration of the MR&T system within the study area, and may ultimately result in a need to increase the height of the Mississippi River levees to provide the required level of flood protection. The numerous bank failures and soil erosion in the lower Red River may require expensive levee setbacks. There is also concern that the current ratio of large-grain sediment between the Mississippi River and Atchafalaya River is out of the targeted range and will eventually result in navigation problems and an increase in bank failures throughout the system. If this were to occur, it would impact the port of New Orleans, as well as the petrochemical industry on which the nation relies so heavily. Much of the infrastructure within the study area would also be affected, resulting in regional and national consequences.

There is no unanimity, even among Corps experts, of the cause or significance of the events being observed in the lower Red, Old, Mississippi, and Atchafalaya Rivers. This is a very complex river system, and effective management requires recognizing subtle changes that will lead to significant problems many years before the problem actually occurs. Constant vigilance and experience are necessary to understand and perceive minor changes that could ultimately alter the system in a negative way. Part of the difficulty is distinguishing subtle changes that are part of a natural cycle from those that are indicators of a detrimental pattern that will destabilize the system.[1]

Study objective

The objective of this study for the ERDC is to provide the MVN with a reliable, scientifically based and technically justified engineering evaluation of sediment diversion characteristics and distributions through the ORCC and evaluation of potential alternatives for increasing sediment diversion.

[1] Report on the 76th Meeting of the USACE Committee on Channel Stabilization, New Orleans, LA, 5–7 October 2010.

Data collection

Data collection served as the primary foundation for increasing the usefulness of additional modeling efforts. The new data was used to improve definition of boundary conditions for numerical sedimentation models. The data was essential for describing the ratio of diversion sediment to river sediment, which is critical information required for calibration and verification of the numerical model results. Without sufficient data for boundary conditions and calibration/verification, confidence level of the model results is significantly lower.

The main objective of the proposed data collection surveys was to determine the integrated transport of water and sediments through the three channels at the ORCC. The goal of integrated surveys was an understanding of the suspended and bed load transport of sand and fines (silt and clay) through the structures and in the adjacent channels. Integrated surveys were needed (1) to ground-truth numerical models and (2) to determine sediment loads into the three channels. The latter was necessary to ascertain if the diversions are operating as designed and to quantify the fraction of the total Mississippi River sediment load being diverted. Quantification of the diverted sediment load will also be valuable for future efforts to describe the shoaling processes and sediment transport in the two-river system.

Geomorphic analysis

The geomorphic assessment utilized available data to document the historic trends and changes in hydrology, sedimentation, and channel geometry for the Mississippi River, Atchafalaya River, and Old River in the vicinity of ORCC. Specifically, the assessment updated portions of the geomorphic assessment conducted as part of the Lower Mississippi River Sediment Study for Louisiana Hydroelectric in May 1999 and also included an analysis of the geometric changes that have occurred in the study area. An update of the entire geomorphic assessment was not attempted as part of this study effort; rather, a limited update was conducted that included extension of the specific gage analysis, and channel geometry analysis. The objectives of the geomorphic assessment were to provide additional definition of the long-term geomorphic trends in the study area and to provide qualitative and quantitative descriptions of changes in channel geometry that could be used for calibration and validation of numerical models.

Numerical model analysis

The numerical model investigations were used to determine if the ORCC structures can be operated in such a manner as to address the sediment accumulation issues. A two-dimensional (2D) investigation focused on screening and refinement of alternatives and multiyear simulations of sedimentation within the model domain using observed or synthesized hydrographs. The 2D investigation was performed with the depth-averaged, shallow-water equation version of the AdH modeling system incorporating quasi-three-dimensional (3D) sediment transport for multiple grain sizes. A limited 3D investigation was performed using the CH3D-SED model to determine whether or not any significant 3D effects not represented in the 2D model were present in the study area.

2 Data Collection

Flow and suspended sediment measurements

On each survey, integrated (suspended + bed load) sediment and water flux measurements were made at the locations shown in Figure 2.1 depending on the operations that were occurring at the time of collection. A vessel-mounted Acoustic Doppler Current Profiler (ADCP) 600 kilohertz (kHz) was used to calculate water discharge and measure acoustic backscatter data at the transect locations. The backscatter data converted to Total Suspended Material (TSM) were coupled with the velocity information to achieve 2D sediment flux measurements.

Figure 2.1. Flow and sediment measurement cross sections.

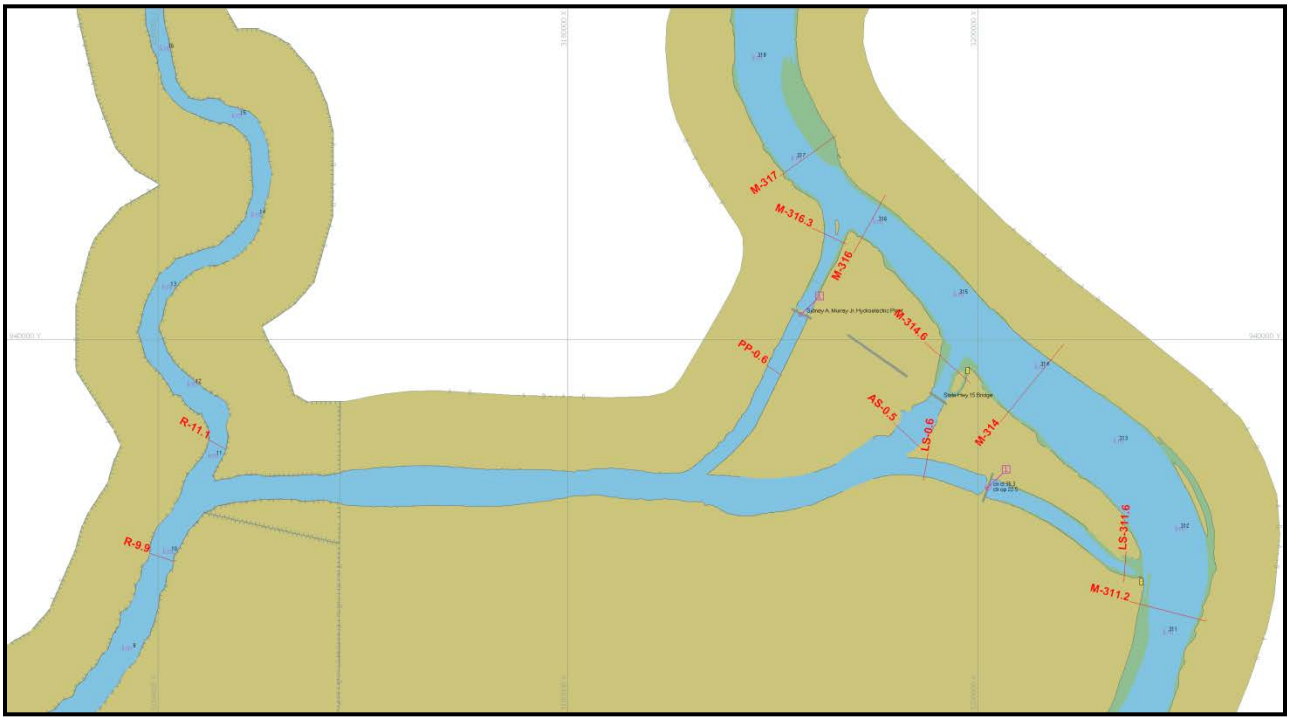

During data collection, the ADCP is capable of measuring vessel velocity, water velocity, water temperature, bottom bathymetry, and acoustic backscatter. The measurement of the velocity of the vessel over the bottom allows the current velocity data to be corrected for the movement of the survey vessel. However, if there is sufficient sediment transport down river at the bottom, the ADCP measurements of the velocity of the survey vessel over the bottom will contain some inaccuracies that will introduce errors

into the calculated current velocities. These were removed by using a global positioning system (GPS) to measure the velocity of the survey vessel. The GPS also provided required heading information to the ADCP system.

A P-6 Isokinetic Point Sampler was used to collect suspended sediment concentration samples from 0.1, 0.3, 0.5, 0.7, and 0.9 fractions of water depth at three or more locations along each ADCP cross section. Sediment was filtered onto preweighed 0.4 micron (μm) filters after presieving the sand (>63 μm) fraction. After drying at 60 °C, samples were weighed and percent sand and fines (silt and clay) calculated. Suspended sediment load (total and sand) was calculated for each cross section using the P-6 data, ADCP velocities, and the acoustic backscatter data from each transect.

All water samples were collected in clean 1-liter (L) HDPE plastic bottles. At each collection point, a five-depth profile at approximately 1 ft below surface, 25% water depth, 50% water depth, 75% water depth, and 1 ft above bottom was collected. The P-6 isokinetic sampler was lowered to each target depth and opened for 30–50 seconds, depending upon flow conditions. Sample bottles were filled to 50%–75% full to ensure that over filling and flushing of sediment from the bottle did not occur. Water flows below 2.0 feet per second (fps) were found to be insufficient to purge the air from within the P-6 sampler and fill the bottle. Therefore, a water pump was used to fill the sample bottles when average flows were below 2.0 fps. In these instances, a water hose was attached to a 100-pound (lb) weight and lowered to each target depth. Sufficient time was allowed to flush the water line before filling a bottle from a specified depth. After collection, samples were stored upright in a cooler and transported back to the lab for analysis.

Laboratory analysis for suspended sediments

Suspended sediment concentrations (SSC)

Each sample for SSC was shaken to resuspend particles and then poured into a 1 L graduated cylinder to record the volume. The samples were then transferred into a ground-glass vacuum filtration system (8 lb vacuum maximum) and drawn through preweighed, 90 centimeter (cm) diameter, glass-fiber filter with 0.7 μm particle retention. The sample bottles, graduated cylinders, and filter towers were rinsed several times with distilled water to make sure that all particles were introduced to the filter.

The filters were then dried in a low-temperature oven overnight at approximately 50˚C. The filters were then reweighed and SSC was calculated for each sample. The SSCs for each sample are reported in Appendix A.

Suspended sediment grain size analysis

The laser diffraction technique was utilized to analyze suspended sediment samples. A Malvern Mastersizer 2000 measured the grain size of all the samples collected. Pretreatments of samples prior to analysis by the laser were consistent throughout all sampling trips. Prior to analysis, a dispersant agent (sodium meta-phosphate) was added to each sample bottle to bring the concentration to approximately 1–2 grams per liter (g/L), sonicated for 60 seconds, and passed through a 850 μm (#20 ASTM) sieve to remove any debris from the sample. Each sample was cycled through the laser at least three times, and an average size distribution was reported. The grain size flux in tons per day (TPD) for the suspended sediment samples are listed in Table 2.1.

Water and sediment flux analysis

ADCP back scatter calibration to suspended sediment concentration data is the means by which sediment flux calculations were made to determine the suspended sediment transport rates out of the various ORCC structures from river mile (RM) 317 to RM 311. The method of calibration has been developed over several years of application. It involves the relationship between the distribution function of the acoustic backscatter energy values and the calibration, distribution function for total suspended sediment concentration (TSM). The ideal calibration TSM data set needs to be collected across the cross sections where ADCP transects are collected.

The range of acoustic back scatter energy values is from 0 to 256. Several representative ADCP transects are read, and the energy values are counted over the range of 0 to 256 to create the distribution function for the acoustic backscatter. The same process is done for all of the TSM samples, each time a concentration value occurs; then a count value is added to a distribution function. The whole premise for the calibration is that the two distribution functions are related for that particular river stage.

Table 2.1. Sediment load (tons per day) by grain size at measured discharge ranges.

Line Designation	Date	Discharge cfs	Grain Size (µm)									
			0-4	4-8	8-16	16-31	31-63	63-125	125-250	250-500	500-1000	1000-2000
AS 0.5	July 1, 2010	44733.74	5236.76	53267.90	6224.85	5858.78	3354.64	774.67	350.03	273.20	21.86	0.00
AS 0.5	March 9, 2011	97136.43	14074.33	20411.83	27774.81	31658.13	21306.90	7855.47	6881.42	8303.57	1106.31	0.00
AS 0.5	May 23, 2011	277924.61	8193.76	9504.10	9013.30	7426.28	4984.58	3662.62	14051.42	23973.79	5733.39	0.00
LS 0.6	July 1, 2010	76885.77	5738.52	6328.85	6547.54	5952.02	3658.29	1195.24	387.42	171.12	8.60	0.00
LS 0.6	September 8, 2010	1328.79	68.92	70.67	42.00	14.52	2.92	0.92	0.23	0.48	0.00	0.00
LS 0.6	March 9, 2011	67265.00	10605.41	14699.79	18800.78	20011.57	13262.81	4268.78	1220.08	572.99	30.19	0.00
LS 0.6	May 23, 2011	209661.26	5229.51	5920.60	5660.55	4803.64	3389.31	2554.39	10925.42	14776.71	2474.44	607.60
LS M311.6	July 1, 2010	57550.91	5011.94	5490.54	5578.21	5037.25	3115.63	1260.44	1059.78	540.06	18.98	0.00
LS-M311.6	February 1, 2010	89740.60	5859.29	9021.20	8071.67	6546.90	3564.59	2989.31	12370.08	14642.98	1849.74	0.00
LS-M311.6	September 8, 2010	934.41	49.50	55.33	39.35	20.14	6.61	1.68	0.22	1.18	0.00	0.00
M311.2	February 1, 2010	985522.36	70269.16	107027.70	90082.75	69443.39	33156.36	22180.80	115203.18	135203.86	9303.62	13.54
M311.2	March 4, 2010	738801.44	34237.59	53993.08	46755.29	36456.99	19726.55	14055.21	62908.01	82294.76	10762.11	0.00
M311.2	April 29, 2010	470239.57	16295.01	24515.61	22483.48	21314.21	13450.68	5090.90	4242.51	4239.74	514.97	0.00
M311.2	July 1, 2010	629651.00	61890.25	131209.43	68356.24	59426.00	36187.02	12305.19	13191.79	12917.24	1236.14	0.00
M311.2	September 8, 2010	312654.92	17636.85	21537.10	19413.51	16399.66	8075.06	2486.06	2070.82	1223.83	117.95	0.07
M314.6	July 1, 2010	56199.66	4751.75	5349.50	5010.39	3905.61	2010.92	590.11	303.18	112.33	97.86	626.36
M314.6	September 8, 2010	24428.93	1389.07	1663.12	1424.68	1181.50	516.24	377.85	1092.69	680.54	5.10	0.00
M316	February 1, 2010	1005514.36	98425.44	158586.07	140872.34	105422.82	49781.15	26832.89	52672.60	46916.80	3751.18	1885.43
M316	March 4, 2010	700158.59	25538.33	41561.50	37011.45	28020.90	11313.58	10346.31	34201.23	24632.80	1176.66	0.00
M316	April 29, 2010	563737.10	21748.84	31134.75	28207.84	26079.88	16074.60	5964.76	7815.77	9463.01	1309.98	0.00
M316	July 1, 2010	735022.00	68628.99	89460.13	75371.77	65215.59	38391.85	12318.29	15419.23	15482.61	1176.12	0.00
M316	September 8, 2010	338757.78	19406.14	23571.67	21364.77	17885.48	9007.64	3019.95	1665.83	676.21	3.08	0.00
M-317	April 29, 2010	658521.52	26354.41	40109.42	36771.25	33989.18	19153.76	7060.31	8528.41	7579.92	818.93	0.00
M-317	July 1, 2010	896398.50	88467.06	113759.31	95300.47	82011.69	48805.94	17241.93	12327.50	8316.74	295.23	0.00

Line Designation	Date	Discharge cfs	Grain Size (µm)									
			0-4	4-8	8-16	16-31	31-63	63-125	125-250	250-500	500-1000	1000-2000
M-317	September 8, 2010	463590.66	28383.58	32941.14	27669.29	21908.51	10617.34	3522.90	2010.23	457.18	0.00	0.00
M-317	March 9, 2011	1085416.07	145009.13	208533.25	240600.51	222492.06	150887.36	94847.13	136176.28	92748.31	4004.91	0.00
M 317	May 23, 2011	1647274.18	46180.66	55747.46	50784.28	38909.81	15438.91	13230.93	134660.90	114685.19	6334.66	0.00
PP 0.6	February 1, 2010	155186.20	13471.18	20690.97	18006.34	12275.36	4945.42	2645.57	2502.99	1055.86	86.50	0.00
PP-0.6	March 4, 2010	123929.58	3204.31	5318.37	4768.13	3648.29	1700.18	1071.93	2000.83	966.56	21.83	0.00
PP-0.6	April 29, 2010	69922.86	2557.99	4887.76	4568.35	3531.00	1439.84	323.34	113.55	49.39	12.28	0.00
PP-0.6	July 1, 2010	115127.28	9641.55	13420.57	11748.47	11155.50	6378.66	1007.12	196.39	91.65	9.30	0.00
PP-0.6	September 8, 2010	96887.78	5729.38	7033.34	5981.17	4487.44	1949.89	438.37	133.49	68.06	0.58	0.00
PP-0.6	March 9, 2011	108714.17	14557.60	19974.09	26516.78	29465.24	20065.49	8007.88	5908.64	5010.58	701.41	0.00
PP-0.6	May 23, 2011	145846.46	1432.25	1624.03	1505.19	1103.59	634.80	388.59	832.50	979.27	143.30	0.00
PP-M316.3	February 1, 2010	168700.25	11082.49	16935.45	15254.63	11975.89	6041.54	4874.49	9299.75	3944.99	1388.42	3193.54
PP-M316.3	March 4, 2010	83539.44	4611.57	6847.33	6024.41	5269.38	2577.47	511.59	138.36	164.85	127.36	0.00
PP-M316.3	April 29, 2010	103735.71	5023.94	5762.01	4812.14	3717.08	1712.80	487.58	325.99	97.03	0.00	0.00
R-11.1	February 1, 2010	217733.81	19233.36	21087.43	17273.97	14392.61	12395.72	19703.56	25251.58	10324.09	1116.35	0.00
R-11.1	March 4, 2010	183505.93	9564.50	11513.74	9551.28	7986.82	5364.58	21832.56	38739.72	14643.41	563.14	0.00
R-11.1	April 29, 2010	28436.12	1278.53	2413.26	2086.87	978.81	66.63	46.83	119.86	13.24	0.00	0.00
R-11.1	September 8, 2010	8055.17	16.83	31.85	39.79	25.15	3.86	1.51	1.65	1.82	0.07	0.00
R-9.9	March 4, 2010	307363.18	10014.17	14494.78	12710.25	10019.61	5163.76	11626.85	18977.83	6324.18	4780.52	63.60
R-9.9	April 29, 2010	207528.28	9204.87	13512.14	12485.21	11870.01	7634.99	4203.34	3354.67	1408.98	131.24	0.00
R-9.9	July 1, 2010	260051.80	24674.39	33484.44	28625.32	25531.39	15178.85	3981.25	2632.62	2067.43	442.91	2499.90
R-9.9	September 8, 2010	118023.31	6877.99	8421.78	7313.30	5733.13	2683.89	667.47	172.78	59.99	9.27	0.01

After the two distribution functions are populated, then the value for each function in 1% increments are paired. These paired values are regressed against each other to define a calibration curve between the two data sets. Usually a second-order polynomial fit gives R-squared values greater than 0.96. That calibration curve is only good for the river stage in which it was collected because the relationship of the acoustic backscatter energy to TSM is a function of the material characteristics in suspension. As the source, size distribution and concentration change with the hydrograph, then the backscatter distribution function will change and take a slightly different shape.

The next step in the calibration process is the conversion of the acoustic backscatter data to TSM values. The calibration equation is applied to the ADCP data to convert backscatter to TSM values. The conversion of backscatter data closer to the bed tends to overestimate the profile as it approaches the bottom. Therefore, a method has been devised that fits a Rouse profile through the concentration data as it approaches the bed. A maximum concentration value has to be supplied by the user to tell the method where to start applying the Rouse profile algorithm to the concentration profile. This value is derived from the actual sample data. The choice of this value is an iterative process to achieve the closest fit to the actual field samples.

Two physical samples were collected at each point in the water column. One sample was analyzed for TSM while the other sample was analyzed for grain size distribution. In addition to the sample data, ADCP velocity and backscatter data were collected during the entire sampling operation. These backscatter data were converted to TSM values for the entire sampling period. The converted TSM values at the specific depth elevation were extracted to compare to the actual physical samples. This comparison showed how well the calibration process worked. If the converted data near the bed were too high as compared to the sample data, then the value of the pick point in applying the Rouse profile in the conversion process would be increased. The process might be repeated several times until the best fit was achieved.

Once the backscatter data were converted as accurately as possible, the next step in the flux calculation process begins. The ADCP collected velocity data as the boat was driven across the channel. The collection rate of the instrument is fixed and the vertical spacing of data in the profile is fixed but

the speed of the vessel as it moves across the channel can vary slightly as different flow conditions arise. Therefore, the cells, or data collection bins, can vary in length as the boat moves across the cross section. In addition to the velocity data for each cell, TSM values for each cell are developed through the calibration process. The dot product of the water flux with the concentration at each cell determines the sediment flux through that cell. This process was done throughout the entire profile at which time the values were summed for the entire cross section. The resultant value is in milligrams per second (mg/sec) which is then converted to tons/day for the cross section. Appendix A presents the calibration equations and resulting suspended fluxes calculated for each collection period.

Bottom (Bed) sediment sampling

Bottom samples were taken each service trip over the entire site to quantify the seasonal changes due to the varying hydrograph, as well as to specify the bed gradation for the numerical models. The types of equipment to be employed are described below along with some of the methods of analysis. Figure 2.2 shows the bed material sampling location cross sections. Five samples were collected along each cross section on the main Mississippi River, three samples were collected along the small channels going into the structures, and five samples per cross sections were collected in the Atchafalaya/Red Rivers, for a total of 57 samples. The samples were collected at each location using one of three different methods, discussed below, depending on the depth of water and flow conditions.

Box core samplers

The box-core sampler is very similar to the petite Ponar in its triggering mechanism and sampling technique. The main difference in the two samplers is where the sample is trapped. The box core sampler has clamshell jaws that scoop the sediment into a clear-plastic square tube. When the sampler is opened at the surface, the sample is visible from a top door on the sampler. From this top door, the trapped sample can be subsampled for more detailed analysis. Figure 2.3 is a picture of the box-core sampler. The subsampling method is to collect only the surface material for analysis each sampling trip because it is the material recently deposited for the time between sampling efforts.

Figure 2.2. Bed material measurement sites.

Figure 2.3. Box core sampler.

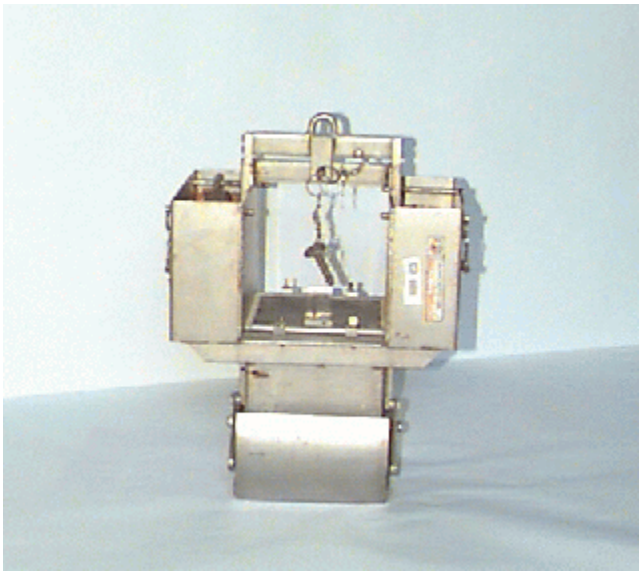

Bed drag sampler

Bottom sediments were obtained with a drag sampler. The bucket was dragged along the bottom on a chain attached to a 100 lb fish. The weight of the chain attached to the open end of the bucket forced it to dig into the bed and fill the bucket with a bottom sample. The sampler was raised to the

surface, and the sample was poured into a sample container for further analysis.

Laboratory analysis of the bottom samples

Prior to introduction to the laser, all bed samples were introduced to and suspended in a solution of sodium meta-phosphate (1–2 g/L) for at least 5 hours (hr). Samples were then sonicated and passed through an 850 μm (#20 ASTM) sieve to remove any large debris from the sample. No sediment grains were ever observed to be retained in the sieve for all samples. Each sample was cycled through the laser at least three times, and an average size distribution was reported. The grain size distributions of the bottom samples are in shown in Figure 2.4 through Figure 2.10 and tabulated in Table 2.2.

Figure 2.4. Grain size for all sample sites a, c, d, e at RM 317.

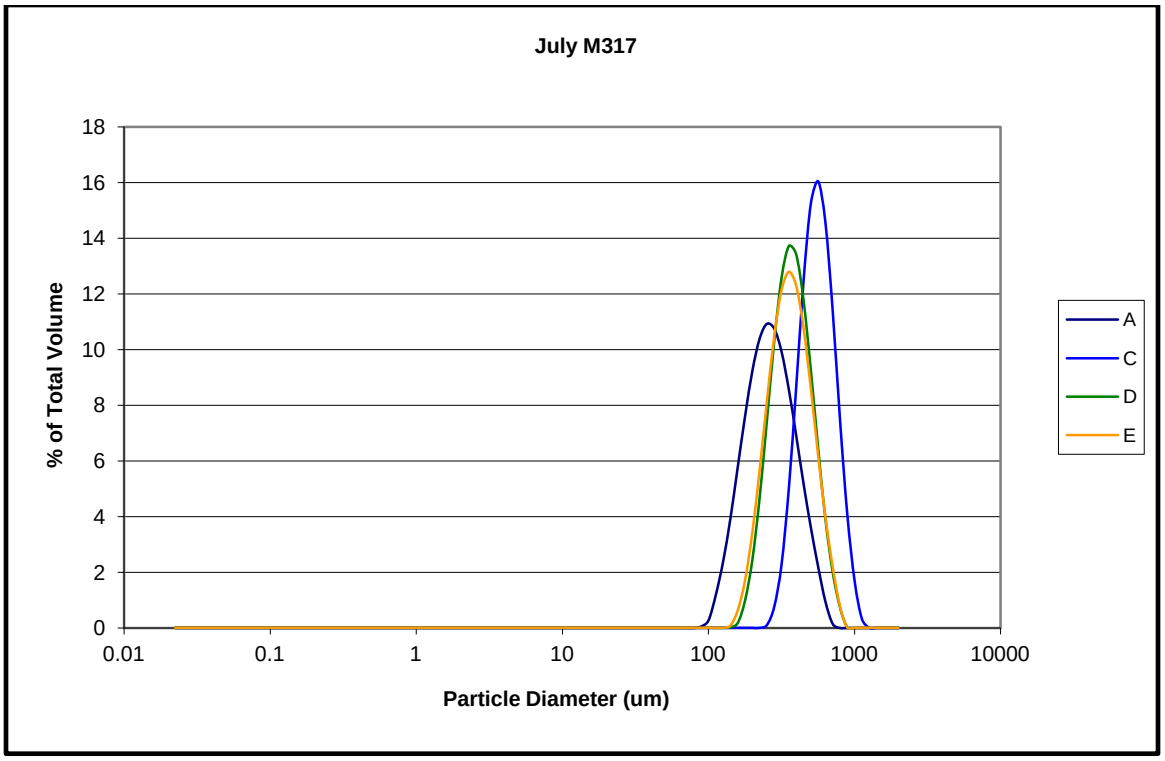

Figure 2.5. Grain size for all sample sites b, c, d, e at RM 316.

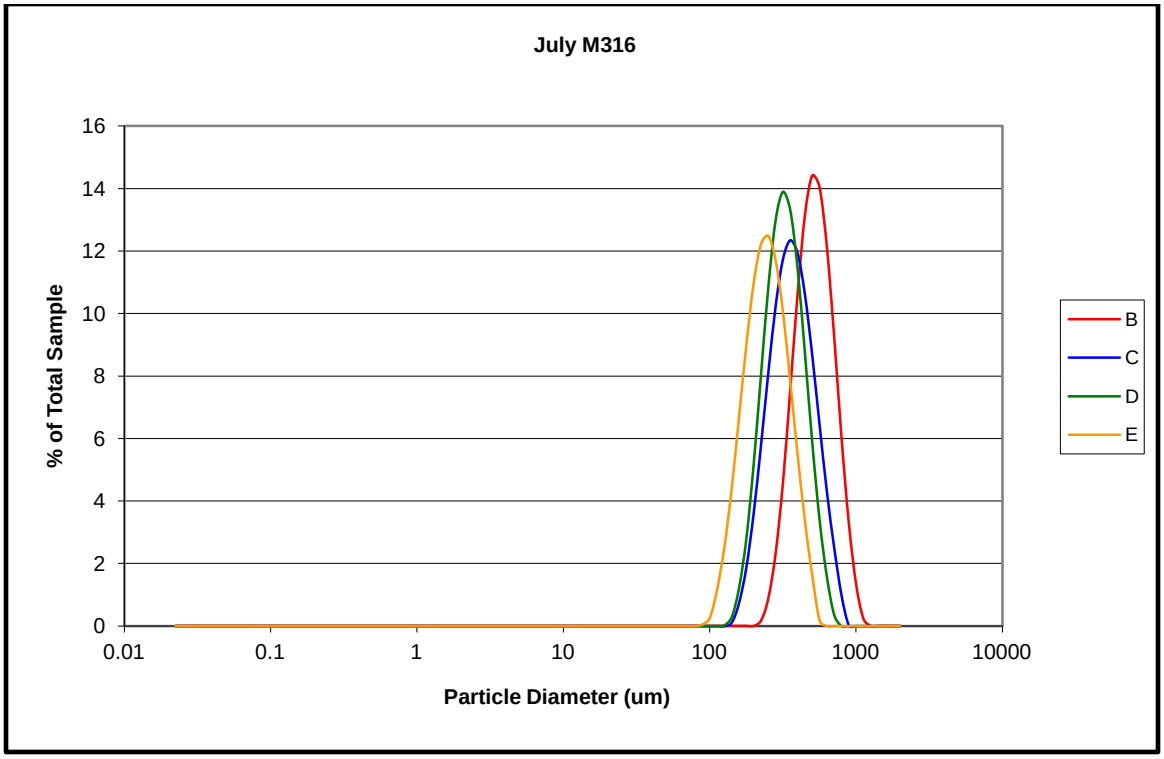

Figure 2.6. Grain size for all sample sites a, b, c, d, e at RM 314.4.

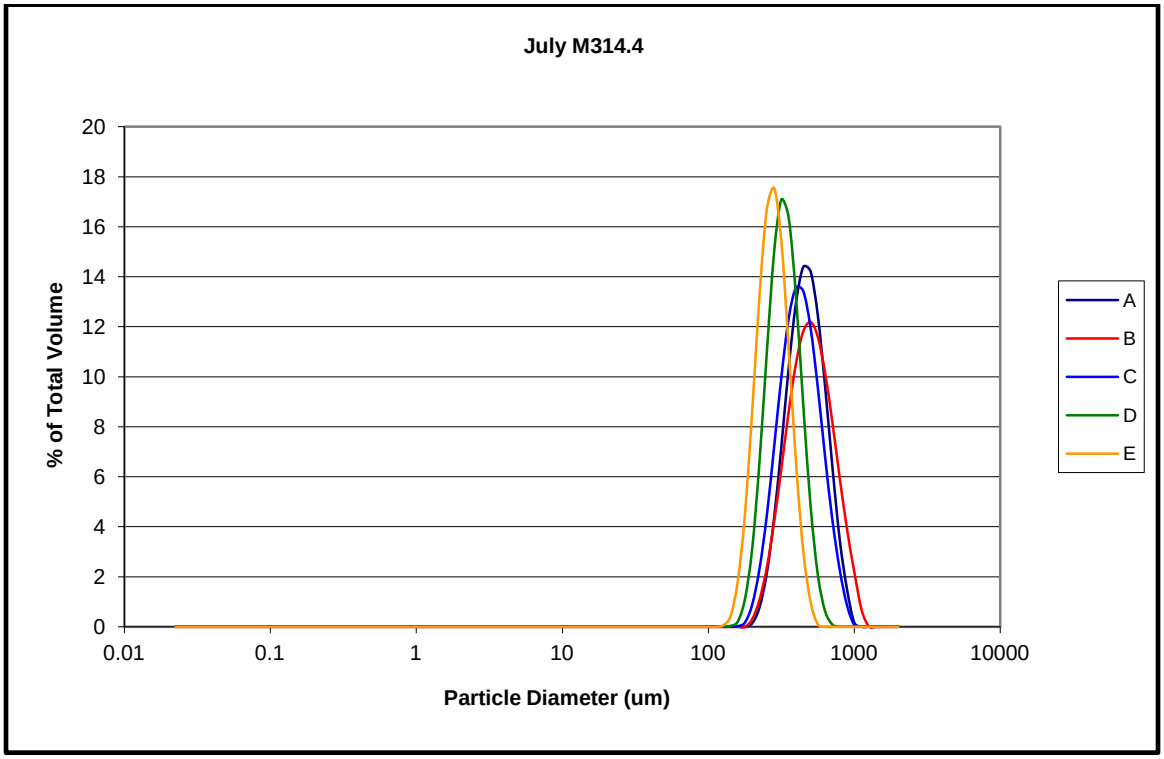

Figure 2.7. Grain size for all sample sites a, b, c, d, e at RM 312.1.

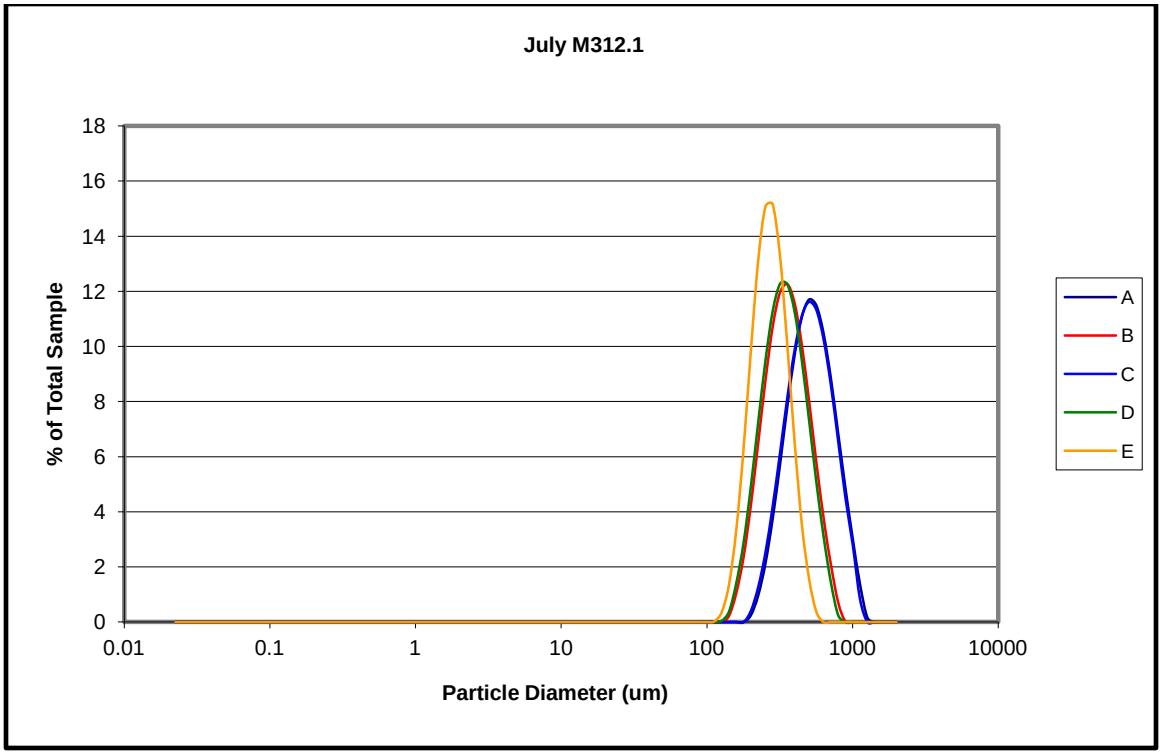

Figure 2.8. Grain size for all sample sites a, b, c, at RM PP0.6.

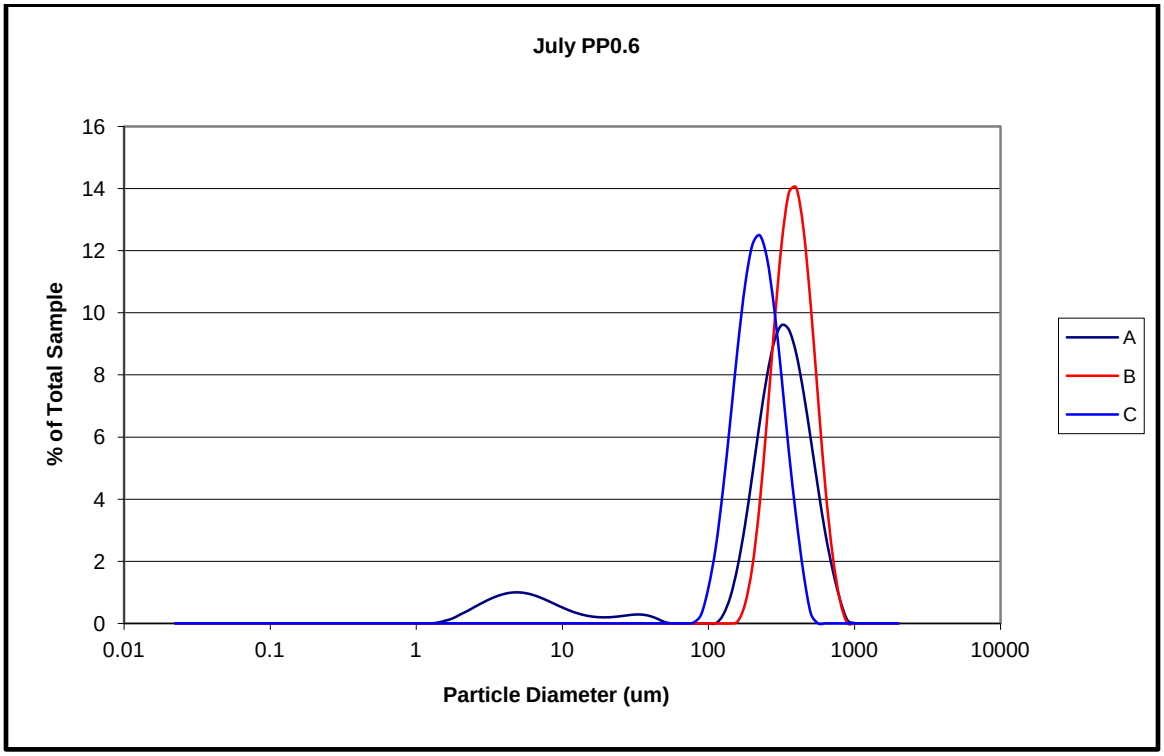

Figure 2.9. Grain size for all sample sites a, b, c, d, e at Red River mile 9.9.

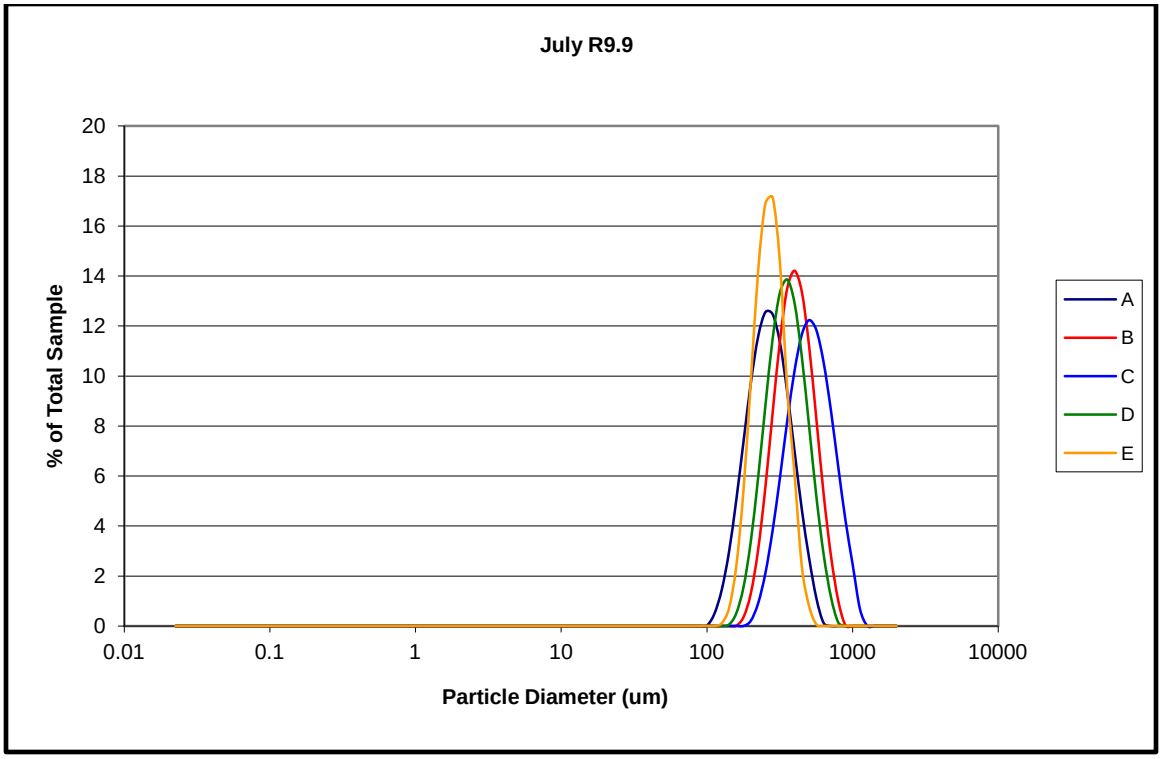

Figure 2.10. Grain size for all sample sites a, b, c, d, at Red River mile 11.1.

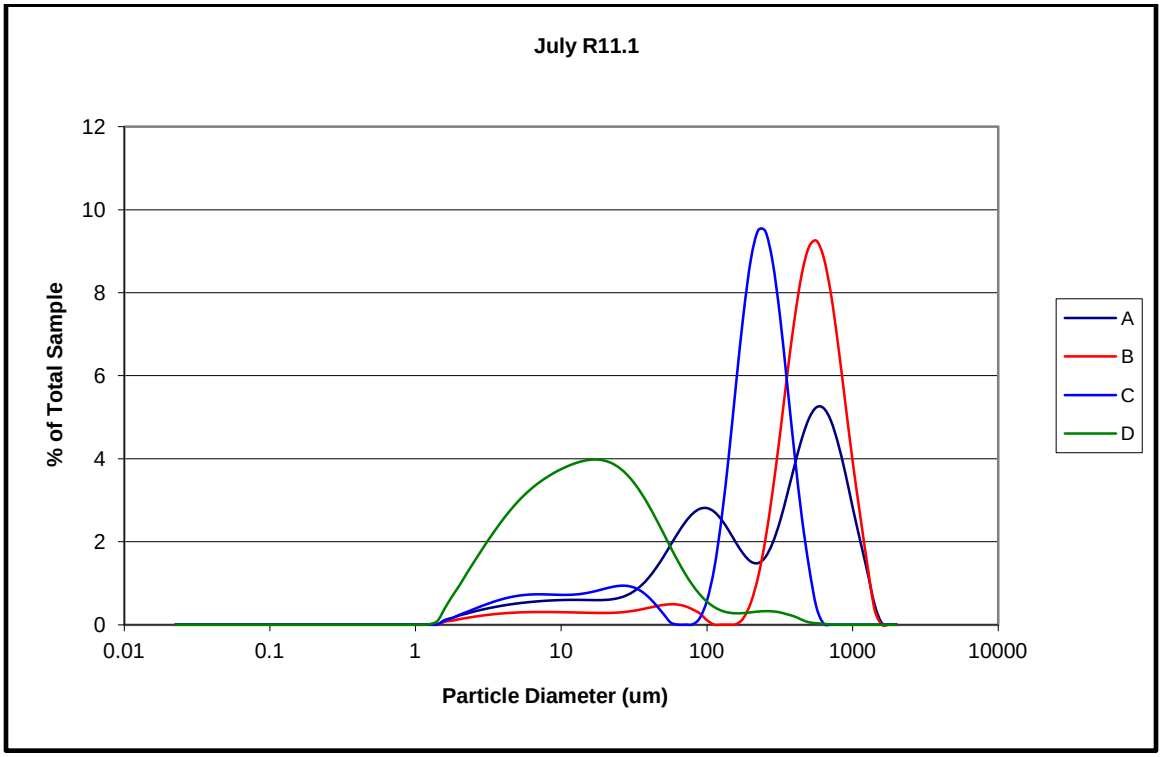

Table 2.2. Bed material sample classification (AGU grain size scale).

Sample	% Sand	%Silt	%Clay	% Very Fine Silt	% Fine Silt	%Med Silt	%Coarse Silt	%Very Fine Sand	% Fine Sand	%Med Sand	%Coarse Sand	% Very Coarse Sand
M311.2-A	100.00	0.00	0.00	0.00	0.00	0.00	0.00	0.00	4.46	64.86	30.68	0.00
M311.2-B	100.00	0.00	0.00	0.00	0.00	0.00	0.00	0.00	26.53	70.12	3.35	0.00
M311.2-C	100.00	0.00	0.00	0.00	0.00	0.00	0.00	0.00	21.13	73.39	5.48	0.00
LS-M311.6-B	100.00	0.00	0.00	0.00	0.00	0.00	0.00	0.00	9.12	63.61	27.28	0.00
LS-M311.6-A	100.00	0.00	0.00	0.00	0.00	0.00	0.00	0.00	0.23	31.68	60.50	7.59
OR-8	90.93	8.06	1.01	1.22	1.41	2.22	3.21	7.23	30.23	42.43	11.05	0.00
OR-15	100.00	0.00	0.00	0.00	0.00	0.00	0.00	0.00	2.49	67.92	29.59	0.00
OR-16	100.00	0.00	0.00	0.00	0.00	0.00	0.00	0.00	1.64	54.70	43.38	0.29
OR-17	100.00	0.00	0.00	0.00	0.00	0.00	0.00	0.00	3.92	55.00	40.63	0.45
OR-18	100.00	0.00	0.00	0.00	0.00	0.00	0.00	0.00	12.39	64.70	22.91	0.00
M314.4-A	100.00	0.00	0.00	0.00	0.00	0.00	0.00	0.00	6.33	69.33	24.34	0.00
M314.4-B	100.00	0.00	0.00	0.00	0.00	0.00	0.00	0.00	1.07	48.11	49.96	0.86
M314.4-C	100.00	0.00	0.00	0.00	0.00	0.00	0.00	0.00	4.90	59.04	36.04	0.02
M314.4-D	100.00	0.00	0.00	0.00	0.00	0.00	0.00	0.00	11.89	65.22	22.89	0.00
M314.4-E	100.00	0.00	0.00	0.00	0.00	0.00	0.00	0.10	41.69	57.31	0.91	0.00
OR-24	17.44	70.22	12.35	14.57	18.08	20.11	17.45	10.13	5.65	1.66	0.00	0.00
M314.6-A	28.63	63.59	7.78	10.75	15.42	20.67	16.76	4.61	9.14	13.74	1.14	0.00
M314.6-B	25.80	63.75	10.45	13.76	19.37	19.98	10.64	5.45	14.17	6.18	0.00	0.00
M316-D	100.00	0.00	0.00	0.00	0.00	0.00	0.00	0.09	27.69	63.92	8.30	0.00
M316-E	100.00	0.00	0.00	0.00	0.00	0.00	0.00	0.08	38.20	60.61	1.11	0.00
PP-M316.3-A	100.00	0.00	0.00	0.00	0.00	0.00	0.00	0.11	34.46	61.76	3.67	0.00
M317-A	100.00	0.00	0.00	0.00	0.00	0.00	0.00	0.04	23.74	64.25	11.96	0.00
M317-E	100.00	0.00	0.00	0.00	0.00	0.00	0.00	0.00	18.32	66.37	15.31	0.00
OR-39	100.00	0.00	0.00	0.00	0.00	0.00	0.00	0.00	12.69	66.76	20.55	0.00

Sample	% Sand	%Silt	%Clay	% Very Fine Silt	% Fine Silt	%Med Silt	%Coarse Silt	%Very Fine Sand	% Fine Sand	%Med Sand	%Coarse Sand	% Very Coarse Sand
PP-0.6-C	100.00	0.00	0.00	0.00	0.00	0.00	0.00	2.08	58.06	39.82	0.04	0.00
PP-0.6-B	100.00	0.00	0.00	0.00	0.00	0.00	0.00	0.00	21.81	65.90	12.29	0.00
PP-0.6-A	88.47	8.76	2.78	2.09	1.25	1.38	4.03	1.62	17.55	49.22	20.08	0.00
PP-3.0-E	96.37	3.52	0.11	0.24	0.20	1.36	1.73	0.00	26.27	66.79	3.31	0.00
PP-3.0-D	100.00	0.00	0.00	0.00	0.00	0.00	0.00	0.00	15.84	63.34	20.83	0.00
PP-3.0-D	100.00	0.00	0.00	0.00	0.00	0.00	0.00	0.00	7.66	61.49	30.85	0.01
PP-3.0-C	100.00	0.00	0.00	0.00	0.00	0.00	0.00	0.00	5.00	58.30	36.59	0.12
PP-3.0-B	100.00	0.00	0.00	0.00	0.00	0.00	0.00	0.00	19.46	66.43	14.11	0.00
PP-3.0-A	100.00	0.00	0.00	0.00	0.00	0.00	0.00	1.35	67.55	31.10	0.00	0.00
R11.1-D	100.00	0.00	0.00	0.00	0.00	0.00	0.00	7.62	50.34	38.70	3.33	0.00
R11.1-C	99.12	0.54	0.35	0.50	0.03	0.00	0.00	0.20	23.14	56.91	18.88	0.00
R11.1-B	100.00	0.00	0.00	0.00	0.00	0.00	0.00	0.01	21.10	60.38	18.51	0.00
R11.1-A	99.23	0.66	0.11	0.39	0.28	0.00	0.00	0.00	10.90	50.84	36.71	0.79
R9.9-B	98.33	1.39	0.28	0.42	0.02	0.57	0.38	1.63	26.94	49.90	19.83	0.04
R9.9-C	100.00	0.00	0.00	0.00	0.00	0.00	0.00	0.00	5.08	66.00	28.92	0.00
R9.9-D	100.00	0.00	0.00	0.00	0.00	0.00	0.00	0.00	0.11	50.86	48.95	0.09
R9.9-E	100.00	0.00	0.00	0.00	0.00	0.00	0.00	0.00	8.37	72.76	18.87	0.00

Bathymetric surveys and bed load measurements

The bathymetric surveys/bed load measurements were conducted with an interferometric (phase measuring) swath sonar. This instrument captures a time sequence of bottom topography, thus allowing the measurement of bed load sediment movement. This information is input into the Integrated Section Surface Difference Over Time version 2 (ISSDOTv2) computational method to obtain bed load transport estimates (Abraham et al. 2011). The swath system (Geo-Acoustics 250 kHz) measures both bathymetry and seabed acoustic backscatter from a hull-mounted transducer, providing coregistered depth soundings and side scan sonar information in water depths ranging from 1.64 to 328 ft. In contrast to fixed-angle algorithms utilized by beam-forming multibeams, interferometric swath systems determine angle and travel time for every sampling interval (~50 milliseconds [ms]). Measuring angles from phase shifts at rapid sampling intervals provides a denser number of soundings at the outer ranges resulting in a wide horizontal swath (approximately 8–10 times water depth) in shallow water and resolution of 3D features ranging in size from inches to feet. Coupled with GPS during the survey, an Applanix POSMV IMU system measured the inertial position of the vessel along with its angular orientation. These measurements are typically acquired at a rate of up to 200 Hz. Each trajectory measurement is described by seven parameters. They are three position coordinates (typically latitude, longitude, and elevation relative to some datum), three angular coordinates (roll, pitch, heading), and a time stamp. These seven parameters completely describe the vessel position and orientation at each sample time.

Bed load measurements

The bed load transport rate was determined using the ISSDOTv2 method. Mississippi River and ORCC bed load measurement sites were selected in cooperation with the MVN. Eleven sites were selected at which measurements were obtained for computation of the bed load portion of the bed material load. The seven data collection or measurement trips were conducted on the dates listed in Table 2.3. The locations of the various sites throughout the Old River Control Complex are shown in Figure 2.11.

Table 2.3. Bed load data collection dates.

Data Collection Dates	
Trip 1	9–10 Feb 2010
Trip 2	3–4 Mar 2010
Trip 3	29–30 Apr 2010
Trip 4	1–3 Jul 2010
Trip 5	1 Sep 2010
Trip 6	9 Mar 2011
Trip 7	23 May 2011

Figure 2.11. ORCC bed load measurement site locations.

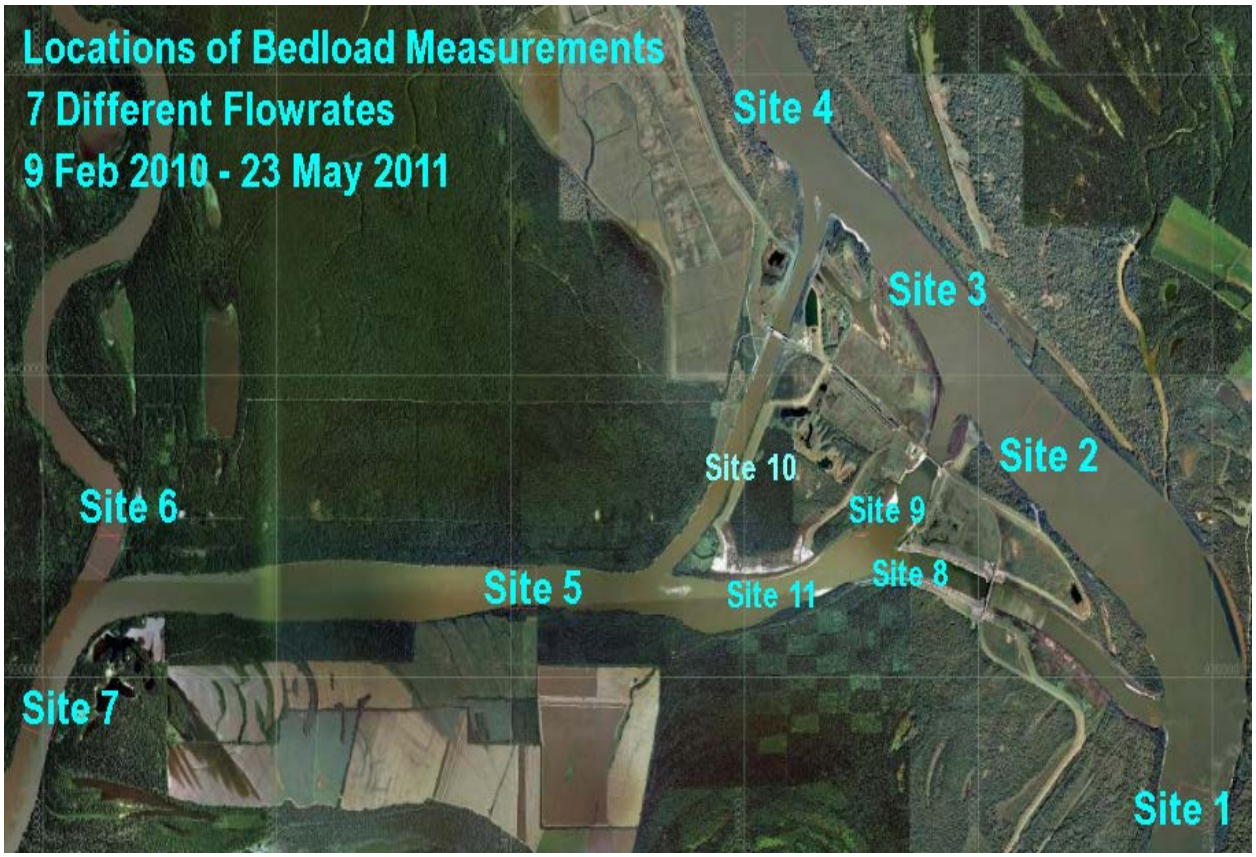

Not all sites were measured on a given trip. Site 4 (upstream of Hydropower) and Site 5 (in the Outflow Channel downstream of the three diversions) are the only two sites where measurements were taken for each trip. The total number of bed load measurements taken for each site are shown in Figure 2.12. Of the 45 multibeam sets taken at the ORCC, 41 were useable. Of these, 22 were on the main-stem Mississippi River (Figure 2.12).

Figure 2.12. Number of measurements made at the various sites.

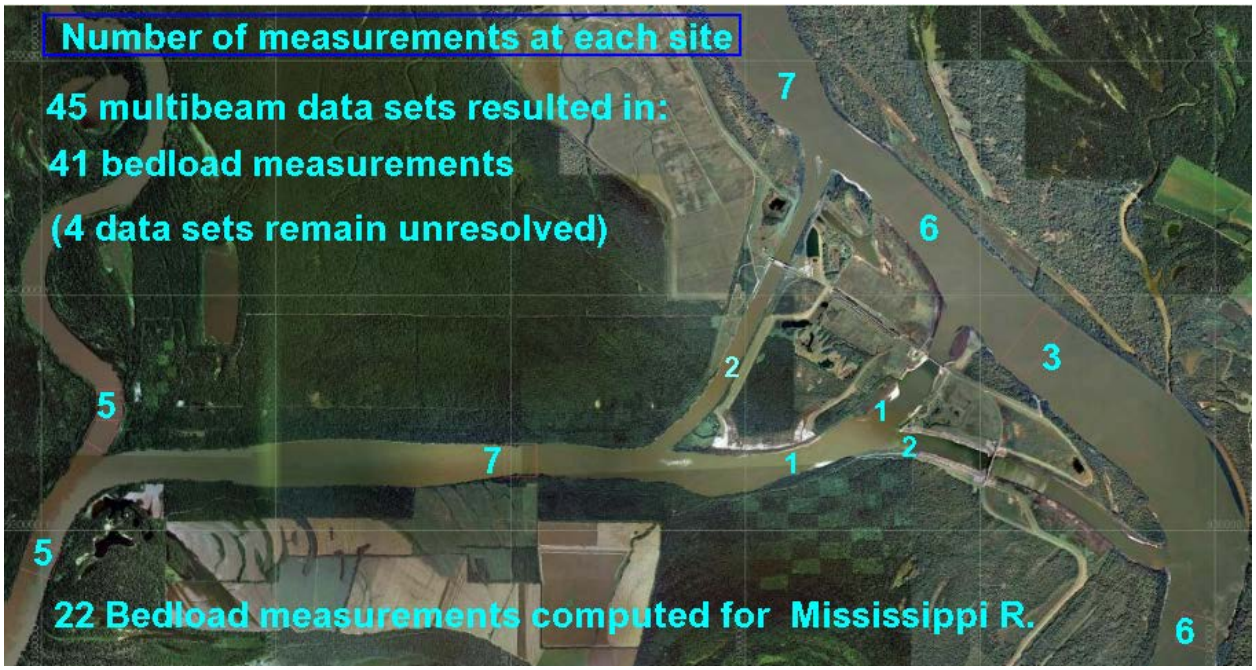

Multibeam data collection methodology

The bathymetric surveys were made from a vessel like that shown in Figure 2.13. The boat is equipped with an inertial motion unit (IMU), multibeam fathometer, and a real-time kinematic (RTK) GPS. All of these components are integrated into a Hydrographic survey package. The multibeam systems are 250 kHz and 500 kHz Geoswath Plus interferometric multibeam sonar with an Applanix PosMV IMU. Real-time GPS corrections are supplied by a Trimble R8 GNSS and broadcast to the PosMV for positioning and crucial time tagging of all instruments. The swath width provided by this system is up to 12 times the water depth per pass with a ranging accuracy of 3.0 mm for the 250 kHz frequency and 1.5 mm for the 500 kHz frequency.

The data collected for use in the ISSDOTv2 methodology must be collected with attention to details not normally important during traditional multibeam survey methods. The data need to be collected over a sufficient length of channel to capture multiple waveforms in a short period of time. It is also desirable to collect as much channel width as possible to capture the lateral variability of the bed forms. The subsequent resurvey swaths must be run along the exact previous survey swath, in the same direction with the same vessel conditions. Swath-to-swath comparisons need to have as many collection conditions the same as possible to get the most accurate results.

Figure 2.13. Bathymetric survey boat.

When data are collected as described above, and properly processed, they are then analyzed with the ISSDOTv2 method to obtain a bed load transport value for the surveyed section of river.

Bed load measurement data analysis

The multibeam data were processed using the Hypack software or the native software of the GeoSwath System; both packages will produce the same results. The first step is to apply the heave, pitch, roll, and position data from the IMU to the raw sonar data. In the process of doing this, the appropriate patch tests must be run on the multibeam calibration data to insure the offsets and latency for the different signal streams are as accurate as possible. These calibrations affect the alignment of data on subsequent resurveys, so it is very important to ensure they are as accurate as possible. Every sensor has different methods of running patch tests, and the best results occur if they are run before the start of each survey.

The next step is to apply the data from the sound velocity probe casts to account for variations of the speed of sound as a function of depth. This data will affect the quality and width of the usable swath if it is not applied correctly. If the data are being collected in deep water where thermoclines

exist, then the data from the sound velocity casts are very important in making corrections to the final bathymetry. If the data is being collected in an area where a salinity gradient is present, then the sound velocity casts are critical and must be taken all along the length of the survey reach during the survey period.

The software packages allow the user to clean the data of outliers after all of the corrections have been applied. Once the swaths have been cleaned, then each individual swath is processed as an individual data set as needed by the ISSDOTv2 method of analysis. This output format from the processing software is a uniform rectilinear grid of elevation data for the bottom topography for each swath. The spacing of the grid is a function of the size of the sediment waves and project area; typically, for large rivers the grid spacing is 5 × 5 ft. The individual swaths can then be processed by the ISSDOTv2 method. Figure 2.14 shows a single swath of bed elevations for Site 5, Trip 4. These data were obtained and processed as described above.

Figure 2.14. ORCC Site 5, Trip 4, swath 2, 0836 hrs.

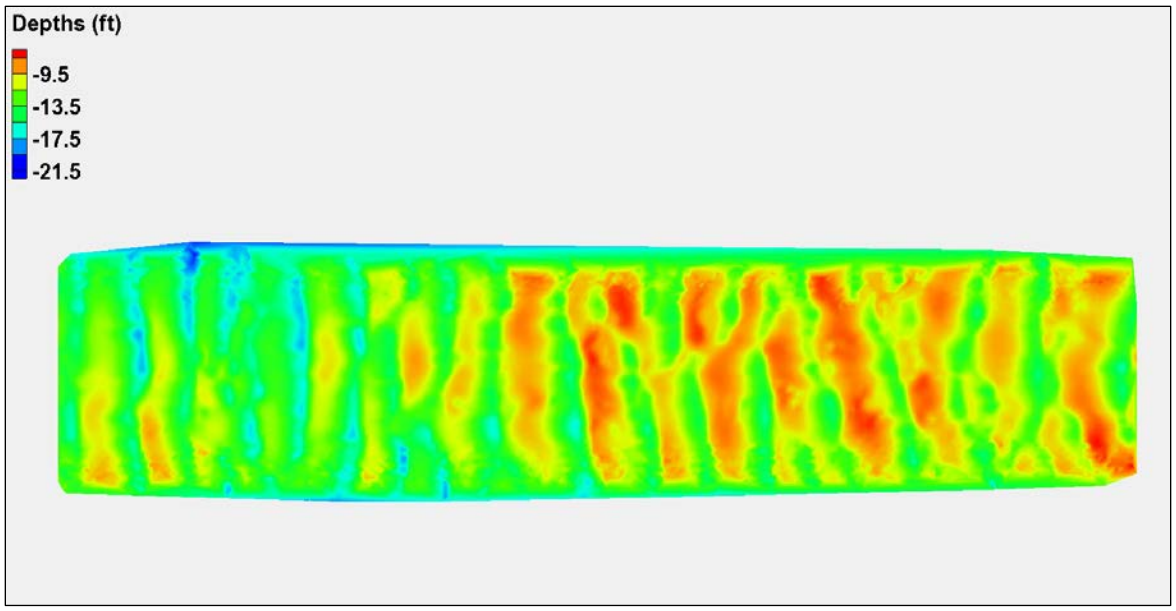

The swath in Figure 2.14 is approximately 300 ft wide and 1340 ft long. The different colors show varying bottom elevations of the river bed, and thus the sand wave pattern is clearly displayed. Average wave dimensions are 70–90 ft long and 5–6 ft high. As the survey vessel continues to make additional passes across the river section, a series of overlapping swaths, as shown in Figure 2.15, is mapped. In most cases, every effort is made to

survey bank to bank within the equipment capability and with respect to safety concerns. When a river section is covered in this manner, the same procedure is repeated over the course of a day. At least three to four repetitions are needed to ensure acquisition of sufficient data for the bed load computations. The successive repetitive swaths, when measured using the constraints mentioned above, can be subtracted from one another to determine bathymetric elevation changes that took place in the intervening time between measurement of the two swaths. A difference plot, like the one shown in Figure 2.16, is then made from the subtraction process which shows areas of the sand waves which aggraded (blue) and those which scoured (red). The ISSDOTv2 method of computing bed load uses the scoured depth and areal extant of each sand wave to determine its scour volume and thus transport rate. These volumes are averaged longitudinally within a given swath and summed by swath across the section.

Figure 2.15. ORCC Site 5, Trip 4, four overlapping swaths.

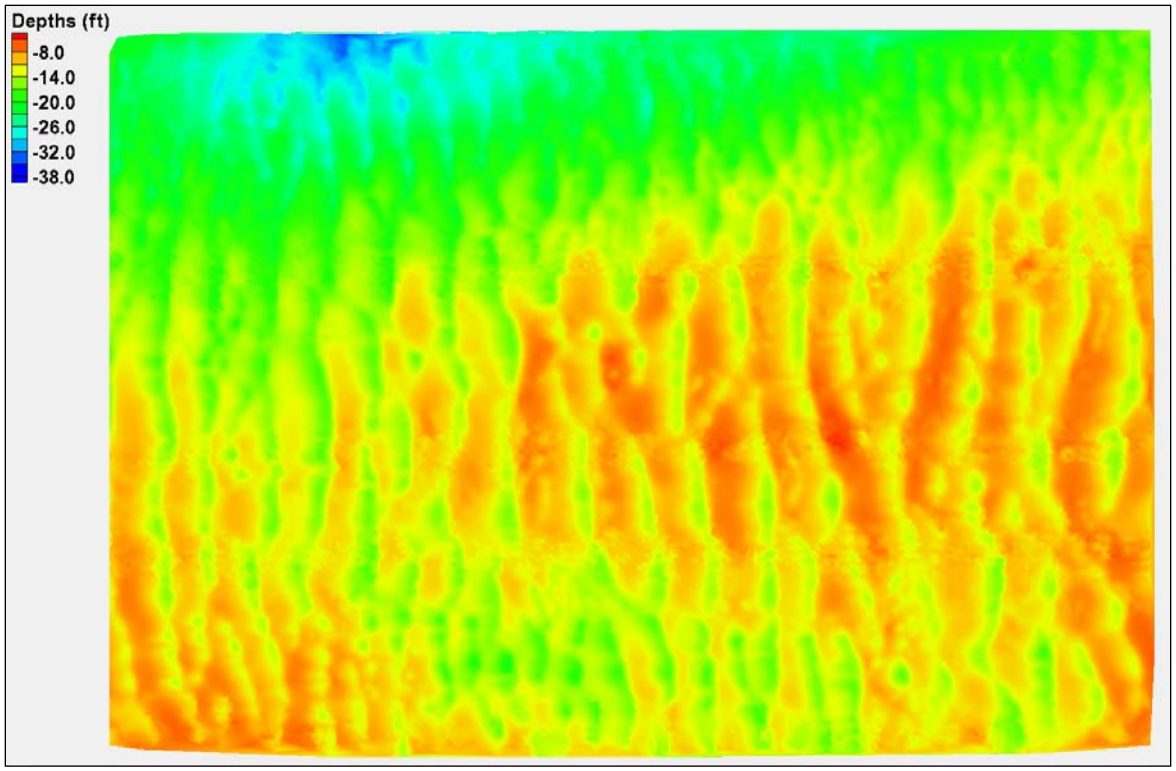

Figure 2.16. ORCC Site 5, Trip 4 difference plot for four swaths.

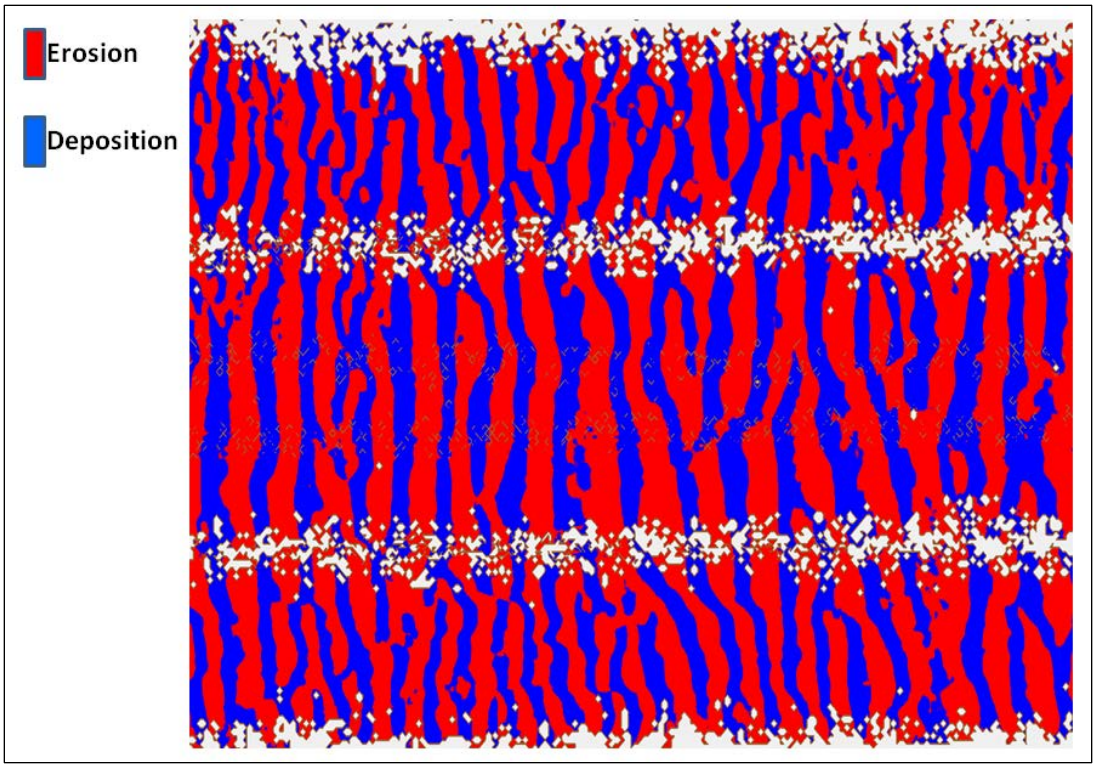

The preceding description was made for specific data obtained in Trip 4 at Site 5. For each of the measurements taken at locations shown in Figure 2.12 for which sufficient data were obtained as in the manner described above, ISSDOTv2 was applied to each of the pairs of swaths for conditions in which an equilibrium transport condition could be determined. An equilibrium condition in this case is defined as a condition over the whole swath in which the difference between scour and deposition was not greater than 20% during the measurement interval. It was determined by dividing the measured scour volume by the deposition volume. Values between 0.8 and 1.2 are considered acceptable. In general, the active sand transport portion of the river was covered at most locations in four to eight swaths depending upon the width of the river and the water depth.

Discussion of sediment load measurements

Results are presented for Sites 1–11 as appropriate in Table 2.4 through Table 2.13 and Figure 2.17 through Figure 2.23. The data for Site 9 were determined to be out of the range of the scour/deposition criteria and thus not useable for bed load computations. The following definitions pertain to the results:

- Wash Load = Fine sediments not found in appreciable quantities in the bed.
- BML = Bed Material Load = Sediment sizes normally found in the bed whether transported in bed-forms or in suspension.
- BL = Bed load = BML on bottom moving in bed-forms, composed of sand for these sites.
- SusBML = The suspended portion of the BML, which is mainly sand for these sites.
- Suspended Load = Wash Load + SusBML.
- Total Load = BML + Wash Load.
- Values are in TPD unless otherwise noted.

Table 2.4. Flow and sediment computations: Site 1.

	Trip 1	Trip 2	Trip 3	Trip 4	Trip 5	Trip 6	Trip 7
Flow (cfs)	985,522	738,801	470,240	629,651	312,655		987,274
BL	36,295	21,051	4,212	9,706	5,045		67,389
SusBML	281,905	170,020	14,088	39,650	5,899		
BML	318,200	191,071	18,300	49,356	10,944		67,389
% BL	11.4%	11.0%	23.0%	19.7%	46.1%		100.0%
Wash Load	369,979	191,170	98,059	357,069	83,062		
Total Load	688,179	382,241	116,359	406,425	94,006		67,389

Figure 2.17. BL and percent BL vs. flow, Site 1.

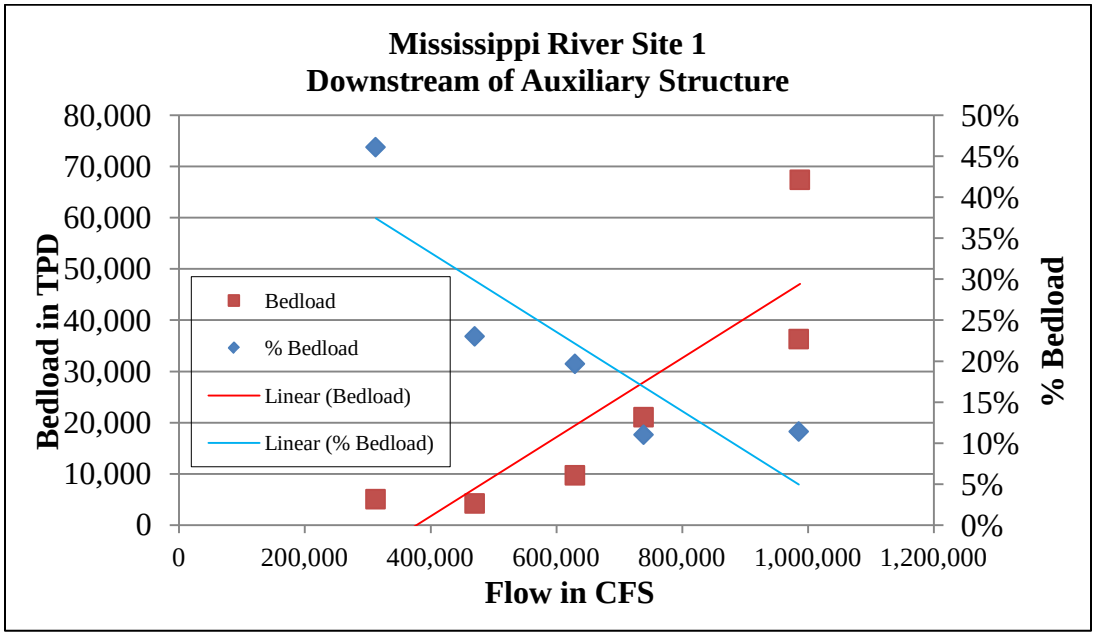

Table 2.5. Flow and sediment computations: Site 2.

	Trip 1	Trip 2	Trip 3	Trip 4	Trip 5	Trip 6	Trip 7
Flow (cfs)				685,000	319,000	879,566	
BL				15,866	3,186	52,904	
SusBML				70,914	4,326		
BML				86,780	7,512	52,904	
% BL				18.3%	42.4%		
Wash Load				308,779	85,407		
Total Load				395,559	92,919		

Figure 2.18. BL and percent BL vs. flow, Site 2.

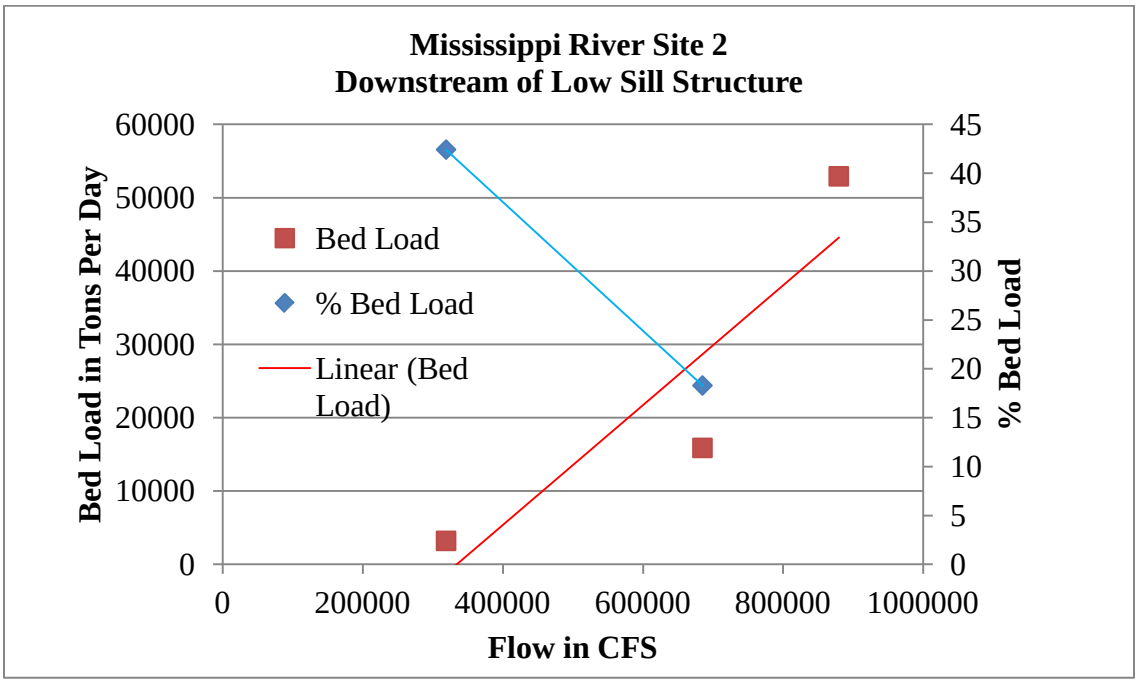

Table 2.6. Flow and sediment computations: Site 3.

	Trip 1	Trip 2	Trip 3	Trip 4	Trip 5	Trip 6	Trip 7
Flow (cfs)	1,005,514	700,159	563,737	735,022	338,758	976,702	
BL	40,914	19,887	14,120	24,700	1,197	40,802	
SusBML	132,059	70,357	24,554	44,396	5,365		
TotBML	172,973	90,244	38,674	69,096	6,562	40,802	
% BL	23.7%	22.0%	36.5%	35.7%	18.2%	100.0%	
Wash Load	553,088	143,446	123,246	337,068	91,236		
Total Load	726,061	233,690	161,920	406,164	97,798	40,802	

Figure 2.19. BL and percent BL vs. flow, Site 3.

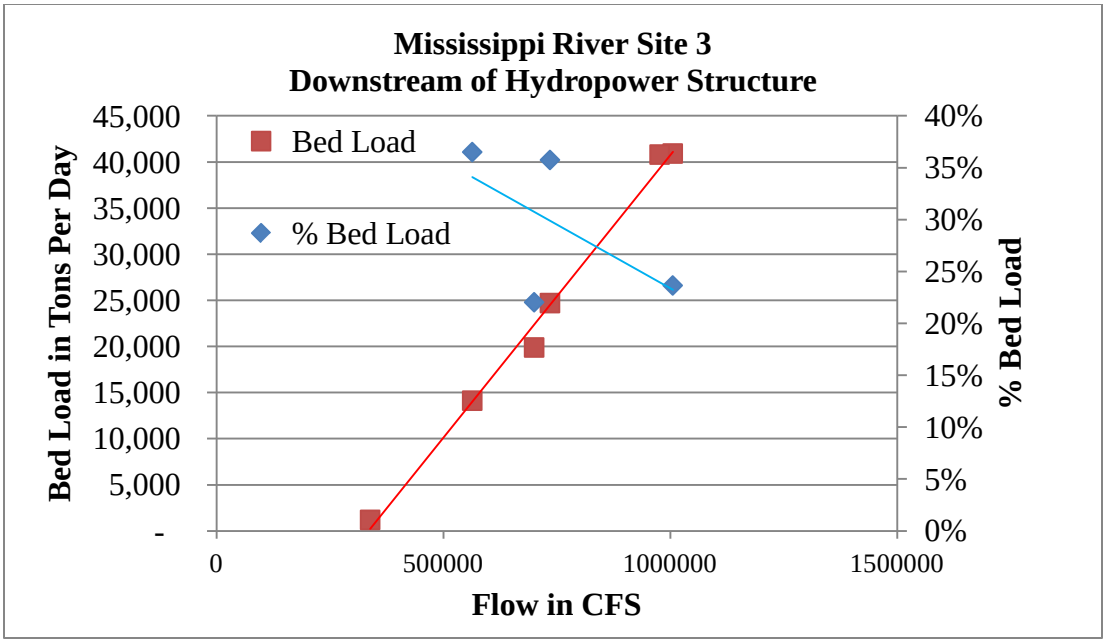

Table 2.7. Flow and sediment computations: Site 4.

	Trip 1	Trip 2	Trip 3	Trip 4	Trip 5	Trip 6	Trip 7
Flow (cfs)	1,099,588	842,747	658,522	896,399	463,591	1,085,416	1,647,274
BL	28,696	18,928	16,044	22,202	4,756	43,383	101,316
SusBML	284,620	72,444	23,988	38,181	5,990	327,777	268,912
BML	313,316	91,372	40,032	60,383	10,746	371,160	370,228
% BL	9.2%	20.7%	40.1%	36.8%	44.3%	11.7%	27.4%
Wash Load	492,772	125,017	156,378	428,344	121,520	967,522	207,061
Total Load	806,088	216,389	196,410	488,727	132,266	1,338,682	577,289

Figure 2.20. BL and percent BL vs. flow, Site 4.

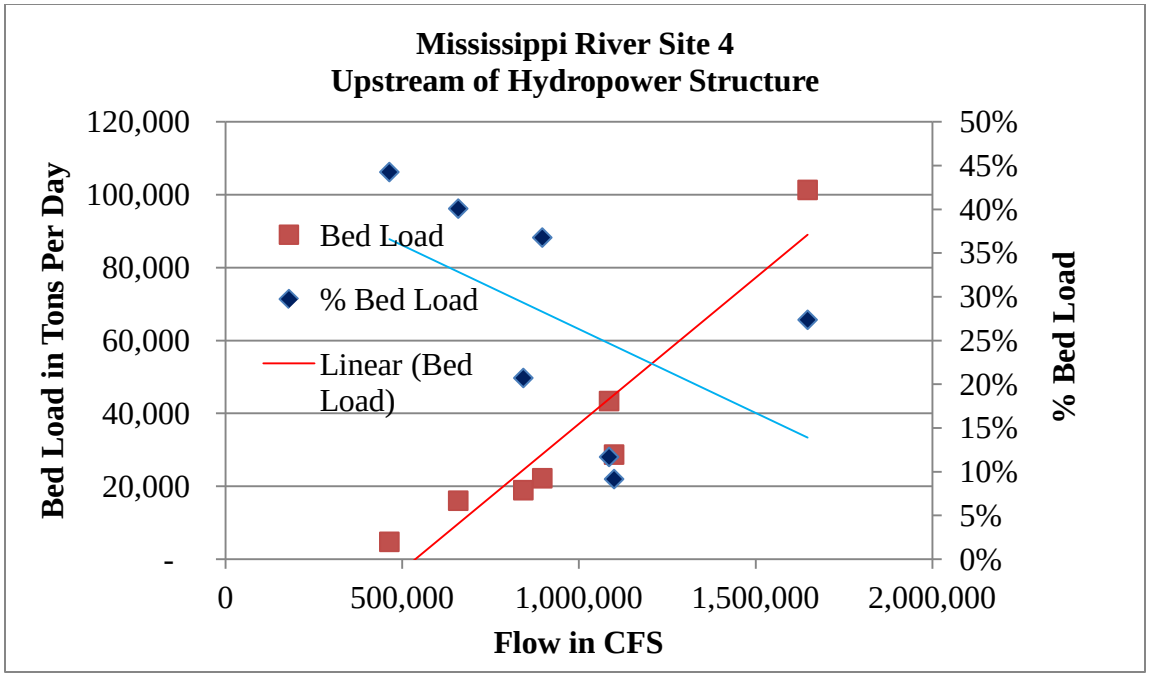

Table 2.8. Flow and sediment computations: Site 5.

	Trip 1	Trip 2	Trip 3	Trip 4	Trip 5	Trip 6	Trip 7
Flow (cfs)	263,000	123,858	155,000	262,000	130,000	318,000	660,000
BL	2,421	1,394	1,385	24,545	541	10,380	41,507
SusBML						76,591	51,092
BML						86,971	92,599
% BL						12%	45%
Wash Load						304,303	47,614
Total Load						391,274	140,213

Figure 2.21. BL vs. flow, Site 5.

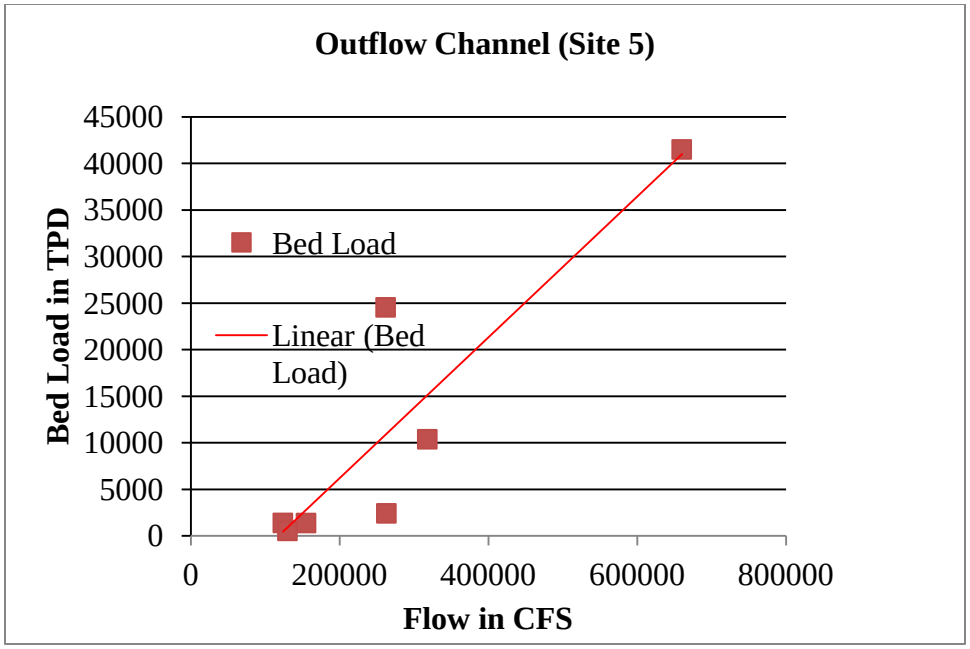

Table 2.9. Flow and sediment computations: Site 6.

	Trip 1	Trip 2	Trip 3	Trip 4	Trip 5	Trip 6	Trip 7
Flow (cfs)	217,000	183,000	28,500	18,400	5,200		
BL	1,624	4,795			1,236		
SusBML	56,396	75,779	180		5		
BML	58,020	80,574			1,241		
% BL	3%	6%			100%		
Wash Load	84,383	43,981	6,824		117		
Total Load	142,403	124,555	6,824		1,358		

Figure 2.22. BL vs. flow, Site 6.

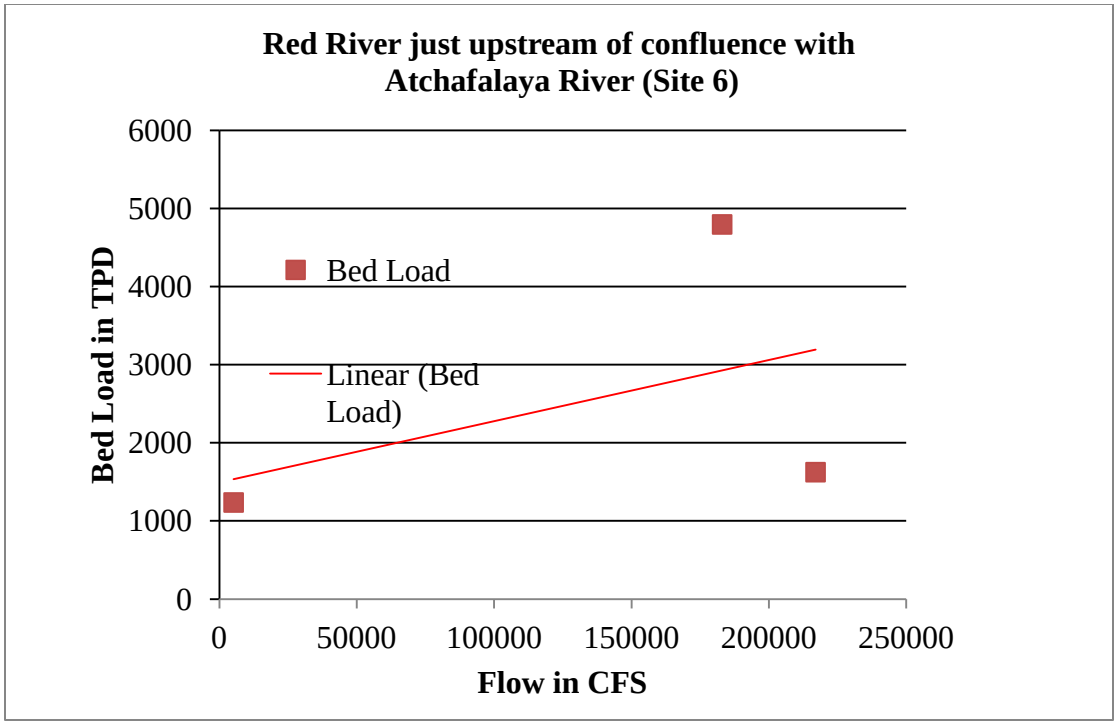

Table 2.10. Flow and sediment computations: Site 7.

	Trip 1	Trip 2	Trip 3	Trip 4	Trip 5	Trip 6	Trip 7
Flow (cfs)	430,000	307,000	205,000	260,000	118,000		
BL	5,333	2,418	1,454	1,592	1,451		
SusBML		41,773	9,098	11,624	910		
BML	5,333	44,191	10,552	13,216	2,361		
% BL		5%	14%	12%	61%		
Wash Load		52,403	54,707	127,494	31,030		
Total Load		96,594	65,259	140,710	33,391		

Figure 2.23. BL vs. flow, Site 7.

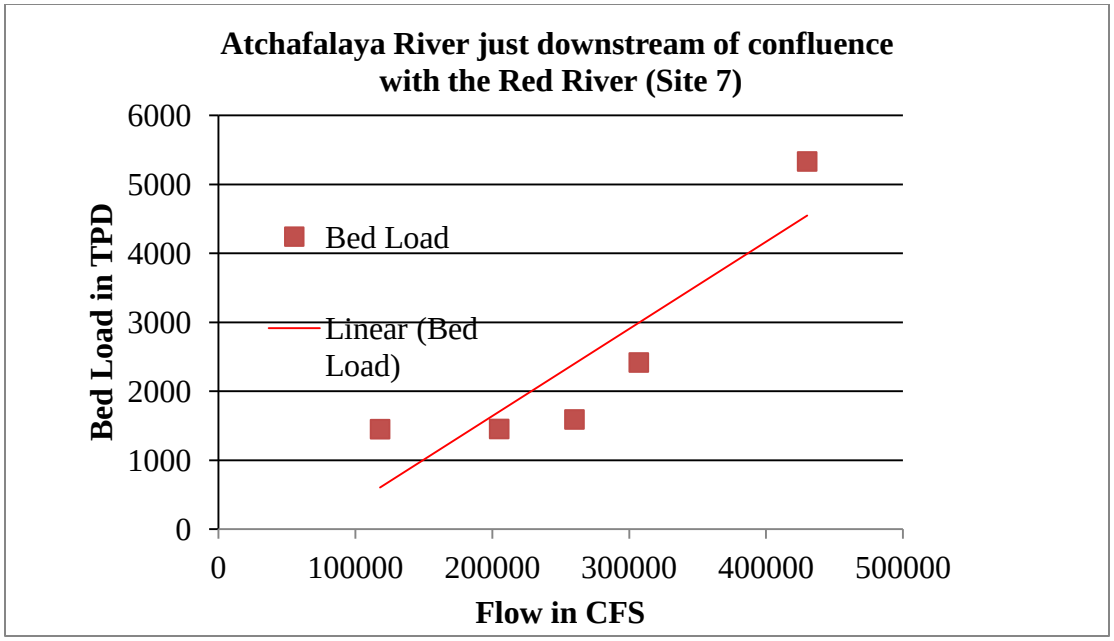

Table 2.11. Flow and sediment computations: Site 8 downstream of auxiliary structure.

	Trip 1	Trip 2	Trip 3	Trip 4	Trip 5	Trip 6	Trip 7
Flow (cfs)				71,000	1,300	67,265	209,661
BL							6,837
SusBML				1,762	2	6,092	31,339
BML							38,176
% Bed Load							18%
Wash load				28,225	199	77,380	25,004
Total Load							

Table 2.12. Flow and sediment computations: Site 10 downstream of hydropower structure.

	Trip 1	Trip 2	Trip 3	Trip 4	Trip 5	Trip 6	Trip 7
Flow (cfs)	154,000	123,000	69,500	115,000	97,000	108,714	145,846
BL							1,547
SusBML	6,291	4,061	499	1,304	640	19,629	2,344
BML							3,891
% Bed Load							39.8%
Wash load	69,389	18,639	16,985	52,345	25,181	110,579	6,300
Total Load							10,191

Table 2.13. Flow and sediment computations: Site 11 confluence of auxiliary and low sill structures.

	Trip 1	Trip 2	Trip 3	Trip 4	Trip 5	Trip 6	Trip 7
Flow (cfs)							
BL							40,382
SusBML							
BML							40,382
% Bed Load							
Wash load							
Total Load							

Seven data collection trips were conducted in the course of this study and are indicated at the top of each table. The dates on which each trip was made are shown in Table 2.3. The flow values are given in cubic feet per second (cfs) and are values obtained by the survey crew at the site using a separate vessel and an ADCP, unless they are shaded in blue, in which case they were inferred from other data. The BL values are those computed using the ISSDOTv2 method and program. The suspended sediment values in the tables, both SusBML and wash load, were obtained by taking suspended sediment samples in the same vicinity as the multibeam data and using a methodology described in the Water and sediment flux analysis section.

Bed load and % Bed load vs. flow

Bed load values are plotted in the graphs and are taken from the “BL” row of the related site table. In general, it can be seen that as flow increases, bed load values increase. These values are shown in the graphs as red squares. This increase of bed load transport with increase of flow will normally occur until flow conditions approach upper-regime sediment transport (Chien and Wan 1999; Graf 1984), which usually begins at Froude numbers above 0.6 to 0.8. In such conditions, the expectation may be to see a decrease in the bed load being transported in the dunes as flow increases beyond these values. This is because the scour volumes used in the method become smaller as more material goes into suspension. This is not to say that bed load is decreasing with flow but that the bedload measured by this method should be expected to drop off at some higher Froude number. This does not appear to have happened in any of the sites in this study, but it is important to consider in analyzing future data at high flows.

The blue diamonds are from the "%BL" row of each table and represent the percentage that bed load comprised of the Total bed-material-load. Wash load is not considered in the computation of the % BL. It has in the past been suggested that bed load comprises approximately 5% to 15% of the total bed-material-load and remains relatively constant. This is possibly a missreading of documents such as USDA (1965), but this is not shown in the data. Values varied with flow from highs near 45% to low values of approximately 10% for all sites for which dependable data were available for suspended bed-material-load, bed load, and flow. The sites with dependable data were Sites 1–4 and which were in the Mississippi River proper.

Bed load rating curve

The consistency of measurements from Sites 1 through 4 as shown in the tables, and plots above lead to the conclusion that a bed load rating curve could be made for the Mississippi River. A plot of all the data points from Sites 1 to 4 is shown in Figure 2.24. The R-squared value shows that the rating curve could be used with some confidence for this portion of the Mississippi River.

Figure 2.24. Bed load rating curve for Mississippi River at ORCC.

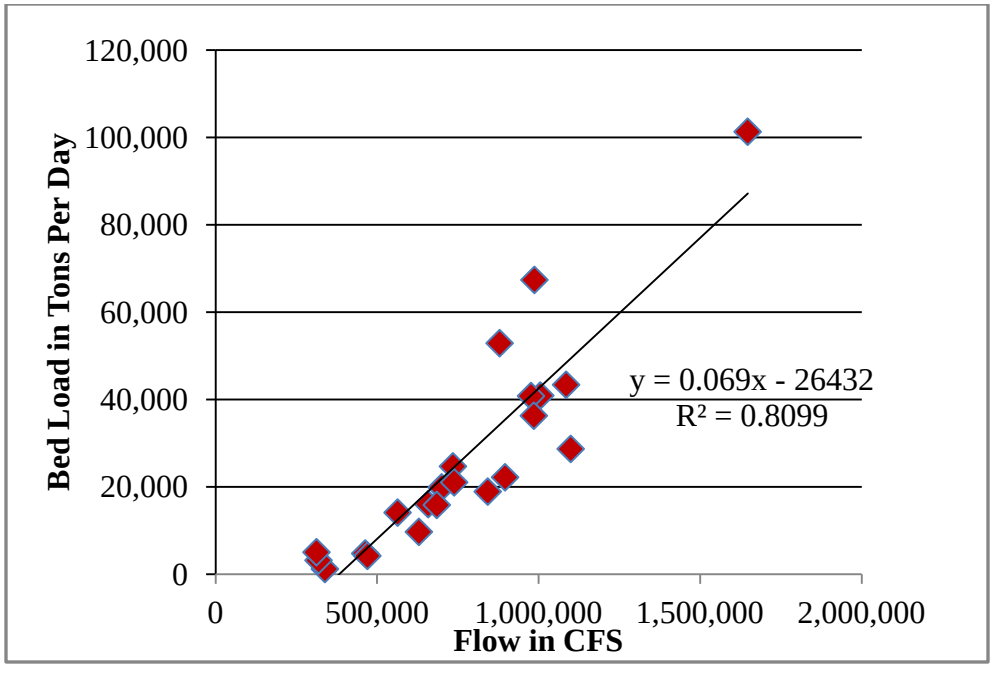

Moving bed load through the ORCC in the Outflow Channel (Site5).

Table 2.14 lists recorded flows through all the structures (auxiliary channel, low sill channel, and hydropower channel) for the dates and trips indicated.

Table 2.14. Flow through ORCC diversions and bed load at Site 5.

	Trip 1	Trip 2	Trip 3	Trip 4	Trip 5	Trip 6	Trip 7
	9-10Feb10	3-4Mar10	29-30 Apr10	1-3 Jul 10	8-Sep-10	9-Mar-11	23-May-11
Aux channel -Q (kcfs)	99	0	70	42	0	88	222
Low Sill-Q(kcfs)	0	0	0	88	28	92	294
**				3 days	1 day	9 days	80 days
Hydro -Q(kcfs)	164	123	85	132	102	138	144
Total Diversion Q (kcfs)	263	123	155	262	130	318	660
Bed Load (TPD)	2,421	1,394	1,385	24,545	541	10,380	41,507

(Note: The row ** in the table has values for the number of days that the low sill structure was open before the bed load measurement was taken.)

It also lists the sum of these flows, which is the total flow that would pass through the outflow channel and Site 5. This is significant because all bed load sediments that will move from the Mississippi River side to the Atchafalaya/Red River side of the complex must be moved through this site. After some initial measurements were made, including Trip 4 in July 2010, and bed load values computed, it appeared that when the Low Sill Structure was open, more bed load moved through Site 5. When more data were collected by the end of the study, it was possible to see if there were some relationship between the operation of the Low Sill Structure and bed load movement through the outflow channel. The result is best shown in Figure 2.25, in which bed load measured at Site 5 is plotted versus the flow through the outflow channel for two conditions. The first condition occurred when the Low Sill Structure was closed and is shown as the blue diamonds. The second condition occurred when the Low Sill Structure was open and is shown by the red squares. The increase of bed load values for conditions when the Low Sill Structure is open is clear both by the numerical values and the slopes of the lines.

Figure 2.25. Bed load vs. flow at Site 5 for open/closed condition of low sill structure.

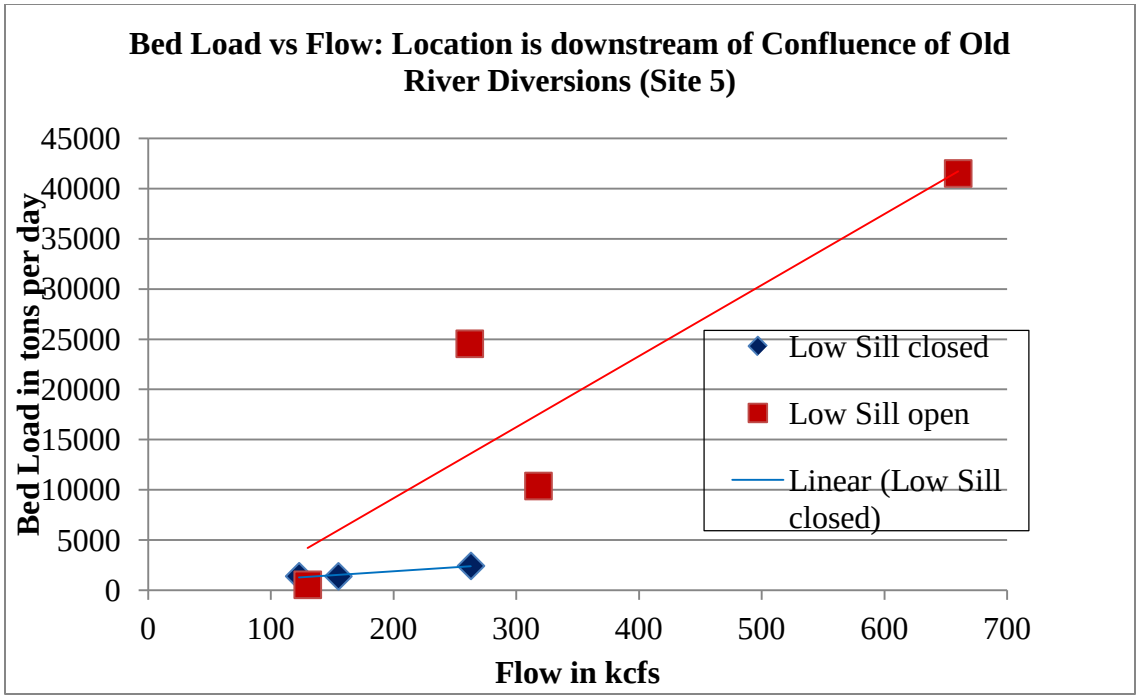

A second way to provide some confirmation of the influence of opening the low sill structure to help move bed load through the outflow channel is to consider the data collected during the record flood of May 2011 (Figure 2.26).

Figure 2.26 shows the computed bed load values (in orange) at sites 8, 10, 11, and 5. Unfortunately, no value is available for Site 9. However, Site 11 minus the value through the auxiliary structure should provide an estimate for the bed load moving through the low sill structure. Bed load at Site 11 minus the bed load at Site 8 is approximately 33,545 TPD. This is nearly five times the transport through the auxiliary structure. Note from Table 2.14, that during this time (Trip 7), the low sill structure only had approximately 1.3 times the flow going through it than the auxiliary structure but about five times the bed load, ignoring storage. At this time, the structures had been open for 80 days, which probably precludes the difference being due to any *slugs* of stored bed material being suddenly mobilized at the time of the measurements.

Figure 2.26. Computed bed load values (orange) in the diversions for the May 2011 flood.

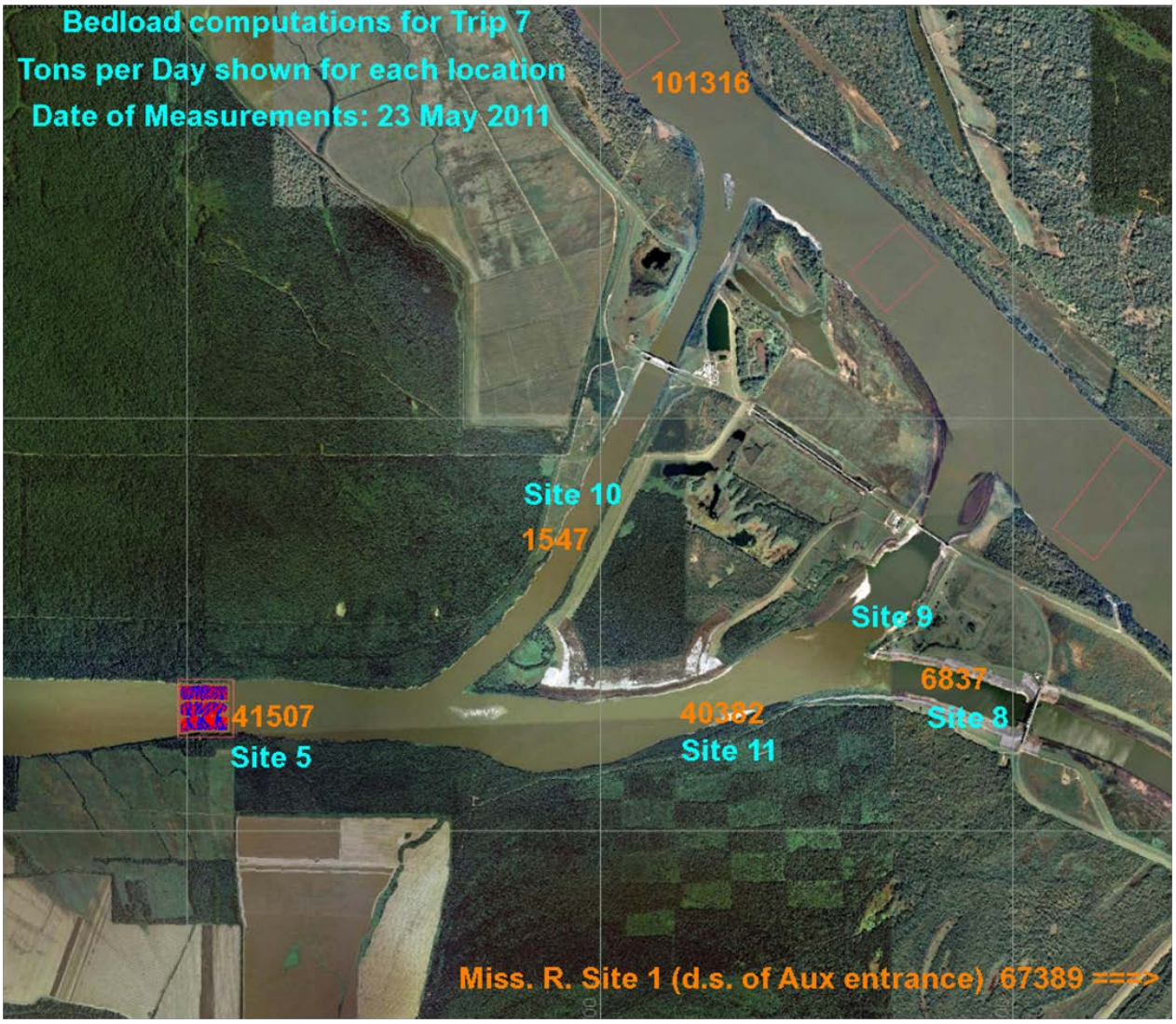

Finally, the values of bed load from Site 11 and Site 10 should reflect the value of material moving through Site 5. Site 11 (40382 TPD) plus Site 10 (1547 TPD) sums to a value of 41,929 TPD, which is approximately 1%–2% higher than the value measured moving through Site 5. Thus, there is a good justification to open the low sill structure in order to move bed material through or across the ORCC. Suspended sediment samples were not obtained at Site 5. Having concurrent suspended sediment information could complete the picture with regards to total movement of bed material through the ORCC.

The sum of this information and the preceding discussion regarding Table 2-14 and Figure 2.25 indicates that the operation of the structures can influence how much bed load moves across the outflow channel. It is

suggested that more measurements for various flows and operational configurations would not only provide better confirmation but also might lead to the development of an *operational schedule* versus bed load rating curve. To enhance the operation of the ORCC, development of a complete bed-material-load and flow measurement scheme, coordinated with structure operations, is recommended.

3 Geomorphic Assessment

Introduction

As part of the Old River Control Complex Sedimentation Investigation, a limited geomorphic assessment was conducted to identify long-term morphological changes on the Mississippi River that may influence the performance of the ORCC structures. The limited geomorphic assessment consisted of an update of selected specific gage records developed as part of the 1999 Lower Mississippi River Sediment Study and an analysis of channel geometry changes that have occurred in the study area since the construction of the low sill structure. The objective of the assessment was to describe the morphologic trends of the Mississippi River in the study area to provide insight into the development and interpretation of the numerical models.

Specific gage record analysis

A specific gage record indicates the trend with time of observed river stage at a given location for a specific discharge. The record provides an understanding of long-term channel stability and can be used to illustrate the rate and magnitude of aggradation and degradation in the river channel over time. However, it should be noted that changes in observed river stage for a given discharge may be a result of changes at the gage location other than bed elevation changes due to erosion or deposition. Care must be used when evaluating the primary causative factor of the specific gage record trends. Selected specific gage records developed as part of the 1999 Lower Mississippi River Sediment Study were updated from 1999 to 2010 for this study. Selected locations on the Mississippi River include Vicksburg, Natchez, Red River Landing, Bayou Sara, and Baton Rouge. Locations on the Atchafalaya River include Simmesport and Krotz Springs. Specific gage record development methods used in the 1999 study were duplicated in this study for consistency. Trends indicated by the specific gage records were evaluated from both a visual assessment and a statistical analysis. An overall trend was determined based on the combination of both visual and statistical trend results.

The specific gage records for the Mississippi River at Vicksburg, MS, and Natchez, MS, are shown in Figures 3.1 and 3.2. The specific gage record

covers the time period 1950–2010 for Vicksburg and 1936–2010 for Natchez. Specific discharges of 300,000 cfs, 700,000 cfs, and 1,000,000 cfs, were used for these stations as well as all Mississippi River stations. It should be noted that these discharges are all less than bank-full flows; thus, the specific gage record does address flood flow conditions. Based on a visual assessment, the specific gage records for both Vicksburg and Natchez indicate a similar trend of general aggradation over the entire time period. There are shorter time periods where the trends are highly variable and indicate periods of degradation, which illustrates the potential problem of basing trend observations on short time periods. An interesting observation for both stations can be seen at the time of the 1973 flood where a period of quick filling was followed by a time of general erosion. A similar period of aggradation followed by degradation can be observed beginning in the late 1980s/early 1990s and continuing into the late 1990s. In general, the overall trend for the entire period of record indicates slight aggradation in the range of 3 to 5 ft.

Figure 3.1. Specific gage record for the Mississippi River at Vicksburg, MS.

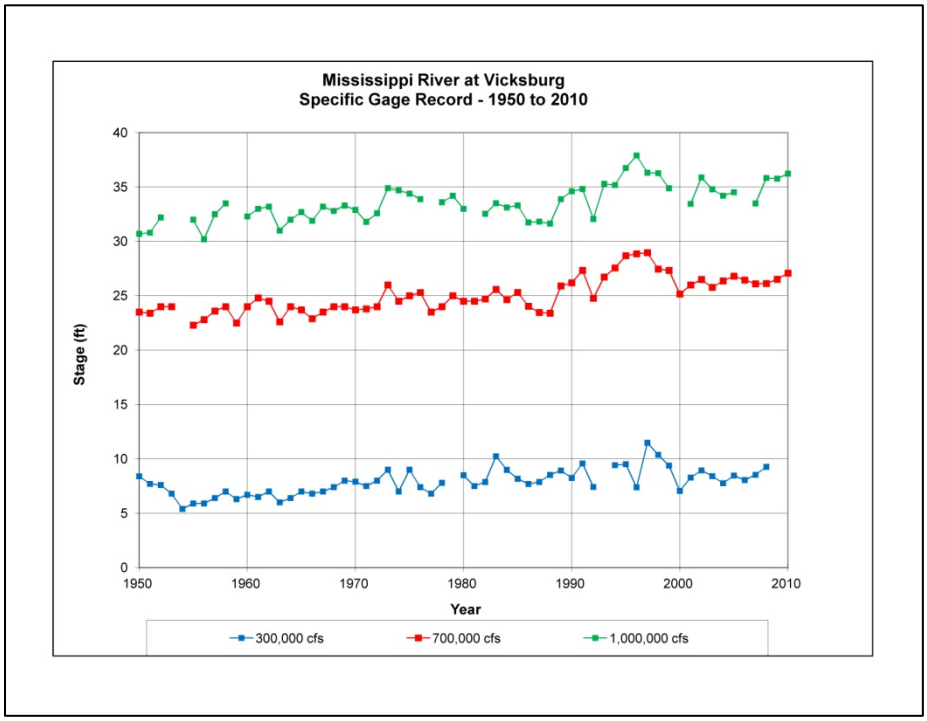

Figure 3.2. Specific gage record for the Mississippi River at Natchez, MS.

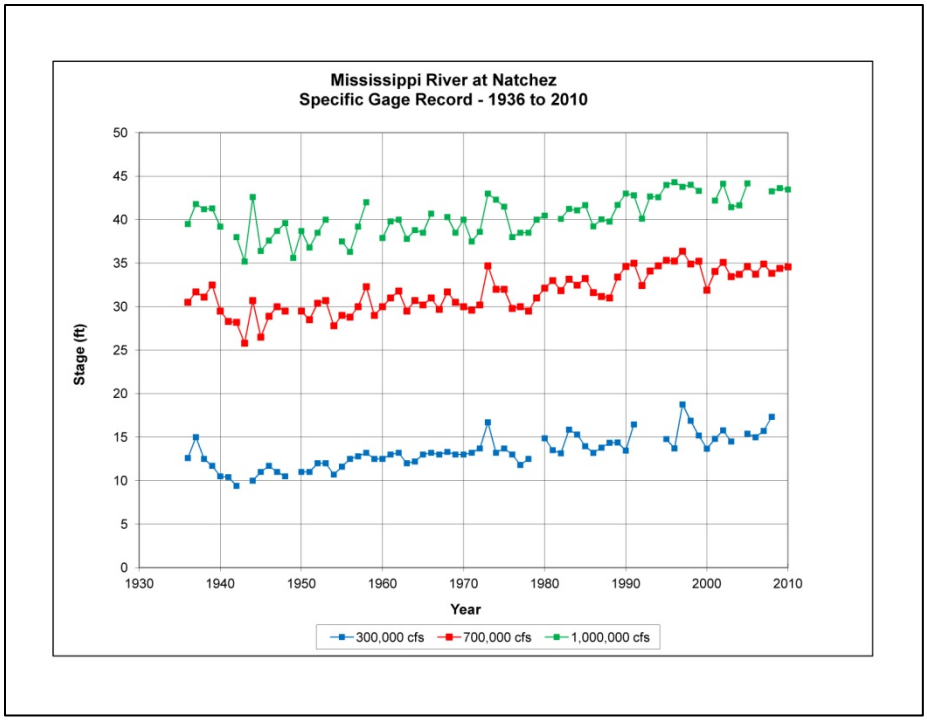

The specific gage record for the Mississippi River at Red River Landing, LA, is shown in Figure 3.3. As seen in the records at Vicksburg and Natchez, the overall trend at Red River Landing for the period of record 1935–2010 is general aggradation of approximately 5 to 7 ft. The records indicate a significant period of filling associated with the 1973 Mississippi River flood as did the Vicksburg and Natchez records; however, the amount of filling is much more pronounced at Red River Landing. The filling period beginning in the early 1990s observed in the Vicksburg and Natchez records is not as evident at Red River Landing, except slightly for the 700,000 cfs record. Notice that the record for the 1 million cfs discharge is much more discontinuous than the other records. This is due to the loss of discharge through the ORCC, resulting in fewer years that achieved a discharge of 1 million cfs at Red River Landing.

Figure 3.3. Specific gage record for the Mississippi River at Red River Landing, LA.

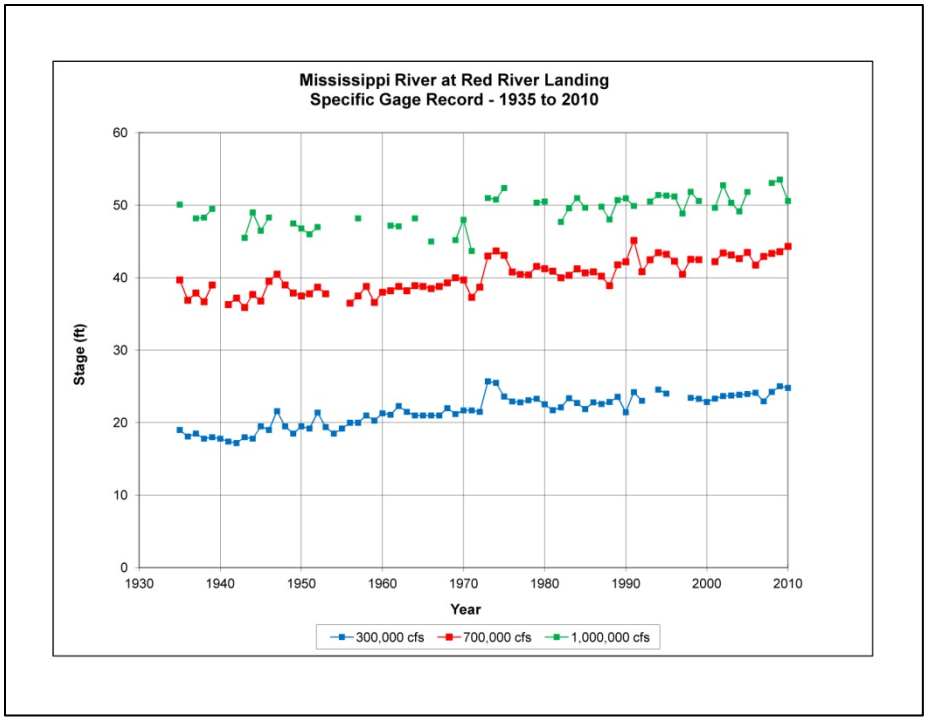

The specific gage record for the Mississippi River at Bayou Sara, LA, for the period of record 1951–2010 is shown in Figure 3.4. Visual assessment of this record indicates several distinct and interesting trends and discontinuities. Observation of the records from the early 1950s to the early 1960s indicates a fairly stable gage, although with year-to-year variation. In the early to mid-1960s, there is a distinct and significant jump in the record, indicating rapid aggradation in the channel. This discontinuity correlates with the beginning of operation of the low sill structure at ORCC. From the mid-1960s to the mid-1970s, the records basically indicate a stable channel. Then, in response to the 1973 Mississippi River flood, the records indicate a period of rapid filling followed by an adjustment period of general degradation. From the early 1980s to 2010, the records indicate a general stability of the channel with no discernible trends. The overall results of the shifts in the gage record are an increase in stage of 5 to 10 ft for the given discharges. For the discharge of 300,000 cfs, river stages are approximately 5 ft higher in 2010 than in the early 1950s. For the discharges of 700,000 cfs and 1,000,000 cfs, the river stages are approximately 10 ft higher in 2010 than in the early 1950s. However, most all of this shift occurred prior to the early 1970s, and from that time to the present, river stages have been very stable.

Figure 3.4. Specific gage record for the Mississippi River at Bayou Sara, LA.

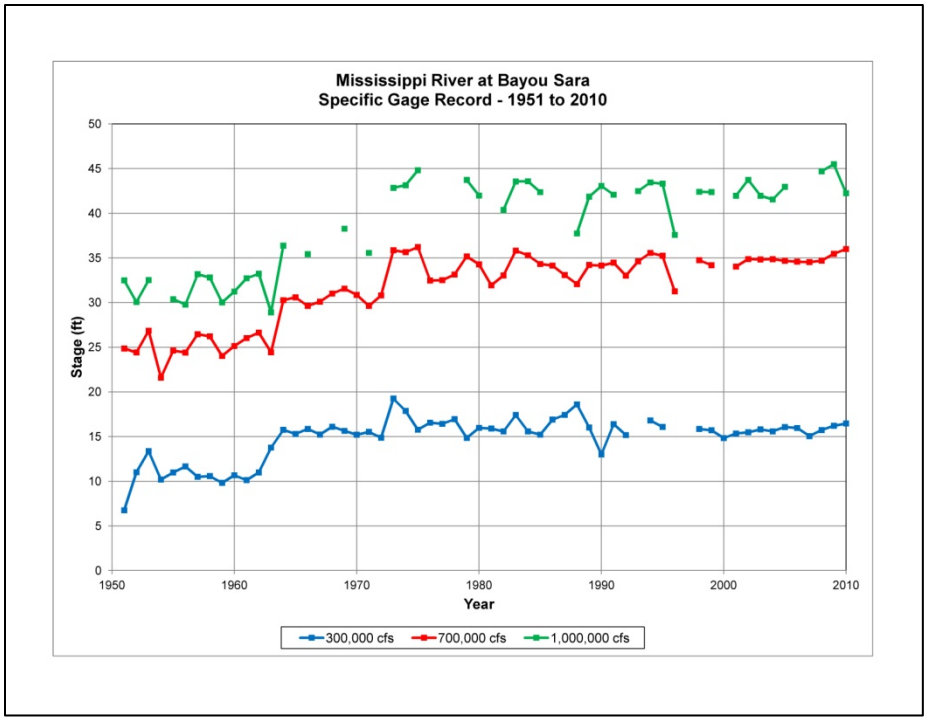

Figure 3.5 shows the specific gage record for the Mississippi River at Baton Rouge, LA. for the period of record 1963–2010. Similar trends and discontinuities are observed with the Baton Rouge specific gage as were observed with the Bayou Sara specific gage in the early 1960s through the mid-1970s. Although the rapid aggradation in the mid-1960s appears to be similar to Bayou Sara, the period of record is not adequate to declare so with any certainty. The response to the Mississippi River flood of 1973 is very similar, and since that time, the specific gage generally indicates a very stable river stage for all three specific discharges.

The specific gage records for the Atchafalaya River at Simmesport, LA, and Krotz Springs, LA, are shown in Figures 3.6 and 3.7. The period of record for the Simmesport specific gage record is 1943–2010, and the period of record for the Krotz Springs specific gage record is 1943–2010. Two specific discharges of 200,000 cfs and 400,000 cfs were used for development of both specific gage records. Both the Simmesport and Krotz Springs specific gage records indicate similar trends. The time period prior to the early 1980s indicates a general trend of significant degradation. Overall, the trends are fairly consistent and result in a general degradation of approximately 15 ft over the period for Simmesport and approximately 12 to 14 ft for Krotz Springs. This degradation trend ended in the early 1980s, and subsequent to that time, there has been no visually discernible trend. The

specific gage for Simmesport is stable for both specific discharges, as is the specific gage for the 400,000 cfs discharge for Krotz Springs. The 200,000 cfs discharge record for Krotz Springs appears to continue a minor degradation trend subsequent to the early 1980s.

Figure 3.5. Specific gage record for the Mississippi River at Baton Rouge, LA.

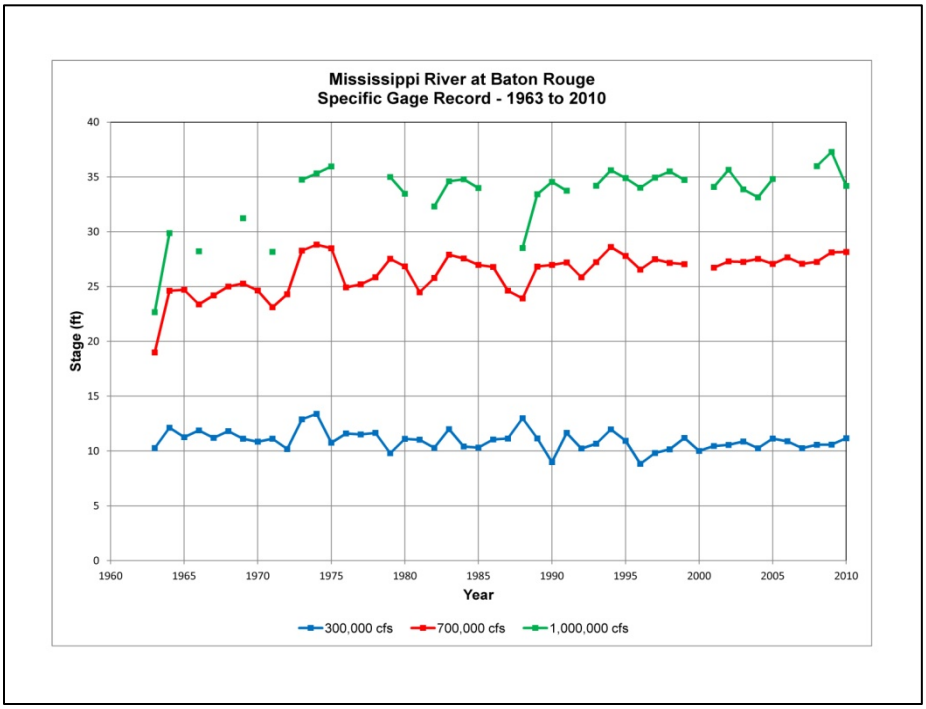

Figure 3.6. Specific gage record for the Atchafalaya River at Simmesport, LA.

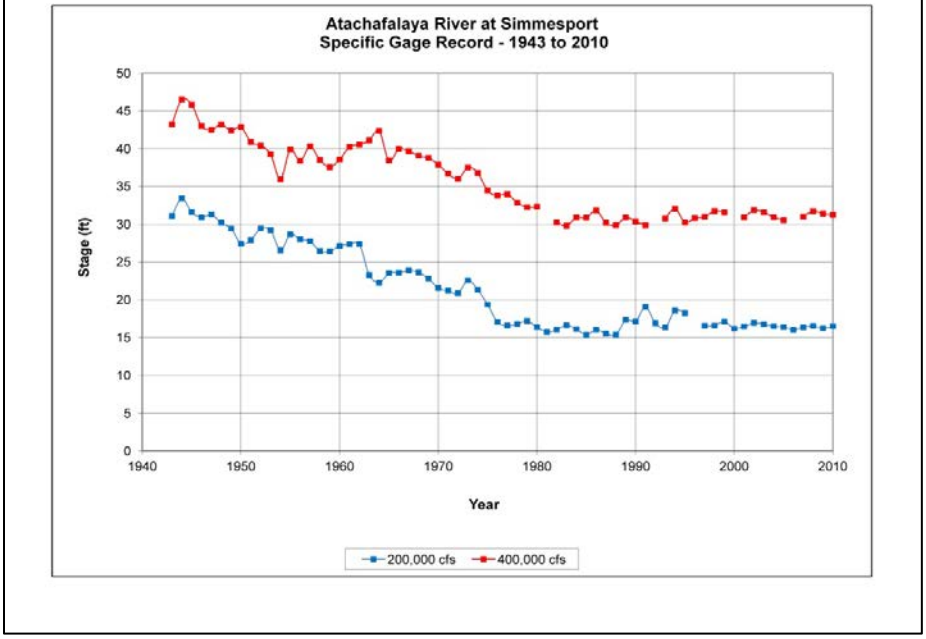

Figure 3.7. Specific gage record for the Atchafalaya River at Krotz Springs, LA.

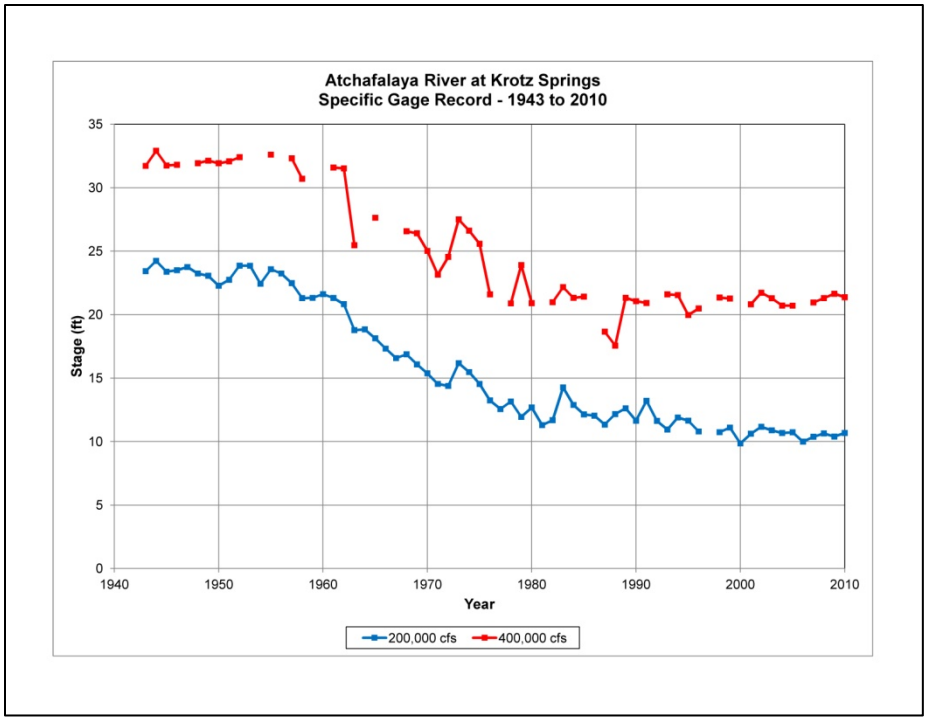

In summary, the visual inspection of the specific gage records for the Mississippi River at Vicksburg, Natchez, and Baton Rouge indicate an overall mild trend of aggradation for the entire periods of record. Discontinuities at the time of the 1973 Mississippi River flood are similar in all three records, indicating aggradation in immediate response to the flood, followed by a period of adjustment by degradation over the following several years. The specific gage records for the Mississippi River at Bayou Sara and Baton Rouge indicate an aggradation response corresponding to the initial operation of the low sill structure at ORCC and the 1973 flood. However, these records indicate a very stable river for the time period following the 1973 flood to the present. In the Atchafalaya River system, a consistent degradation trend is noted for both Simmesport and Krotz Springs from the early 1940s to approximately 1980. This trend of degradation has resulted in approximately 10 to 15 ft of river bed lowering in the Atchafalaya River. A distinct shift in trend occurs in the early 1980s, and from that point to the present, the specific gage record indicates very little change and a generally stable river.

Although visual inspection of specific gage records usually provides an acceptable assessment for very distinct trends, there are often instances when the trends are not as obvious. For this reason, a statistical analysis of the record was conducted to determine if a valid trend does or does not

exist. In order to analyze the observed visual trends in this study, the specific gage record was linearly regressed, and the coefficient of determination (R^2) and P-value were calculated. The coefficient of determination expresses the proportion of the variance of Y (stage) that can be explained by the variations in X (time), and its range is 0 to 1. The P-value is used to determine if a trend defined by the regression slope is or is not real. The P-value describes the probability that the relationship between the variables found in the sample is a chance occurrence. The P-value criteria used as part of the 1999 Lower Mississippi River Sediment Study were used to accept or reject the null hypothesis that the regression line slope was not significantly different from zero. If the P-value was less that 0.01, the null hypothesis is ejected, and the regression line slope is classified as being significantly different from zero: a trend does exist. If the P-value is greater than 0.10, the null hypothesis is accepted, and the regression line slope is not significantly different from zero: there is no significant trend. If the P-value falls within the range of 0.01 to 0.10, the results are inconclusive. Inconclusive results are generally interpreted that no statistically significant trend of aggradation or degradation exists and that the reach is generally stable.

For the statistical analysis, linear regressions for two time periods were used. For the Mississippi River stations, regressions were computed for the entire periods of record and the post-1973 time period. These periods were selected because of the observed changes that were evident by the discontinuities in the specific gage records at the time of the 1973 flood. For the Atchafalaya River stations, regressions were computed for the pre-1980 and post-1980 time periods. These periods were selected based on the visibly obvious shift in trends that occurred in approximately 1980. The results of the specific gage record statistical analysis are presented in Table 3.1. In addition to the statistical trend results, an overall trend is presented based on the visually observed trend as well as the statistical trend.

The statistical analysis of the Mississippi River specific gage records for the period of record regressions indicates a statistically significant increasing, or aggradation, trend for all specific discharges, except for 300,000 cfs at Baton Rouge, which was inconclusive. The statistical analysis of the post-1973 regressions for Vicksburg indicates a not statistically significant result and an inconclusive result for the 300,000 cfs and 1,000,000 cfs discharges, respectively, and a statistically significant increasing trend for

Table 3.1. Statistical analysis results for specific gage records for Mississippi River and Atchafalaya River.

Station	Discharge (kcfs)	Trends During Time Period					
		Period of Record[a]			1973 - 2010		
		Statistical Trend[b]	R^2	Overall Trend[c]	Statistical Trend[b]	R^2	Overall Trend[c]
Miss. River at Vicksburg, MS (1950-2010)	300	S, (+)	0.41	IT	NS, (+)	0.06	NT
	700	S, (+)	0.59	IT	S, (+)	0.32	IT
	1,000	S, (+)	0.50	IT	I, (+)	0.18	NT
Miss. River at Natchez, MS (1936-2010)	300	S, (+)	0.60	IT	S, (+)	0.24	IT
	700	S, (+)	0.61	IT	S, (+)	0.40	IT
	1,000	S, (+)	0.43	IT	S, (+)	0.41	IT
Miss. River at Red River Landing, LA (1935-2010)	300	S, (+)	0.77	IT	NS, (+)	0.06	NT
	700	S, (+)	0.69	IT	S, (+)	0.22	IT
	1,000	S, (+)	0.39	IT	NS, (+)	0.09	NT
Miss. River at Bayou Sara, LA (1951-2010)	300	S, (+)	0.37	IT	I, (-)	0.06	NT
	700	S, (+)	0.68	IT	NS, (+)	0.03	NT
	1,000	S, (+)	0.69	IT	NS, (+)	0.001	NT
Miss. River at Baton Rouge, LA (1963-2010)	300	I, (-)	0.13	NT	I, (-)	0.15	NT
	700	S, (+)	0.37	IT	NS, (+)	0.06	NT
	1,000	S, (+)	0.38	IT	NS, (+)	0.03	NT
Atch. River at Simmsport, LA (1943-2010)	200	S, (-)	0.93	DT	NS, (+)	0.01	NT
	400	S, (-)	0.74	DT	I, (+)	0.24	NT
Atch. River at Krotz Springs, LA (1943-2010)	200	S, (-)	0.92	DT	S, (-)	0.55	DT
	400	S, (-)	0.80	DT	NS, (+)	0.04	NT

[a] For Atchafalaya River stations, table entries are for Pre-1973 Period instead of Period of Record.

[b] Trend indicated by statistical analysis:
S = statistically significant
NS = not statistically significant
I = statistically inconclusive
(+) = increasing slope of linear regression line
(-) = decreasing slope of linear regression line

[c] Overall trend based on statistical analysis and visual observation of data:
DT = Decreasing stage trend
IT = Increasing stage trend
NT = No stage trend

the 700,000 cfs discharge. For the Natchez gage, all three discharges indicated statistically significant increasing trends. For the Red River Landing gage, not statistically significant results were indicated for the 300,000 cfs and 1,000,000 cfs discharges, while a statistically significant increasing trend was observed for the 700,000 cfs discharge. For both the Bayou Sara and Baton Rouge gages, inconclusive results were indicated for

the 300,000 cfs discharge, and nonsignificant results were observed for both the 700,000 cfs and 1,000,000 cfs discharges.

The statistical analysis of the Atchafalaya River specific gage records for the pre-1980 regressions indicates a statistically significant decreasing, or degradation, trend for all specific discharges for both Simmesport and Krotz Springs. For the post-1980 time period regressions, a statistically nonsignificant trend was observed for the 200,000 cfs discharge at Simmesport, and an inconclusive result was determined for the 400,000 cfs discharge. For the Krotz Springs gage, a statistically significant degreasing trend was observed for the 200,000 cfs discharge, where a no-significant-result was observed for the 400,000 cfs discharge.

The overall trend assessments for the Mississippi River specific gage records for the entire periods of record indicate a general increasing, or aggradation, trend over time. Approximately 3 to 5 ft of aggradation is noted for Vicksburg (1950–2010) and Natchez (1936–2010), and approximately 5 to 7 ft of aggradation for Red River Landing (1935–2010), most of which has occurred fairly uniformly over the entire period of record. As much as 5 to 10 ft of stage increase was noted from the specific gage records for Bayou Sara (1951–2010) and Baton Rouge (1963–2010), although almost all of this occurred prior to 1973. Also, distinct discontinuities indicating rapid increase that corresponded to the initial operation of the ORCC low sill structure and the 1973 Mississippi River flood were noted for both Bayou Sara and Baton Rouge. Similar responses to the 1973 flood were observed for all Mississippi River stations, which suggest that significant river channel response and subsequent adjustment occurred during this large flood. For the post-1973 flood time period, an overall increasing trend was determined for Natchez for all specific discharges, but only one of three discharges for Vicksburg and Red River Landing indicate an increasing trend. The specific gage records for the other discharges indicate no trends for Vicksburg and Red River Landing; thus, there are essentially no significant trends during this time period. For Bayou Sara and Baton Rouge, overall trends for the post-1973 flood periods indicate no significant trends and a relatively stable reach.

For the Atchafalaya River gages for the pre-1980 time period, an overall decreasing, or degradation, trend was observed for both Simmesport (calculated from 1943–1980) and Krotz Springs (calculated from 1943–1980). As much as 15 ft of base level lowering through degradation

occurred in these reaches during this time period, with the changes occurring fairly uniformly with time. However, the specific gage records indicate a discernible shift occurred in the early 1980s, with a transition to very stable reaches with no significant trend observed from that time to 2010.

Geometric data analysis

An analysis of the long-term channel geometry changes on the Mississippi River was conducted from historical hydrographic survey data. Surveys included the comprehensive hydrographic surveys of 1975, 1983, 1992, and 2004. These surveys provided the widest area of coverage for the study area but are limited to survey transects on approximate 1000 ft spacing. Multibeam bathymetric surveys conducted in 2004, 2006, 2008, and 2010 were also used. These surveys provided very dense data point coverage that yielded a high-definition description of the channel bed but were limited in spatial coverage. All survey data were imported into GIS, and Triangulated Irregular Network (TIN) surfaces were developed. Cross sections were extracted from each survey TIN and compared for changes. Contour maps were generated for each survey. These analyses were performed for the Mississippi River channel only and did not address the Atchafalaya River or the ORCC outflow channels.

Comparative cross sections for each survey were evaluated in the ORCC reach of the Mississippi River at the locations shown in Figure 3.8. Not all multibeam surveys had complete coverage for all cross-section locations, but sufficient data were available to have comparisons from at least 1975 to 2008 at all cross sections. All cross section plots are oriented looking downstream from left bank to right bank. It should be noted that there is variability in the survey data due to the dynamic nature of the lower Mississippi River channel, and quantitative changes are often difficult to ascertain. However, qualitative assessment of trends can generally be achieved.

Comparative cross section data for the section located upstream of the hydropower channel at approximate RM 318.5 is shown in Figure 3.9. The cross section is located in the bend upstream of the hydropower channel, as can clearly be seen from the shape of the channel. In general, this section has been fairly consistent in shape from 1975 to 2008. The overall depth of the channel has decreased slightly by approximately 6 to 7 ft. Depths are consistent from 1975 to 1983 and then decrease through 1992 to 2004.

Depths are consistent from 2004 to 2008. The sloping face of the channel bed on the inside of the bend has changed the most, with approximately 15 to 20 ft of filling occurring from 1975 to 2008. Although the cross-sectional area was not computed, it is clear from visual inspection that the channel section is much smaller in 2008 than in 1975.

The cross sections plots for the section located at the hydropower channel at approximate RM316.2 are shown in Figure 3.10. Again, a general decrease in overall channel depth can be seen from 1975 to 2008. The approximately 15 ft of filling occurred between 1975 and 1983 and from 1992 to 2004. Depths from 2004 to 2008 have been fairly consistent. No major change in channel shape is noted.

Figure 3.8. Locations for comparative cross sections.

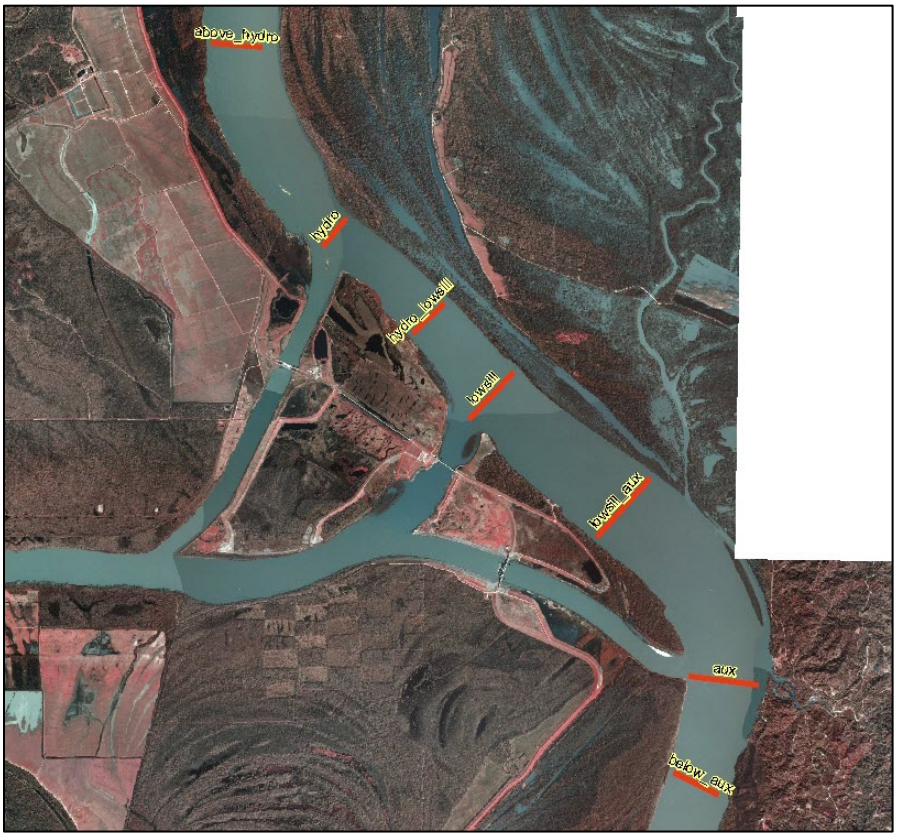

Figure 3.9. Comparative cross sections upstream of hydropower channel (RM 318.5).

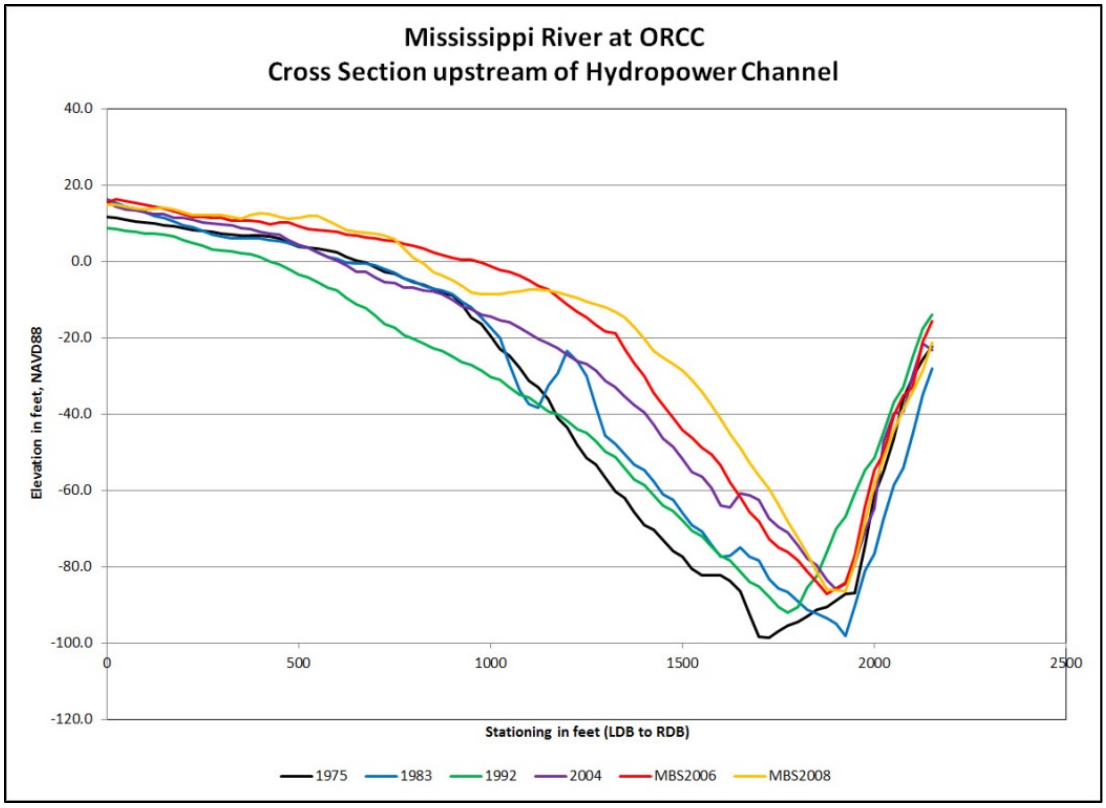

Figure 3.10. Comparative cross sections at hydropower channel (RM 316.2).

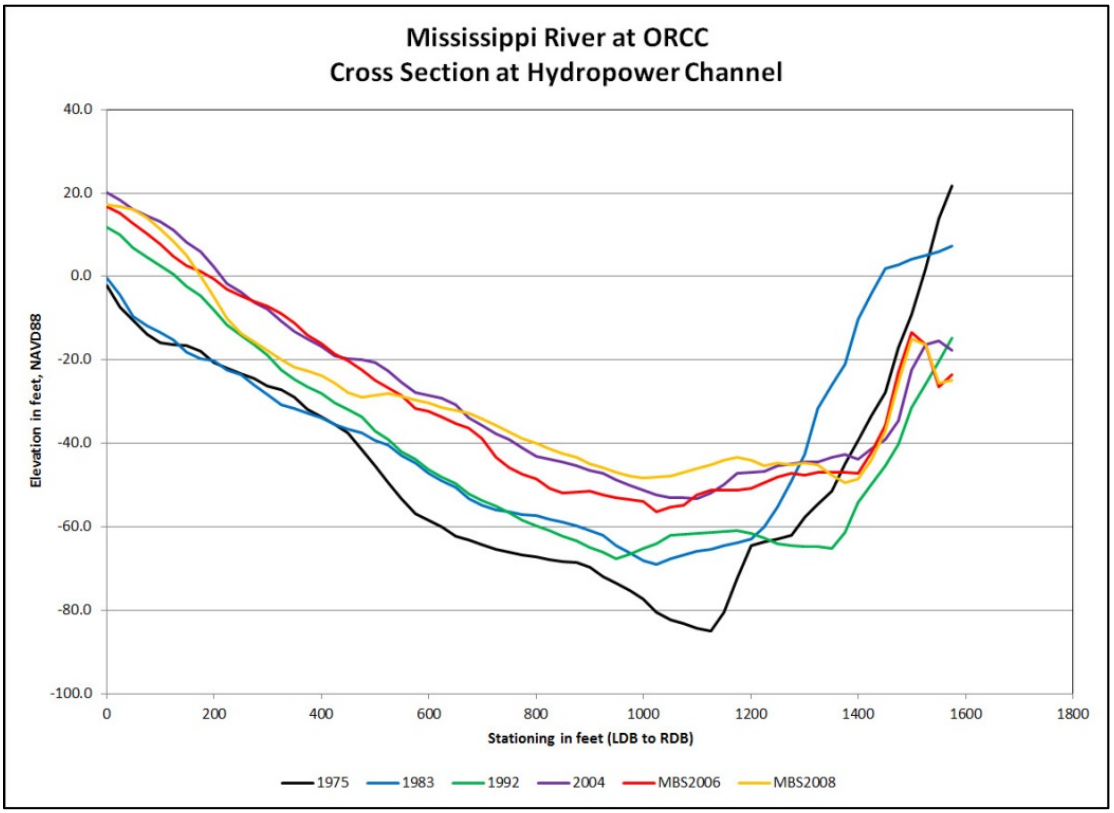

Figure 3.11 shows the comparative cross section plots for the section midway between the hydropower channel and the low sill channel at approximate RM 315.5. The comparative cross section plots indicate significant filling of the channel, with a decrease in overall channel depth of approximately 40 to 45 ft between 1975 and 2008. Filling occurred at a fairly constant rate between 1975 and 1992, with approximately 12 to 15 ft of depth lost. However, the rate of filling significantly increased from 1992 to 2004, with approximately 25 to 30 ft of filling occurring during this time. The elevation of the channel bed between 2004 and 2008 is fairly consistent, although fluctuations of 4 to 6 ft are observed. The shape of this channel at this location is indicative of a section in a crossing, with the channel bed very uniform and somewhat level.

Figure 3.11. Comparative cross sections midway between hydropower channel and low sill channel (RM 315.5).

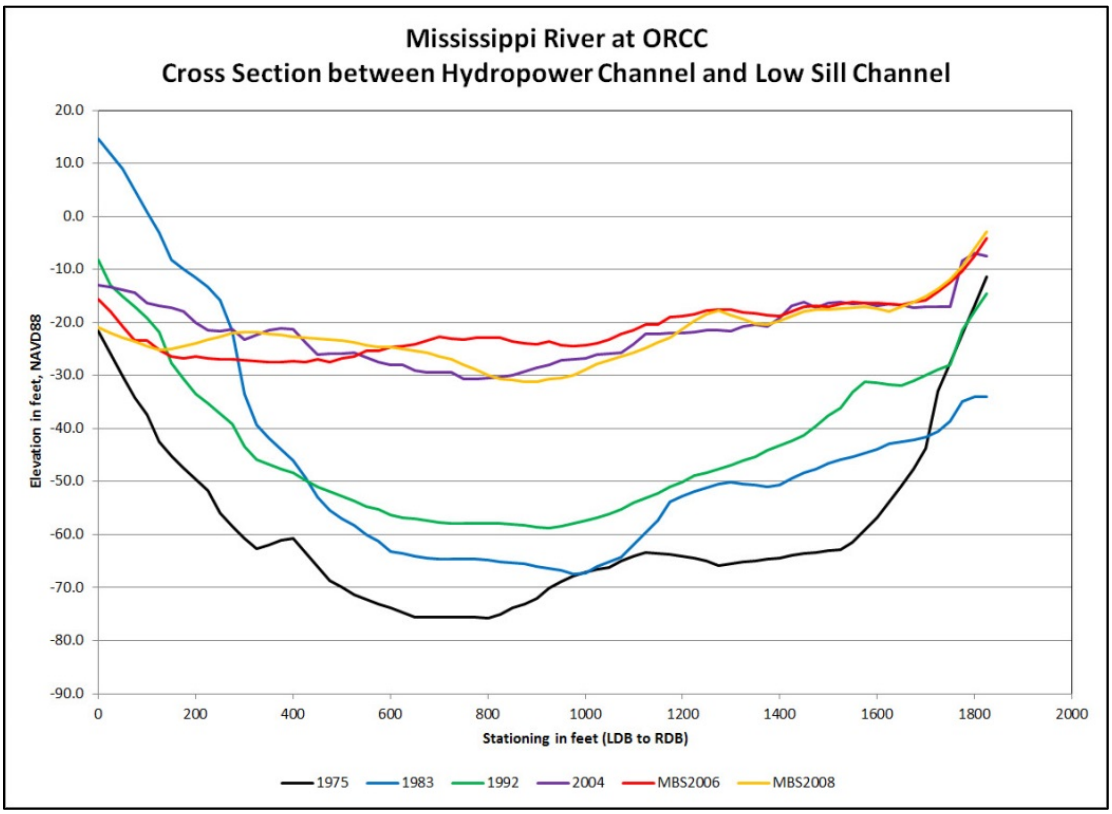

The comparative cross section plots for the section located at the low sill channel at approximate RM 314.5 are shown in Figure 3.12. The depth of the channel thalweg at this location varied between 1975 and 1992 by as much as 16 ft, with the deepest channel occurring in 1983. From 2004 to 2010, the channel shape has been fairly consistent, with an overall depth reduction of approximately 16 to 18 ft from 1983. A noteworthy

observation is the reduction in channel depth in the right side of the section in the area immediately adjacent to the entrance of the low sill inlet channel, where approximately 10 to 20 ft or more of filling has occurred. Loss of depth of this magnitude could have significant adverse impacts on the operability of the low sill structure. Another interesting observation is the apparent shift of the channel thalweg toward the left descending (east) bank that occurred between 1992 and 2004.

Figure 3.12. Comparative cross sections at low sill channel (RM 314.5).

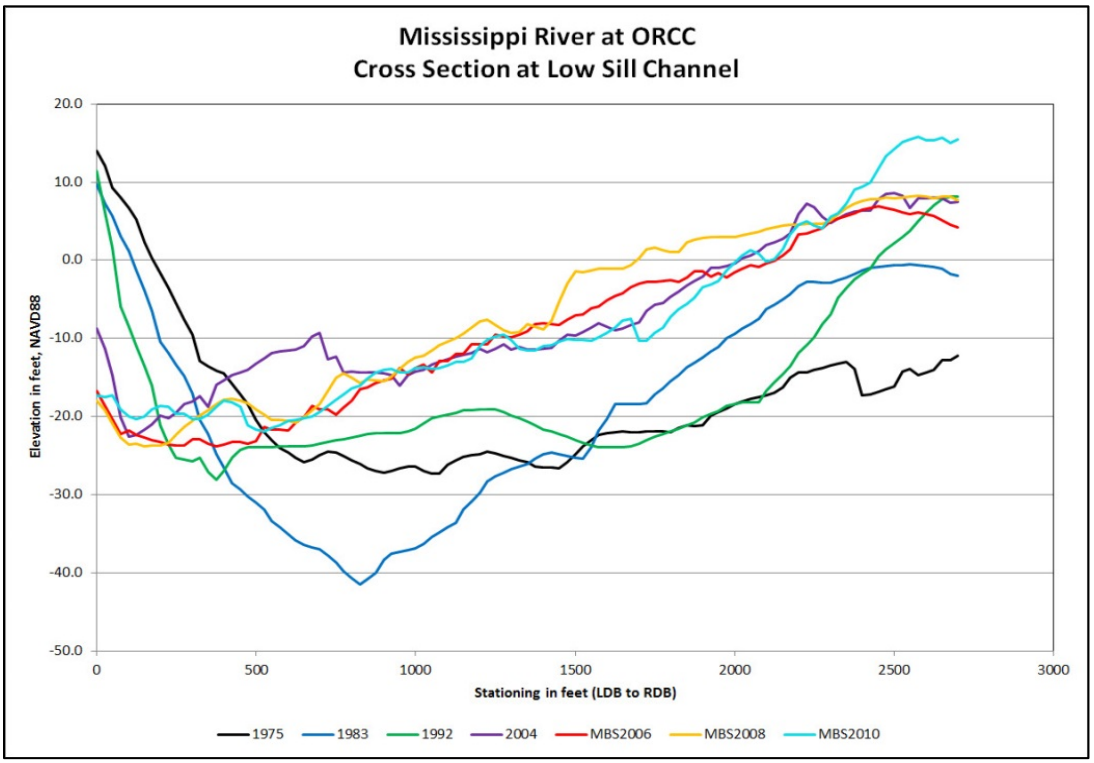

Figure 3.13 shows the comparative cross section plots for the location midway between the low sill channel and the auxiliary channel at approximate RM 313. An overall reduction in channel depth and a change in channel shape are observed at this location. An overall depth reduction of approximately 10 to 12 ft occurred between 1975 and 1992, and an additional 8 ft of reduction took place between 1992 and 2006. In 1975, the shape of the channel showed the thalweg located along the right descending (west) bank and a bar along the left portion of the section, forming a configuration typically found in a bend. This shape was generally still maintained in 1992, but from that point shifted to a shallower and uniform elevation cross section. The deep portion of the section in 2010 is still located along the right descending bank, but the channel bed elevation across the entire section is fairly uniform.

Figure 3.13. Comparative cross sections midway between low sill channel and auxiliary channel (RM 313.0)

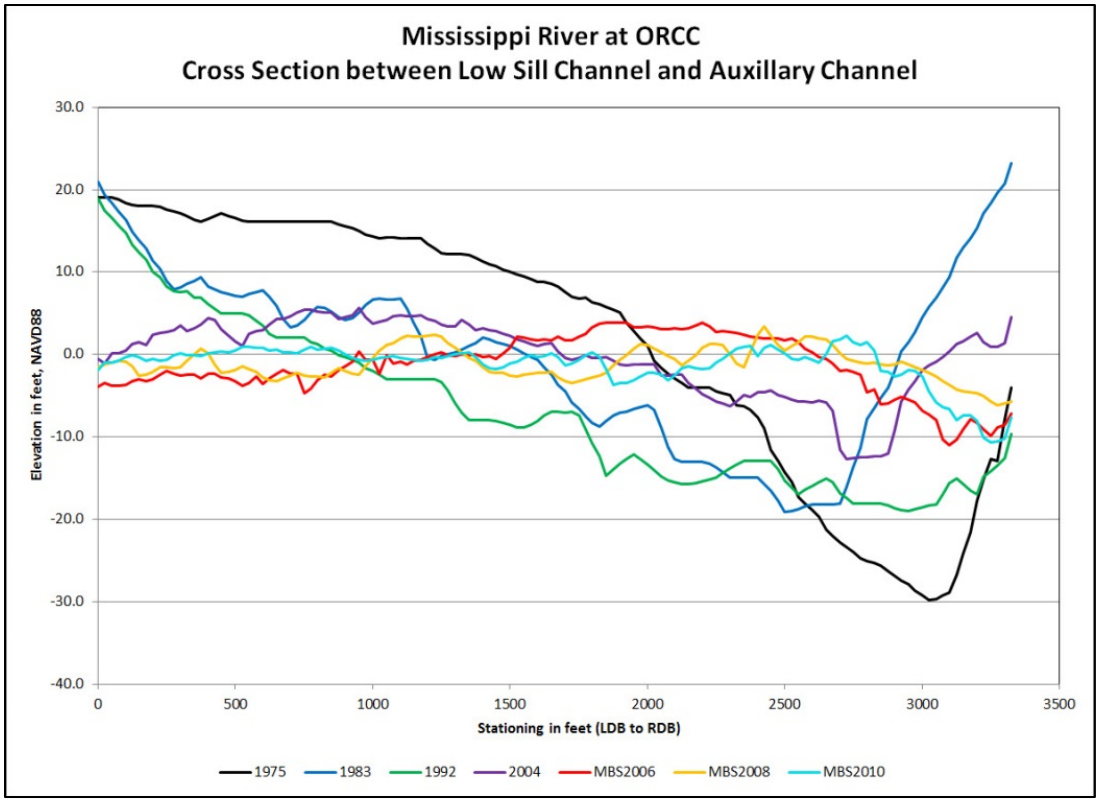

Figure 3.14 shows the comparative cross section plots for the section located at the auxiliary channel at approximate RM 311.5. A reduction in overall channel depth is noted here along with a change in channel cross-section shape. A reduction in depth of approximately 20 ft occurred between 1975 and 1983, followed by a scouring of approximately 16 ft between 1983 and 1992. From 1992 to 2010, channel filling resulted in a depth reduction of approximately 20 ft. Overall depth reduction from 1975 to 2010 is approximately 24 to 26 ft. The plot also indicates significant filling in the middle portion of the section of approximately 20 ft from 1992 to 2004. This deposition seems to correlate with the development of the downstream end of a middle bar deposit between the low sill channel and the auxiliary channel. There is a fair degree of variation in the maximum elevation of the *hump* of this deposit, indicating that the middle bar may erode and reform during high water events. A shift in the channel thalweg toward the left descending bank also occurs between the 1992 to 2004 timeframe.

Figure 3.14. Comparative cross sections at auxiliary channel (RM 311.5).

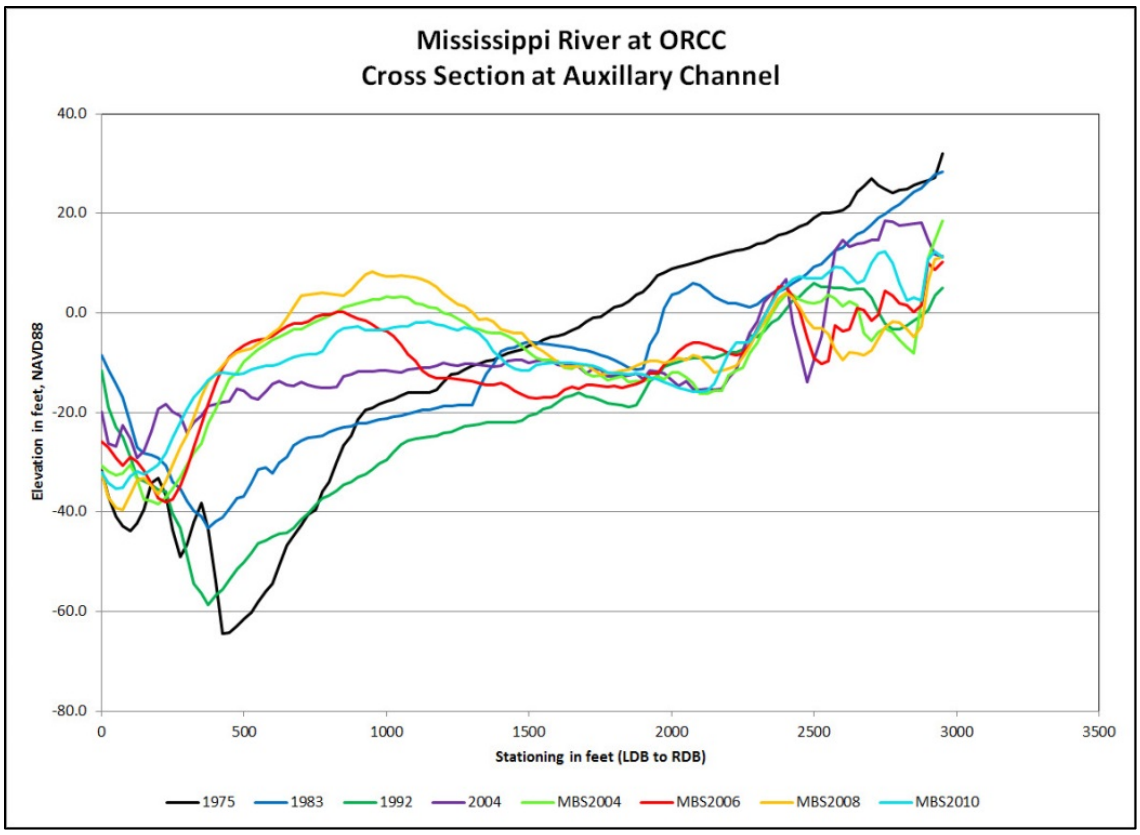

The comparative cross section plots for the section located just downstream of the auxiliary channel at approximate RM 310.5 is shown in Figure 3.15. A reduction in overall channel depth and a slight shift in the channel thalweg are noted at this location. A reduction in depth of approximately 22 to 25 ft occurred between 1975 and 2004, with a slight regain in depth of approximately 6 ft occurring between 2004 and 2008. In addition, there is a very slight shift in the channel thalweg toward the left descending bank over the time period of 1975 to 2008. The channel shape is generally the same over the time period, with a slight flattening of the point bar slope observed.

The assessment of comparative cross sections within the immediate reach of the ORCC indicates that there has been a general deposition trend of the river channel in this reach. Although some channel depth reduction occurred between 1975 and 1992, the comparative cross sections indicate that the majority of deposition takes place between 1992 and 2004, particularly immediately downstream of the hydropower channel. The most notable changes were observed between the hydropower channel and the low sill structure channel, where approximately 25 to 30 ft of filling occurred between 1992 and 2008. Deposition in the range of 10 to 20 ft was

also observed for the river channel in the vicinity of the low sill channel entrance, which could be problematic for reliable operation of the low sill structure. In addition to the reduction in channel depth, a shift in the channel thalweg location toward the left descending bank is observed in the vicinity of the low sill channel and the auxiliary channel beginning with the 1992 survey. This shift is most likely a result of less frequent use of the low sill structure for normal ORCC operations after the commencement of auxiliary structure and hydropower plant operations.

Figure 3.15. Comparative cross sections downstream of auxiliary channel (RM 310.5)

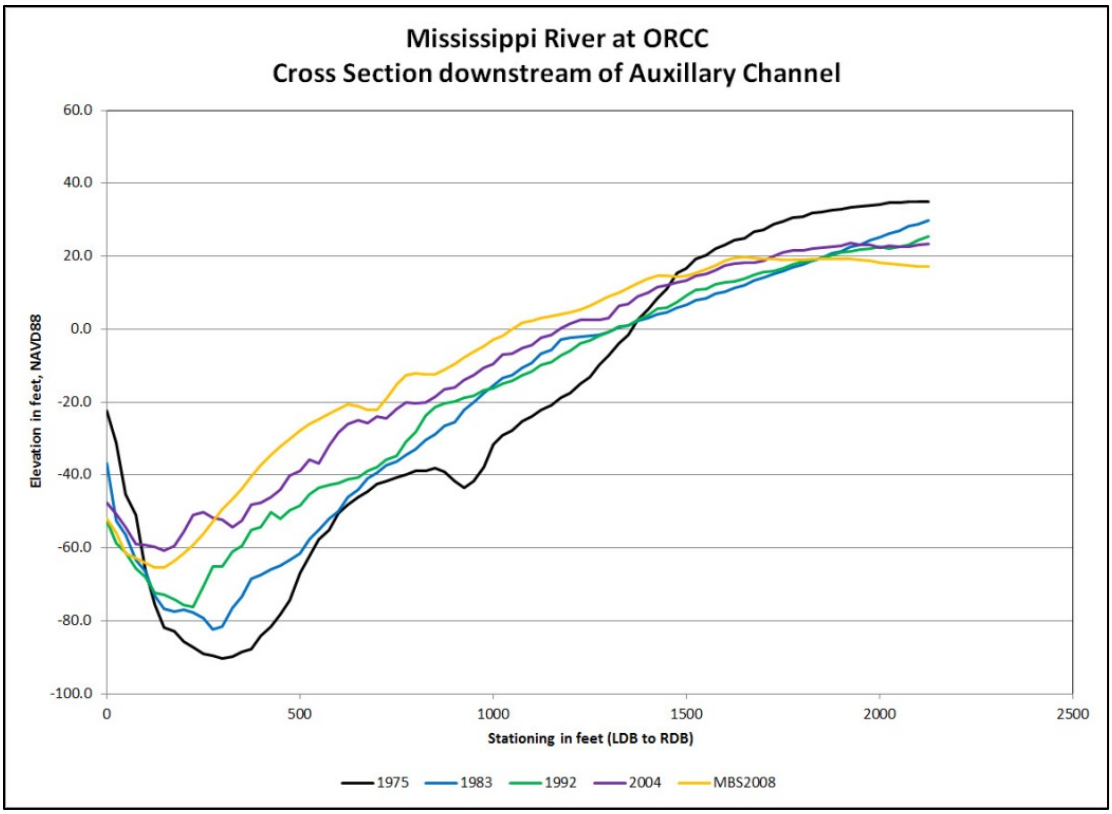

Channel bed elevation contour plots were generated from the comprehensive hydrographic surveys and the multibeam surveys, although the multibeam surveys are limited in spatial coverage. The contour maps were used to evaluate local channel pattern changes that have occurred in the immediate reach of the ORCC. This evaluation is based primarily on the contour maps of the comprehensive hydrographic surveys, as they provide complete coverage of the study reach for all years. The contour maps from the multibeam surveys were used to evaluate channel pattern changes in the limited areas where consistent coverage was available.

The contour map for the 1975 comprehensive hydrographic survey is shown in Figure 3.16. The map indicates a very deep thalweg channel hugging the right descending bank upstream of the present-day hydropower channel. This deep channel extends all the way to the low sill channel entrance. Downstream of the low sill channel, the thalweg channel is less deep due to the loss of discharge through the low sill structure and a wider channel width, and the thalweg basically continues along the right descending bank. Near the present-day location of the auxiliary channel, the thalweg channel crosses over to the left descending bank, where the channel deepens and the channel width narrows. A large channel bar near the left descending bank is present in the reach between the low sill channel and the current auxiliary channel.

Figure 3.16. Contour map for the 1975 comprehensive hydrographic survey.

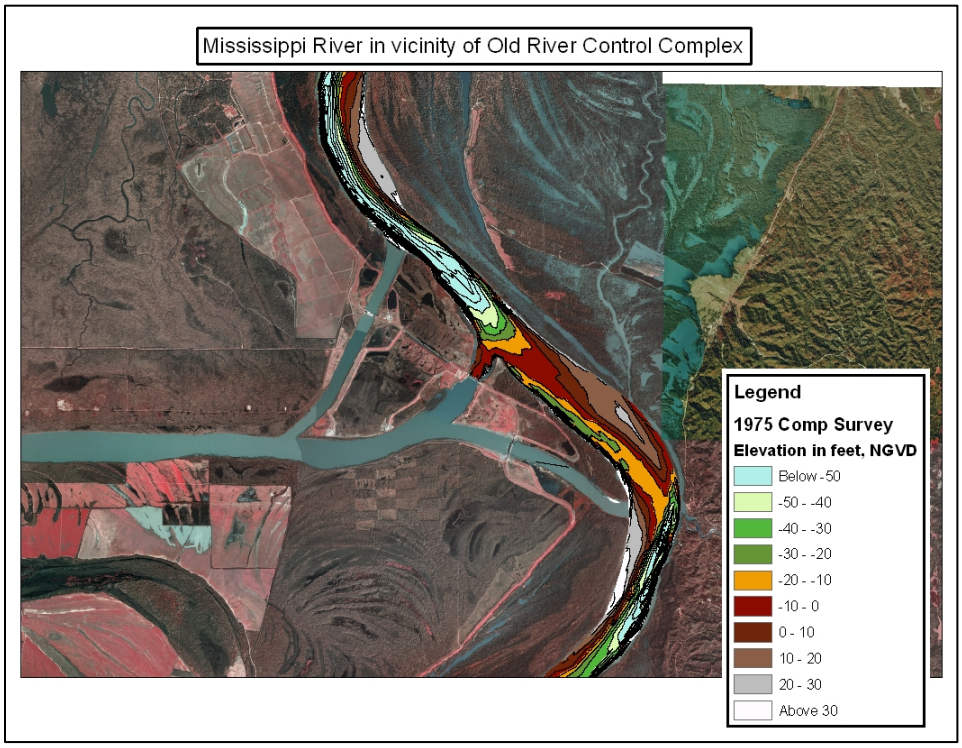

The contour map for the 1983 comprehensive hydrographic survey shown in Figure 3.17 indicates a similar channel pattern to the 1975 survey, which is expected since the auxiliary and hydropower structures were not yet operational. Notable changes between the 1975 and 1983 channel are a better-defined thalweg channel immediately downstream of the low sill structure and a decrease of the large middle bar between the low sill channel and the present-day auxiliary channel.

Figure 3.17. Contour map for the 1983 comprehensive hydrographic survey.

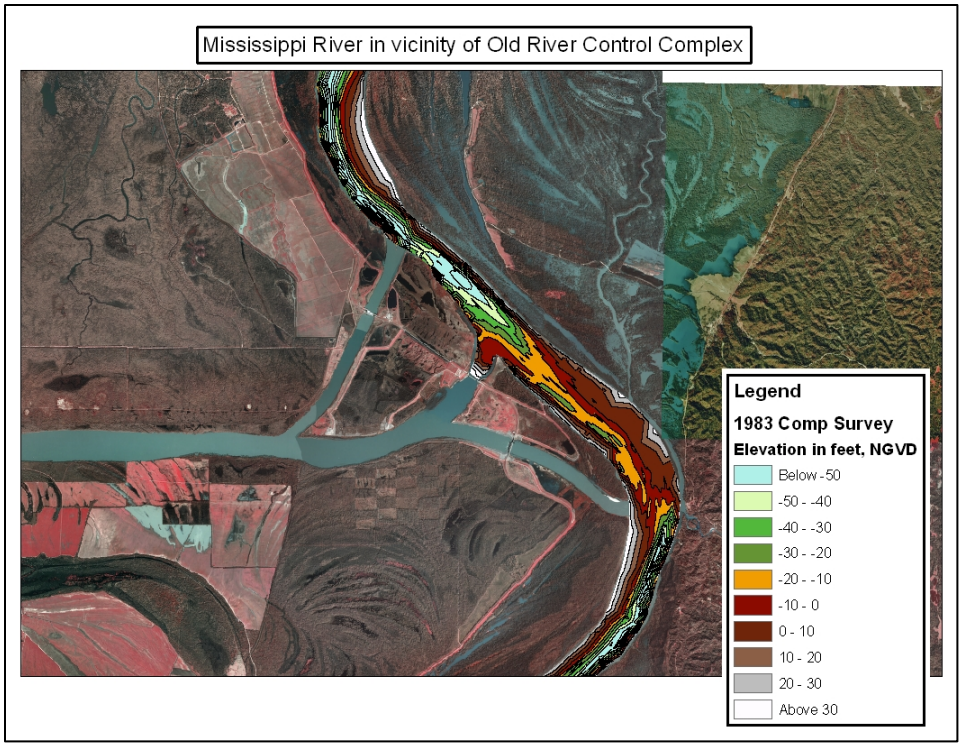

The contour maps for the 1992 and 2004 comprehensive hydrographic surveys are shown in Figures 3.18 and 3.19. The 1992 contour map illustrates the conditions subsequent to the commencement of operations of the auxiliary and hydropower structures. Changes in channel pattern between 1983 and 1992 are somewhat subtle. The thalweg channel between the low sill channel and the auxiliary channel appears better defined, and the middle bar has been further removed, particularly the downstream portion. This is most likely in response to a percentage increase in discharge through the reach as ORCC operations were shifted from the low sill structure to the auxiliary structure. Observed changes between the 1992 and 2004 surveys are less subtle, as several notable adjustments are seen. First, there is a decrease in the depth of the thalweg channel between the hydropower channel and the low sill channel, yet the deep channel still exists upstream of the hydropower channel. In the vicinity of the low sill channel, the thalweg channel of the river has shifted toward the left descending bank as deposition has occurred in front of the low sill channel. There is a less defined and shallower thalweg channel along the right descending bank downstream of the low sill channel than previously existed. A very short channel crossing from the left descending bank to the right descending bank now occurs immediately downstream of the low sill channel. In addition, the channel bar between the low sill

channel and auxiliary channel has increased in elevation and spatial extent and extends farther downstream, although the height of the bar is still less than 1975 conditions.

Figure 3.18. Contour map for the 1992 comprehensive hydrographic survey.

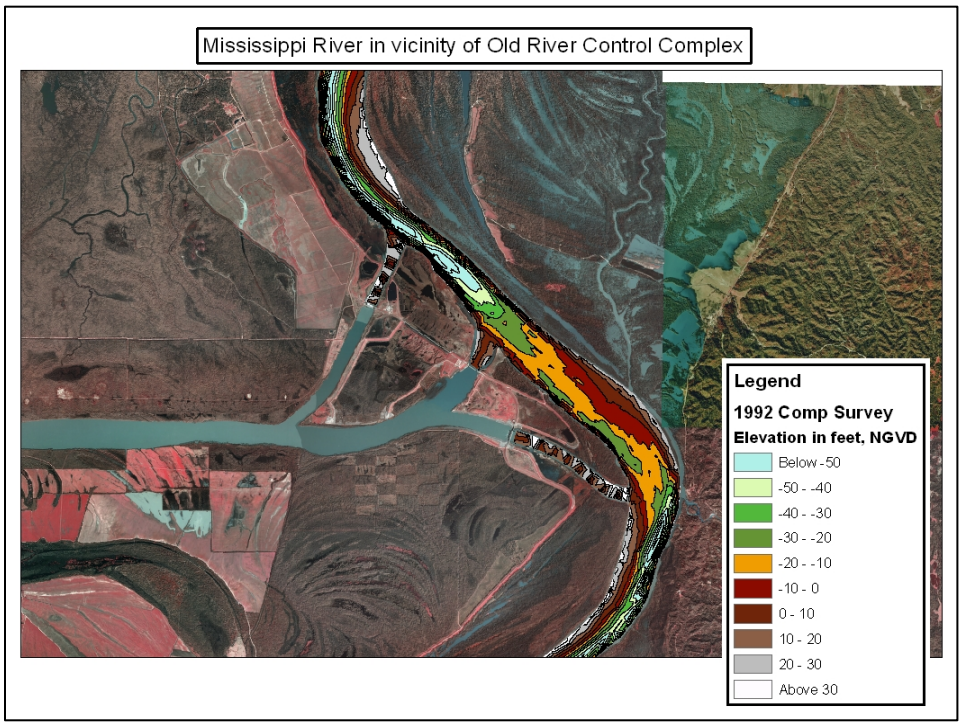

Figure 3.19. Contour map for the 2004 comprehensive hydrographic survey.

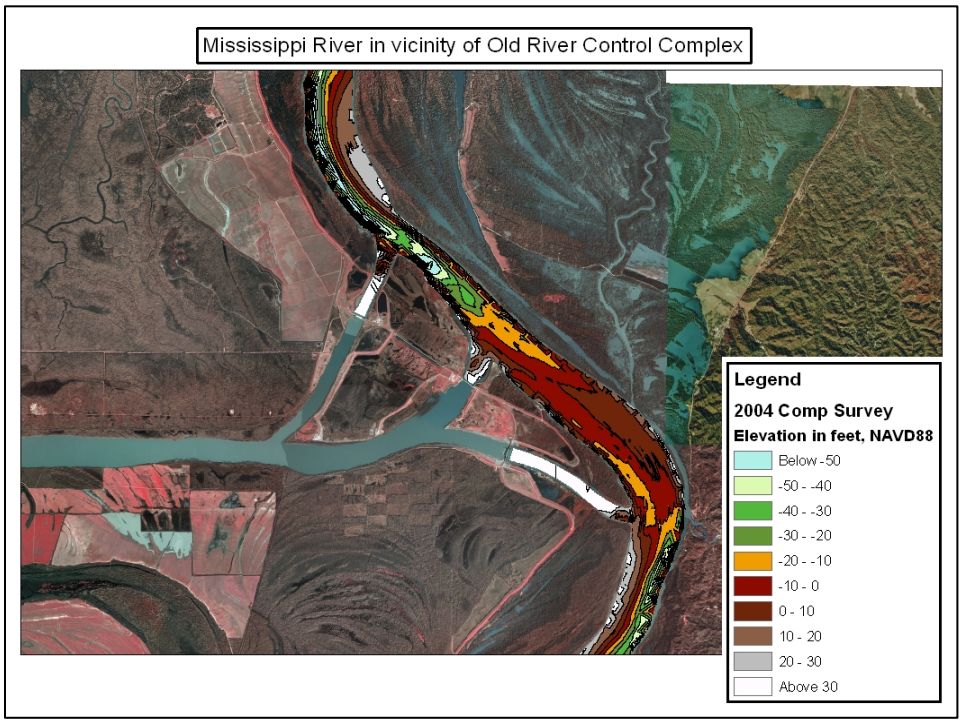

Contour maps developed from the multibeam surveys of 2006 and 2008 of the reach between the hydropower channel and the low sill channel are shown in Figures 3.20 and 3.21. These maps depict the same general channel conditions as were observed with the contour map of the 2004 comprehensive hydrographic survey in this reach. It is evident that the thalweg channel shallows considerably downstream of the hydropower channel. Also, the location of the thalweg channel has shifted toward the left descending bank between the hydropower channel and the low sill channel. The development of a bar at the entrance of the low sill channel is evident.

Figure 3.20. Contour map for the 2006 multibeam survey, hydropower to low sill reach.

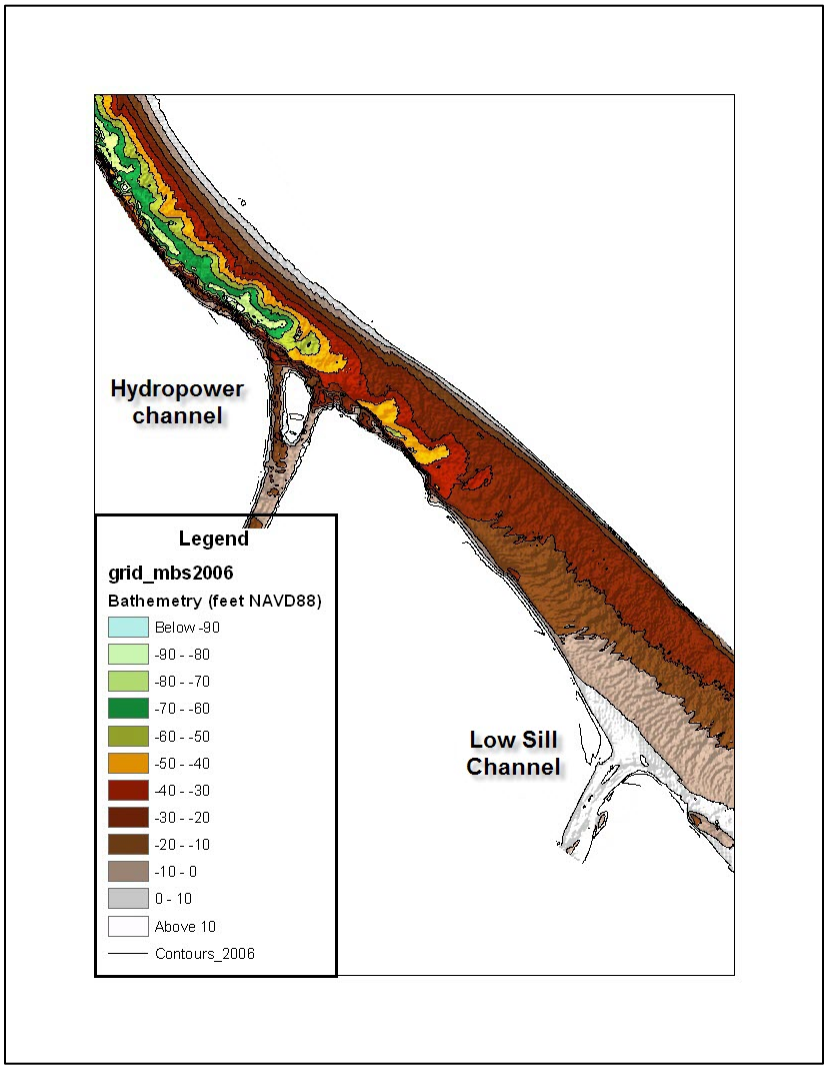

Figure 3.21. Contour map for the 2008 multibeam survey, hydropower to low sill reach.

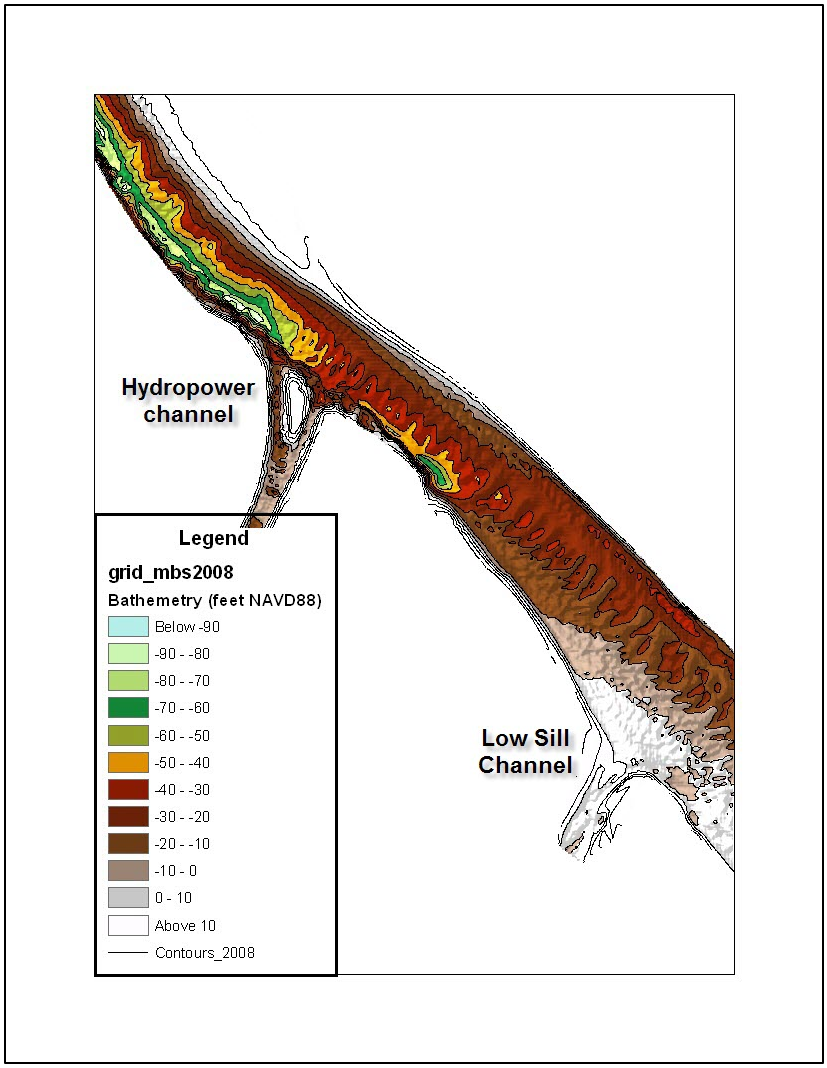

Contour maps for the multibeam surveys from 2006, 2008, and 2010 for the reach between the low sill channel and the auxiliary channel are shown in Figures 3.22 through 3.24. This reach encompasses the area of the channel bar deposit upstream of the auxiliary channel. The contour maps indicate the channel bar has eroded slightly from 2006 to 2010, in contrast to the growth of the channel bar observed between the 1992 and 2004 comprehensive hydrographic surveys. This suggests that the channel bar may erode and reform as high water events are experienced. Also evident in these contour maps is the short channel crossing from the left to right descending bank that occurs just downstream of the low sill channel near the upstream end of the channel bar. The maps show that deep water also exists along the left descending bank adjacent to the downstream end of the channel bar, basically forming a midchannel bar.

Figure 3.22. Contour map for the 2006 multibeam survey, low sill to auxiliary reach.

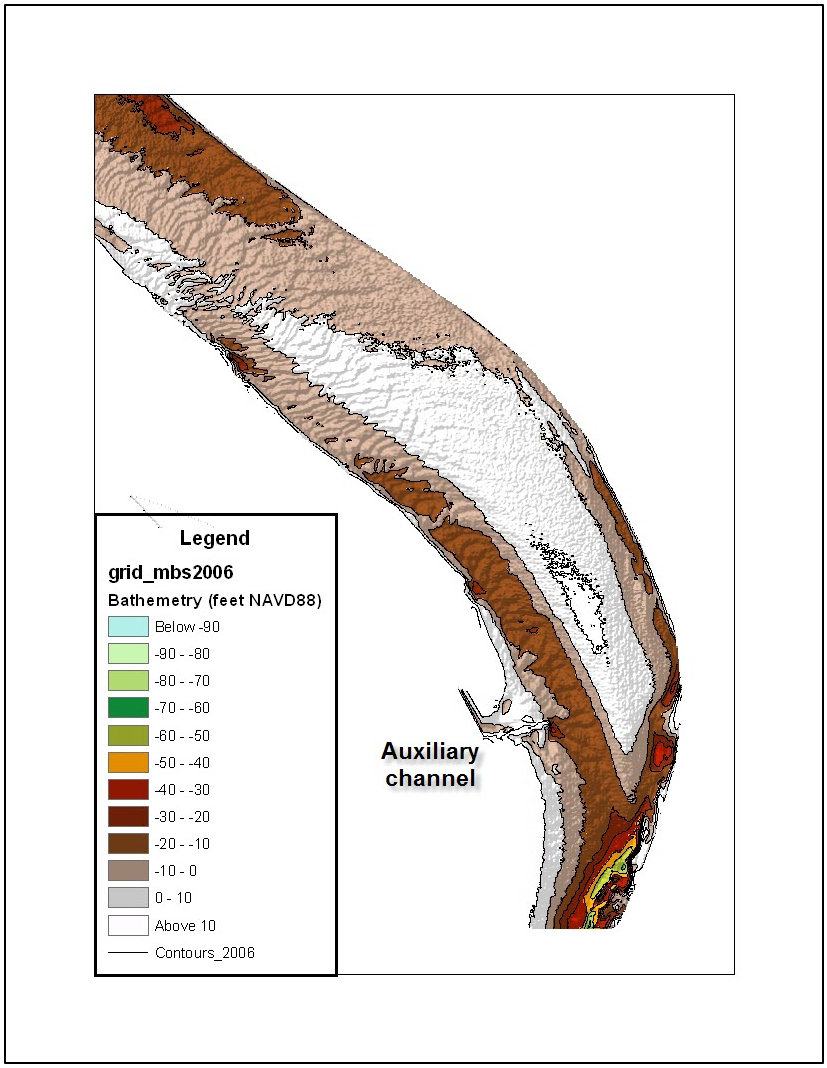

Figure 3.23. Contour map for the 2008 multibeam survey, low sill to auxiliary reach.

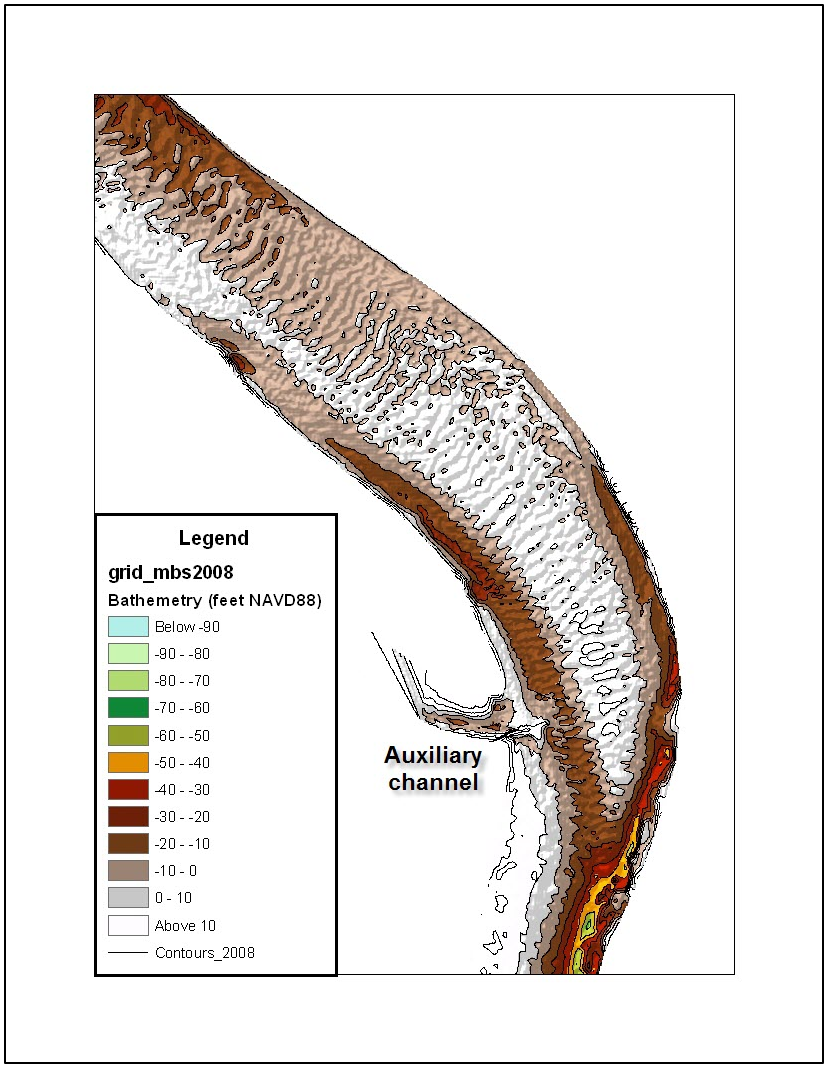

Figure 3.24. Contour map for the 2010 multibeam survey, low sill to auxiliary reach.

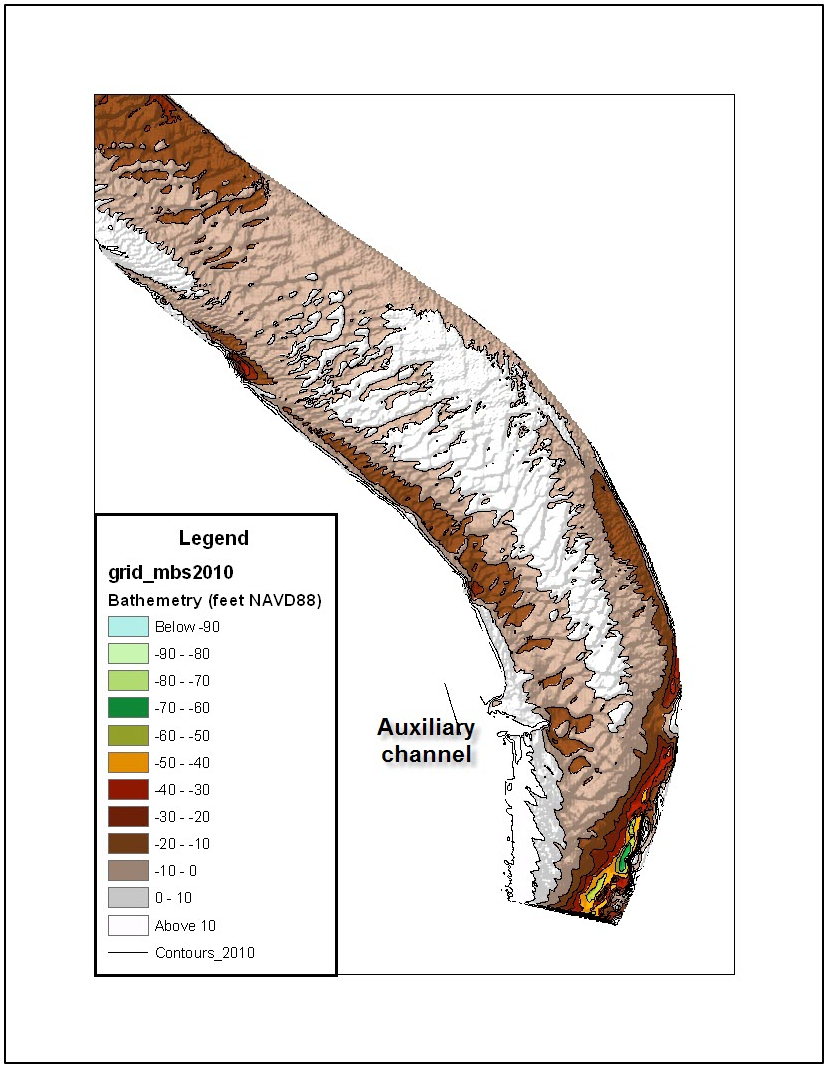

Overall assessment

The overall assessment based on this limited geomorphic analysis is that the local reach of the Mississippi River in the vicinity of the ORCC has experienced a reduction in overall depth due to channel filling. Geometric data analyses indicate that filling has occurred throughout the time period of 1975 to 2010, but the majority of the filling occurred subsequent to 1992. The reach between the hydropower channel and the low sill channel has experienced significant filling, as much as 25 to 30 ft, during this time period. The location of the thalweg channel has also shifted from the right to left descending bank during this time, resulting in deposition of material in the vicinity of the low sill channel entrance. These changes most likely reflect the river adjustment to discharge changes resulting

from the added operation of the hydropower and auxiliary structures in the mid-1980s and early 1990s.

Specific gage analysis also indicates a long-term trend of increased stages for the Mississippi River stations at Vicksburg, Natchez, Red River Landing, Bayou Sara, and Baton Rouge. As much as 5 to 10 ft of stage increase was noted for the long-term periods of record for these stations. However, for the post-1973 flood period, there were no significant trends observed for these stations, with the exception of Natchez where the stage trend was still increasing and Vicksburg and Red River Landing where trends were more uncertain.

Interpretation of the results of the specific gage results with the findings of the geometric data analysis suggests that most of the changes on the Mississippi River in the vicinity of the ORCC are likely local responses to changes in operation of the ORCC with the addition of the hydropower and auxiliary structures. The reach has experienced a long-term, system-wide increase in stage; therefore, the overall changes are likely a combination of a systematic adjustment of this reach of the Mississippi River as well as local responses at the ORCC structures. Due to the spatial limitations of the geomorphic assessment, the potential impacts of these changes on Mississippi River reach-scale morphology is uncertain, as well as the possible effects on flood stages.

4 ORCC Vegetation Change and River Capacity Analyses

Vegetation change task overview and objectives

As a component of the ORCC numerical model investigations, vegetation change analyses were performed with the primary goal of quantifying the impacts of these changes to the Mississippi River channel. Three data sets were used in these analyses: the 1992 U.S. Geological Survey (USGS) Land Cover (Vogelmann et al. 2001); the 1992 land cover compiled for the Mississippi River Supplemental Environmental Impact Statement (MRSEIS) (USACE 1998); and digital imagery of the 2011 flood event.

Methodology

Digital imagery of the 2011 flood event was captured during the peak of the event within the Mississippi River & Tributaries Project in the State of Louisiana. Spatial extents of the imagery extend from above ORCC southward along both the Mississippi and Atchafalaya Rivers to the Gulf of Mexico (Figure 4.1). Time period of capture is 17 May through 1 June 2011. The digital imagery was ortho-rectified and mosaiced into a single image with a 1.5 ft resolution. A subset of this imagery was extracted from north of the ORCC to north of the city of Baton Rouge, LA. A supervised classification was performed on this 4-band color infrared imagery. Approximately 50 individual class signatures were digitized for input to a supervised classification model using the maximum likelihood method. Results were combined into four primary classes of water, fields, bare earth, and vegetation and subsequently into two classes of land and water (Figure 4.2).

Measured ground-truth information was not available to perform accuracy assessments of the 2011 land/water classification. Evident within the imagery, flood waters extended through large open areas covered by forested wetlands. The images captured the trees, but it can be assumed that flood waters extended beneath the canopy throughout the area. Thus, the canopy was classified as vegetation even though the region was flooded.

Figure 4.1. 2011 High water imagery extents.

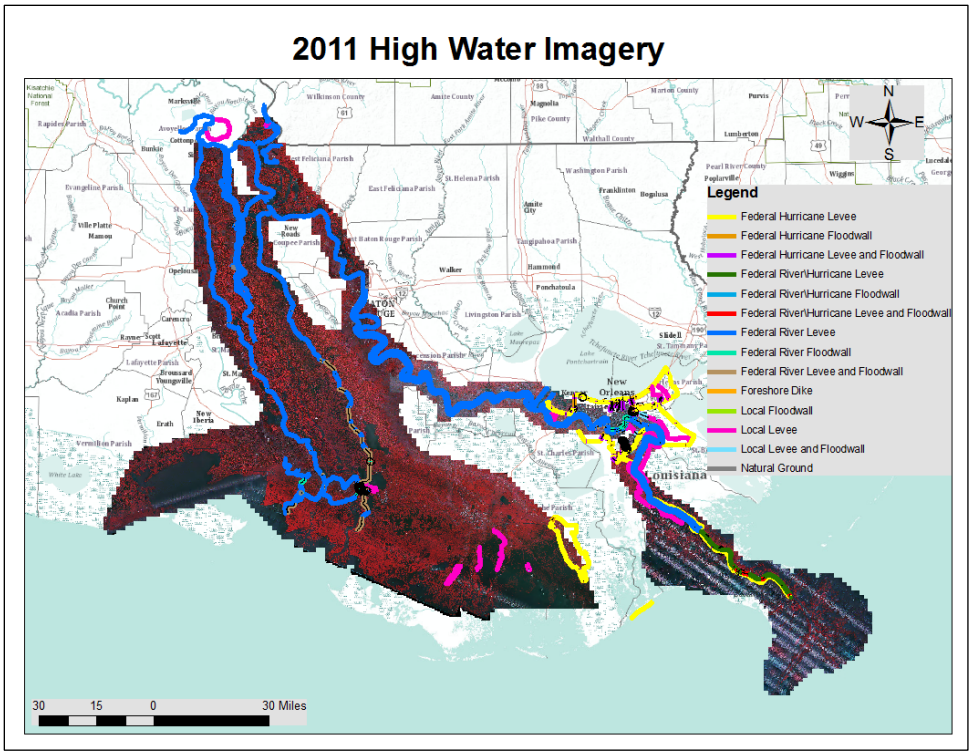

Figure 4.2. 2011 Flood water derived from digital imagery.

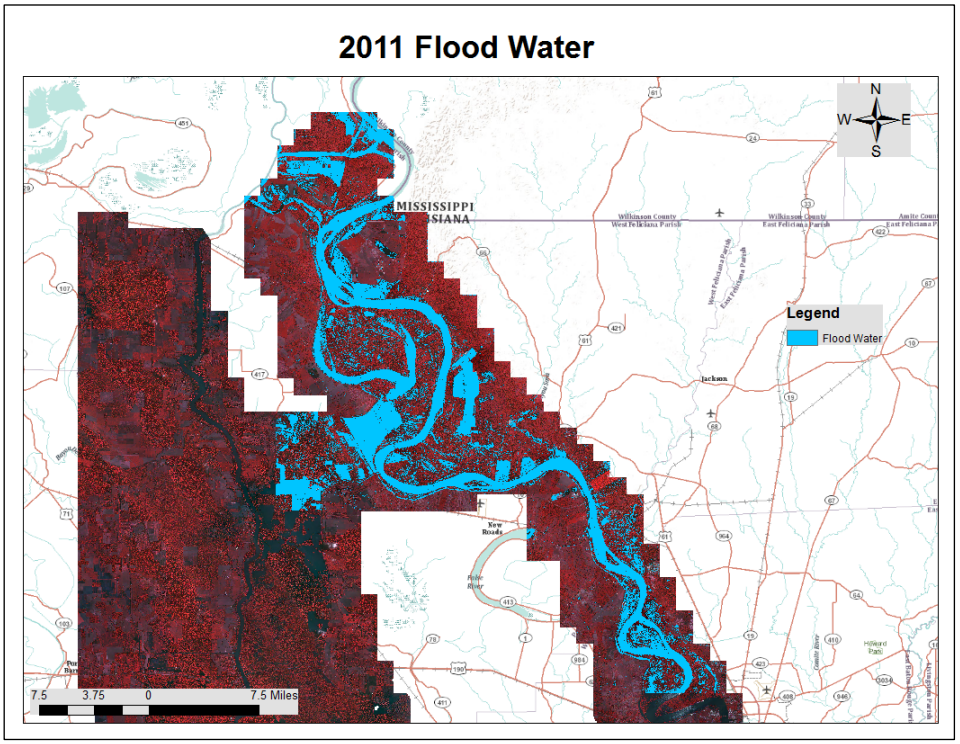

The 1992 USGS Land Cover data set (Figure 4.3) is a historic layer which contains 23 individual land classes, including water. The 23 classes are defined according to the USGS habitat data categories and were derived from satellite imagery at a 25 meter (m) resolution. This data covers the State of Louisiana, and the project study region was extracted to overlay the 2011 flood imagery extent.

Figure 4.3. 1992 USGS Land Cover.

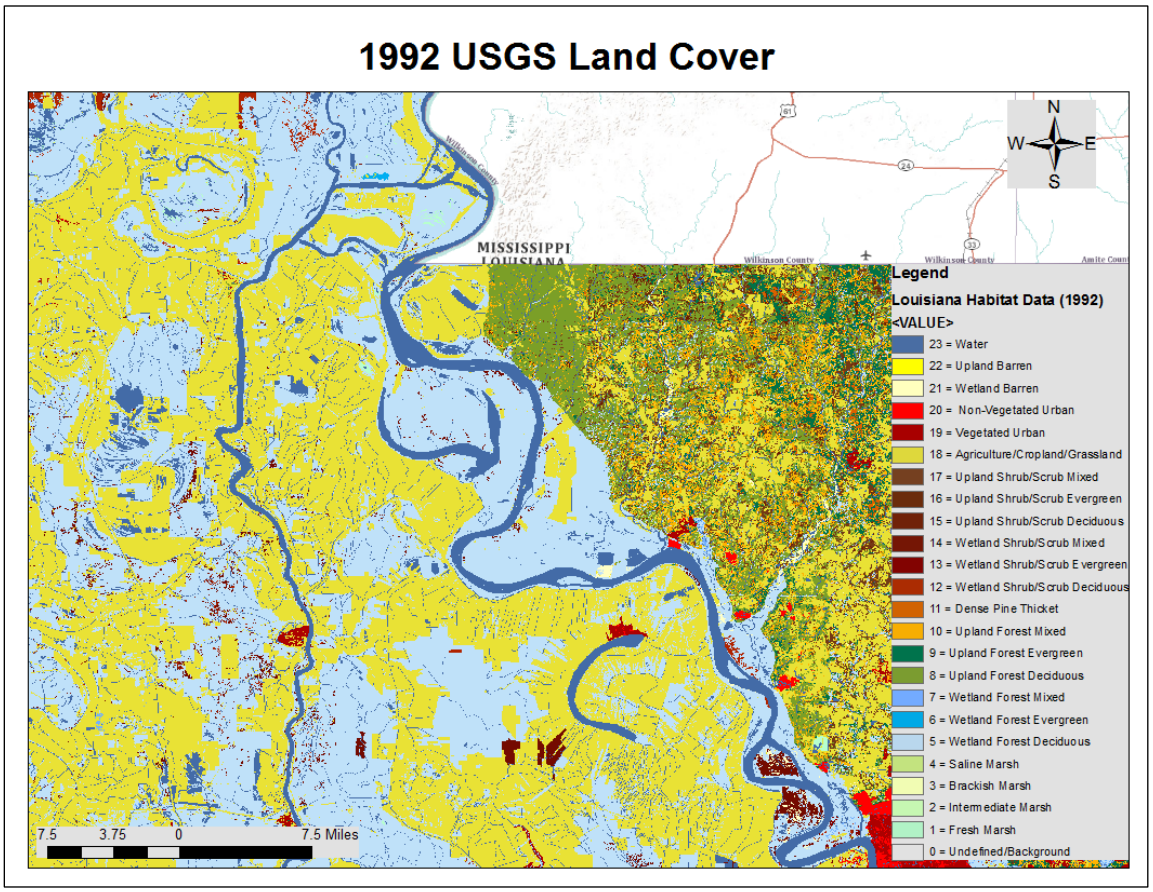

The 1992 MRSEIS land cover was derived from 1992 aerial imagery for the entire length of the Mississippi River. Approximately 35 land cover classes were digitized from georectified scanned imagery in support of a supplemental environmental impact statement. These were compiled for the region within the levee protection through 200 ft on the protected side of the levees (Figure 4.4).

Figure 4.4. 1992 MRSEIS Land Cover classes.

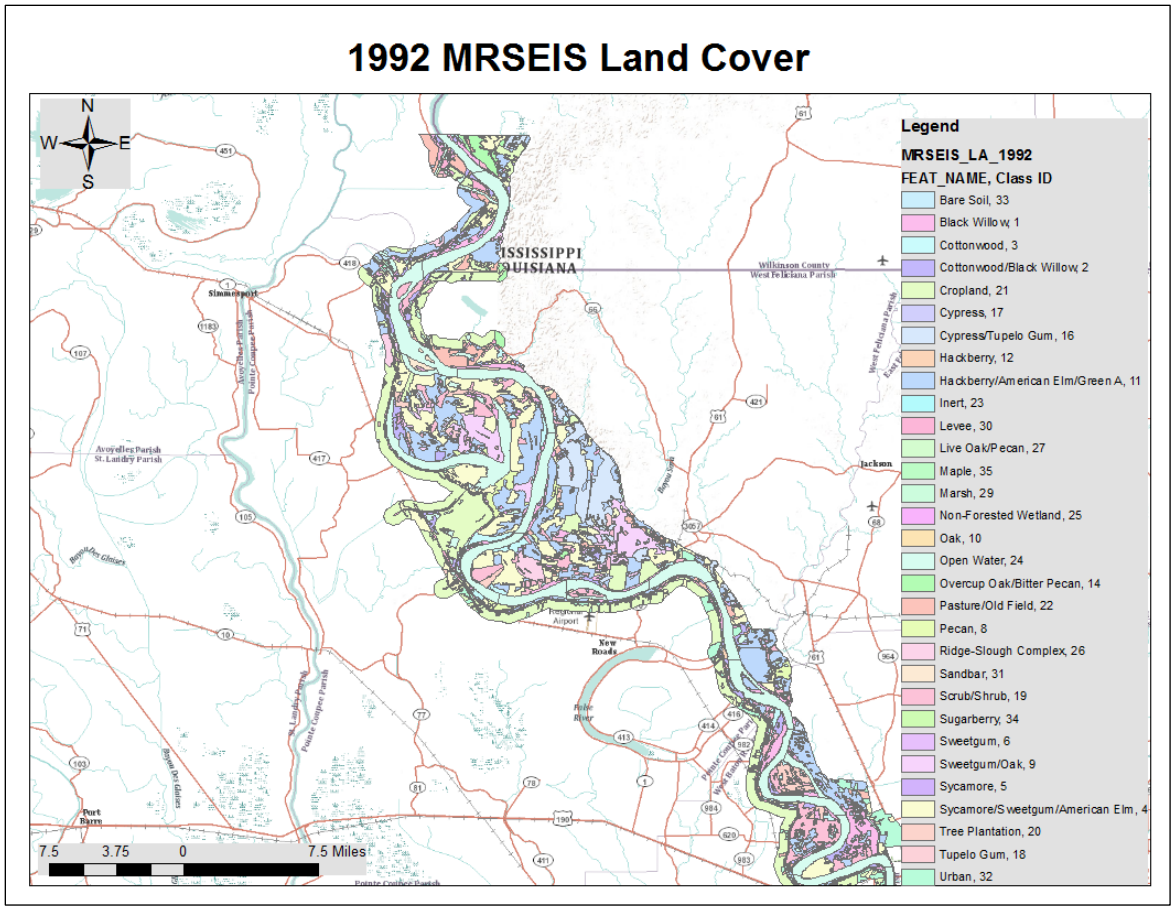

Each of the 1992 data sets were overlaid onto the 2011 Flood Water layer to compute changes in land cover (vegetation) between 1992 and 2011 and quantify the land inundated in the 2011 flood event.

Vegetation change summary of results

A cross-correlation spatial analysis was performed to compute the acreages of flooded land. Analyses were constrained to the extents of the intersection of each 1992 data layer to the 2011 Flood Water layer. Approximately 112,000 acres of the 1992 USGS habitat lands were computed to be inundated by the 2011 flood event. This is in relative agreement with approximately 119,000 acres of the 1992 MRSEIS land cover data set (Figure 4.5). Although, as previously mentioned, the total water inundation area is somewhat larger due to unavoidable classification of tree canopy as vegetation.

Figure 4.5. 2011 Flood inundation, 1992 acres.

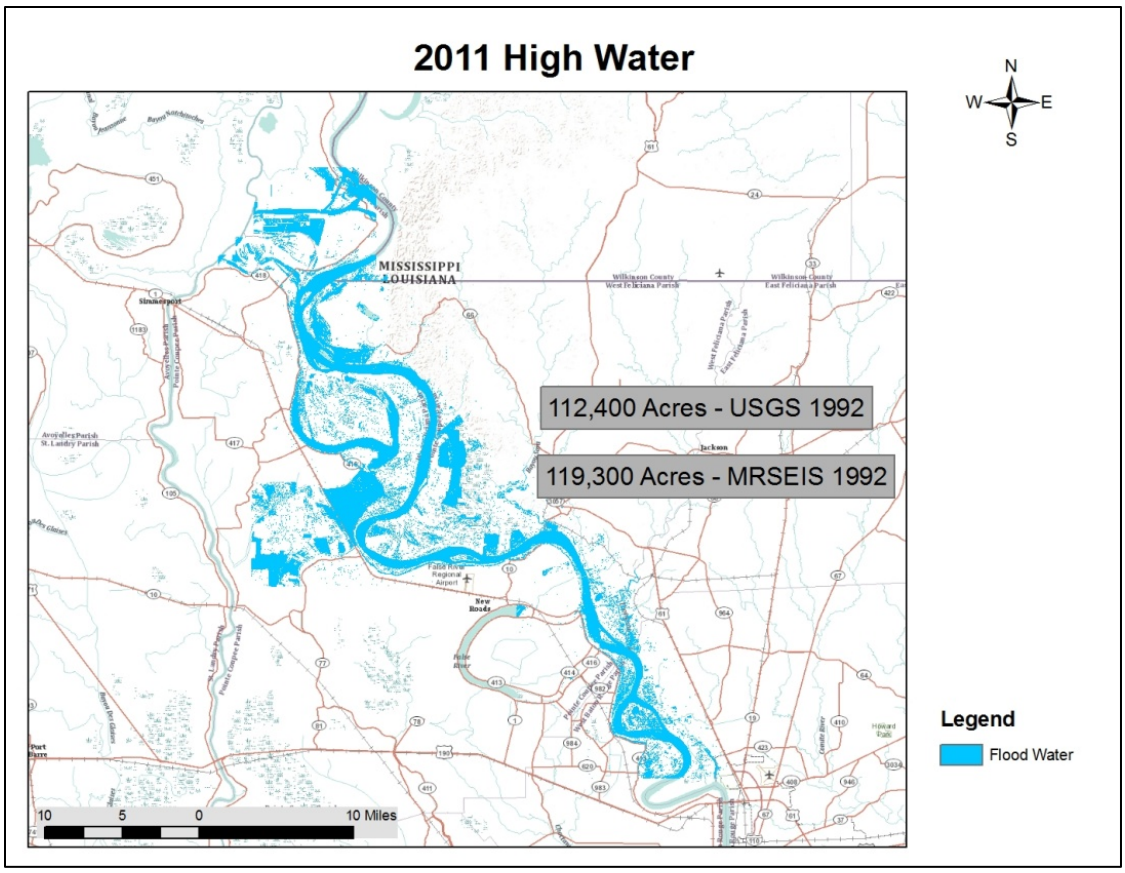

River capacity analyses task overview

The primary objective of this task is to determine any trends, either quantitatively or qualitatively, in the Mississippi River's discharge capacity (increase or reduction) given the period of record for the available data sets. A river's capacity to pass flow can be approximated by computing the channel *conveyance*. The river discharge (Q) in terms of Manning's n is computed by

$$Q = \left(1.0 / n\right) AR^{2/3} S^{1/2} \tag{4-1}$$

where:

A = Area
R = hydraulic radius
S = slope

The channel conveyance (K) is based upon its geometry and

$$K = \left(1.0 / n\right) AR^{2/3} \quad (4\text{-}2)$$

or

$$Q = KS^{1/2} \quad (4\text{-}3)$$

In order to use these equations, the entire cross-sectional geometry of the river is needed for each respective time period. Mississippi River full-channel, cross-section surveys are generally acquired approximately every 10 yr.

Conveyance estimates

Historic river channel cross section surveys have been archived by MVN although all years for individual sections cannot readily be compared due to survey inconsistencies ranging from vertical and horizontal datums, traverse base lines, as well as reference bench mark locations. Due to these issues, a selection of three sections were extracted for the years 1992 (posthydropower initiation) and 2004. These ranges are designated as ranges R300.35, R295.5, and R294.5 and cross the Carr Point and Hog Point revetments (Figure 4.6). These ranges were selected based on proximity to the ORCC as well as the volume of shoaling computed at these locations (Section 6). Cross section views of R294.5 for 1992 (Figure 4.7) and 2004 are shown (Figure 4.8) and clearly show shoaling in the channel at this site.

Conveyance (K) for these sections varied considerably between cross sections as well as between time periods of 1992 and 2004. An equivalent approximate channel slope and Manning's n value was used to compute conveyance and discharge capacity for each year. A water surface elevation of 40 ft was used for all sections. A significant reduction (41×10^6 cfs) is realized at R294.5 with conveyance and channel capacity in 1992 of approximately 1.162 million cfs and approximately 1.112 million cfs in 2004. The conveyance at R295.5 increased from approximately 1.1 million cfs in 1992 to 1,191 million cfs in 2004. These results indicate some decreased but also high variability of channel capacity and localized differences. A full-channel capacity analysis is beyond the scope of this effort but would provide a complete summary of the historic change in river capacity.

Figure 4.6. Mississippi River revetments and cross section locations.

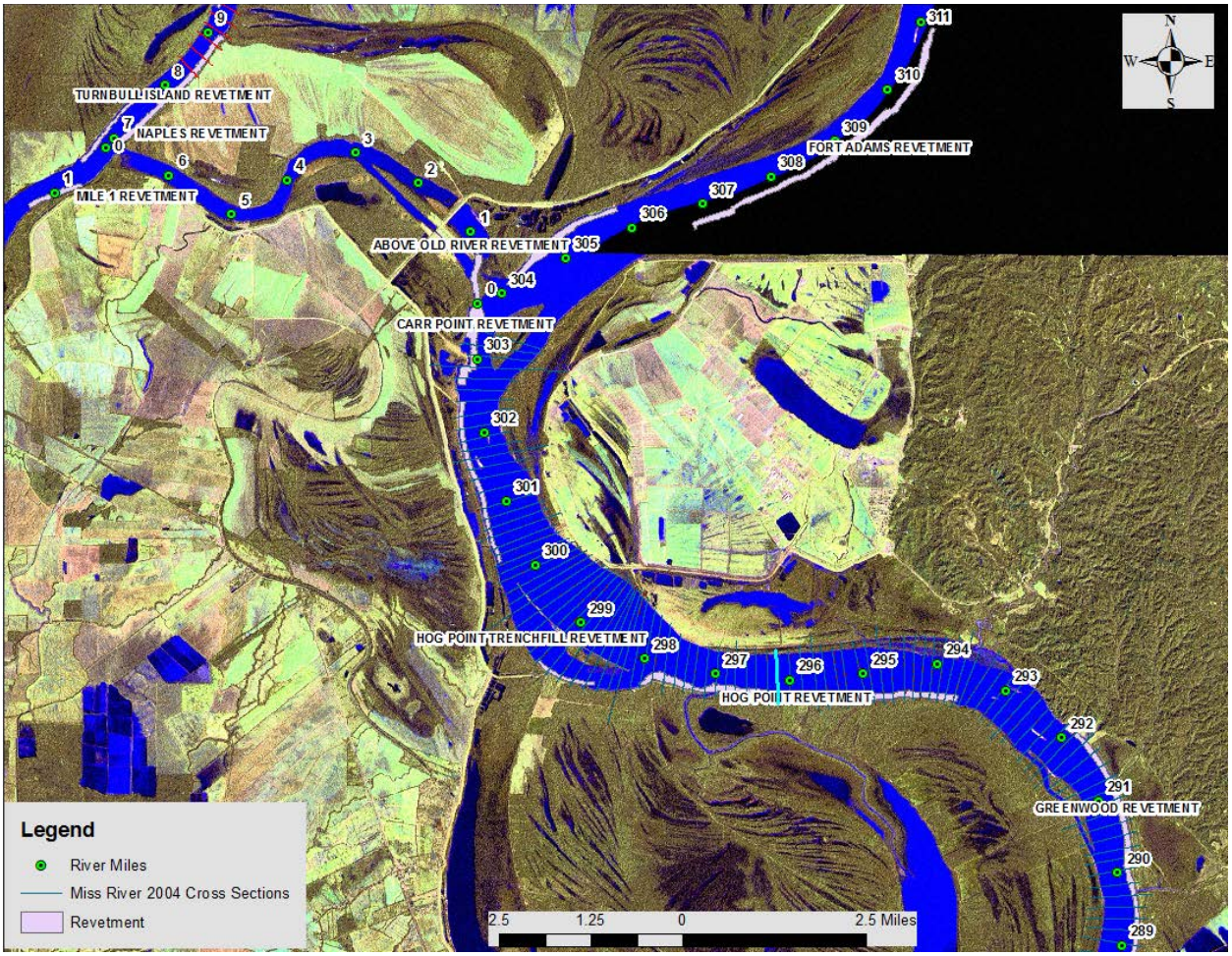

Figure 4.7. Range R294.5 year 1992 survey.

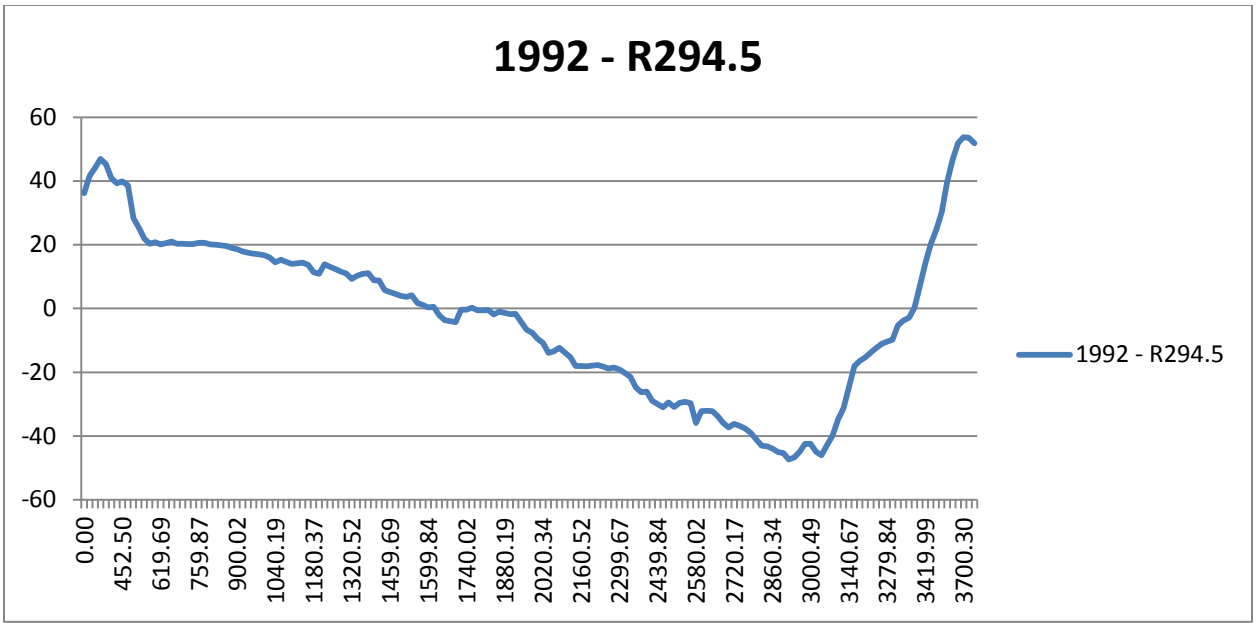

Figure 4.8. Range R294.5 year 2004 survey.

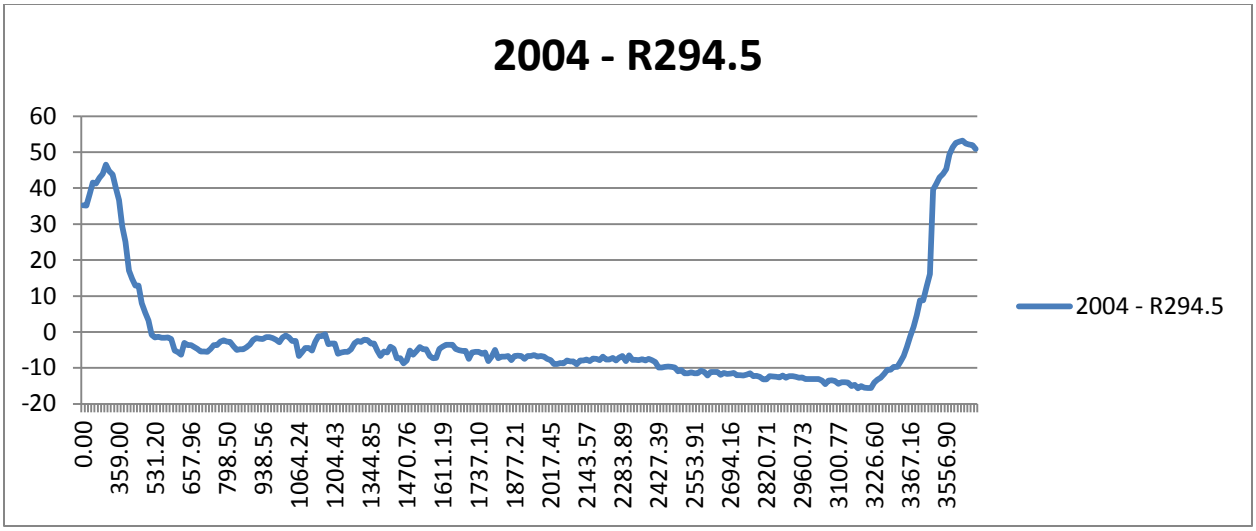

Volume computation analyses

MVN computed shoal and scour volumes for all 85 river revetment locations. These quantities represent the change in volume between individual survey year and the *base* year. The base year is defined as the year of initial revetment placement. Each revetment range section for each survey year was intersected with the base range survey section. Positive differences were totaled for all sections as shoal and negative differences as scour. Volumes were calculated based upon distance between range sections.

Summary statistics and graphics were produced for each location (85) by year as well as totals for all revetments across the full time period of analyses from 1992 through 2011. Revetment locations in the vicinity of ORCC are shown in Figure 4.9. Yearly shoaling and scour volumes are shown for the Fort Adams, Carr Point, Above Old River, and Hog Point revetments (Figures 4-10 through 4-13). All locations show significant shoaling vs. scouring with the largest at Carr Point (~140×10^6 ft^3, 5.19×10^6 yd^3) and Hog Point (~160×10^6 ft^3, 5.93×10^6 yd^3) revetments. Carr Point revetment is adjacent to the large sandbar in the main river channel which gradually developed over the last 15 to 20 yr.

Figure 4.9. Revetment locations in vicinity of ORCC

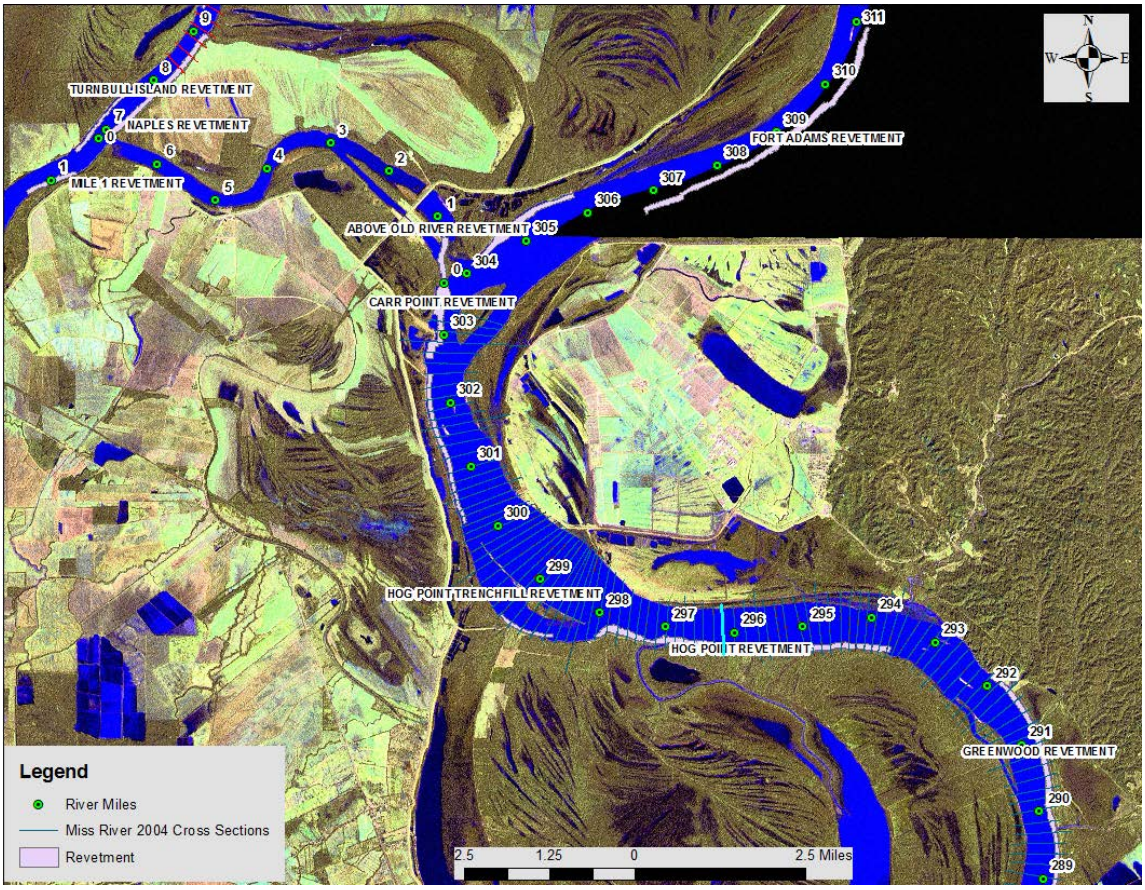

Figure 4.10. Fort Adams revetment scour and shoal volumes.

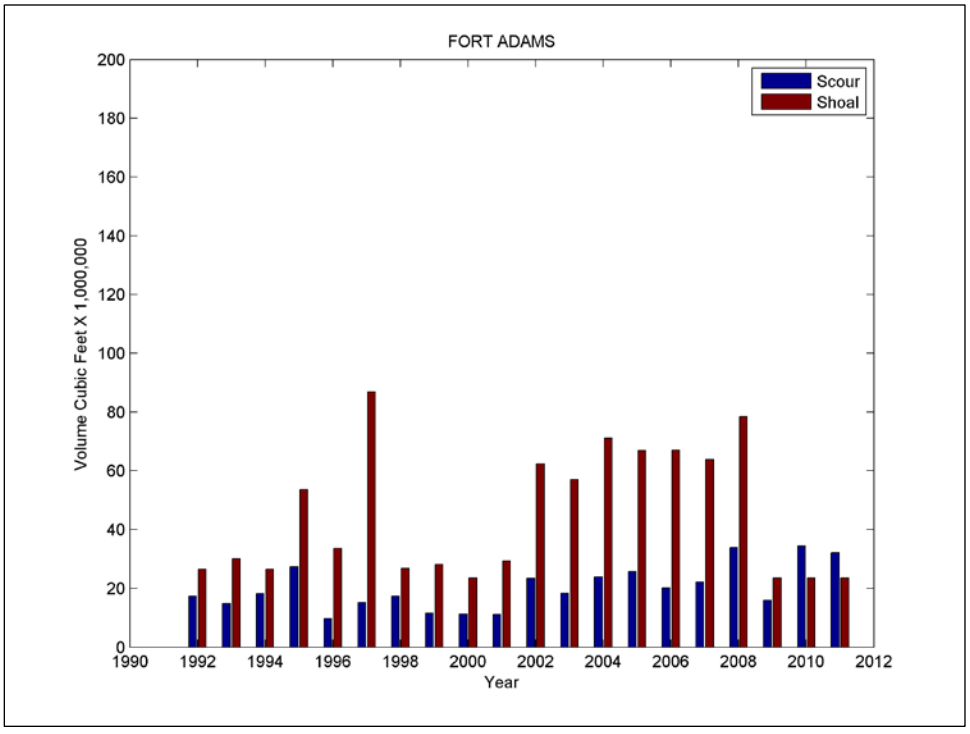

Figure 4.11. Above Old River revetment scour and shoal volumes.

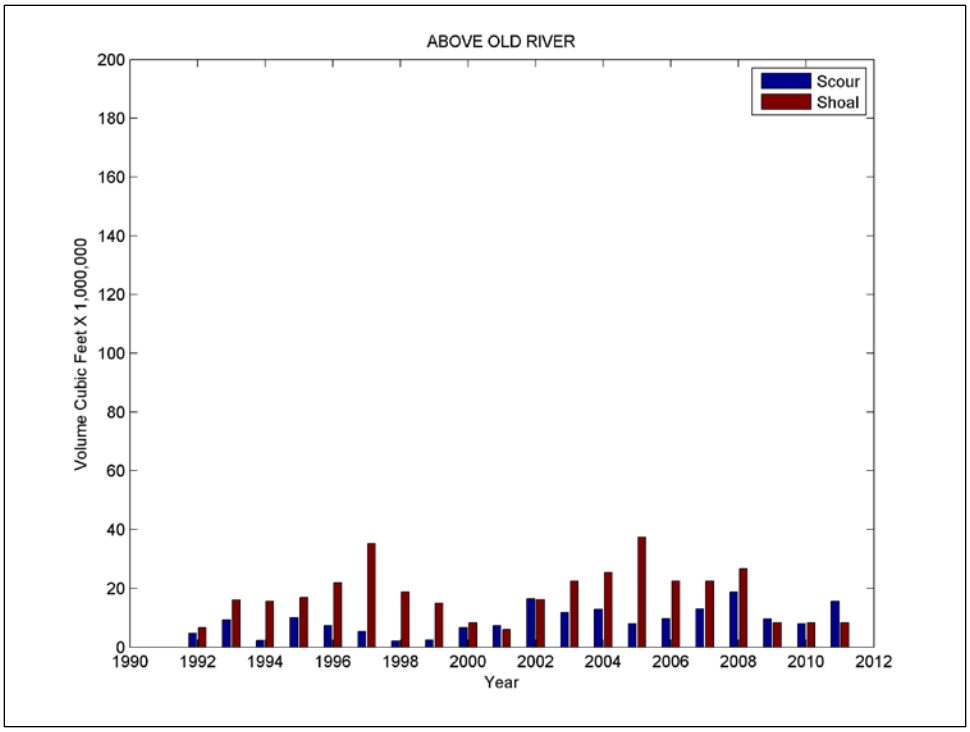

Figure 4.12. Carr Point revetment scour and shoal volumes.

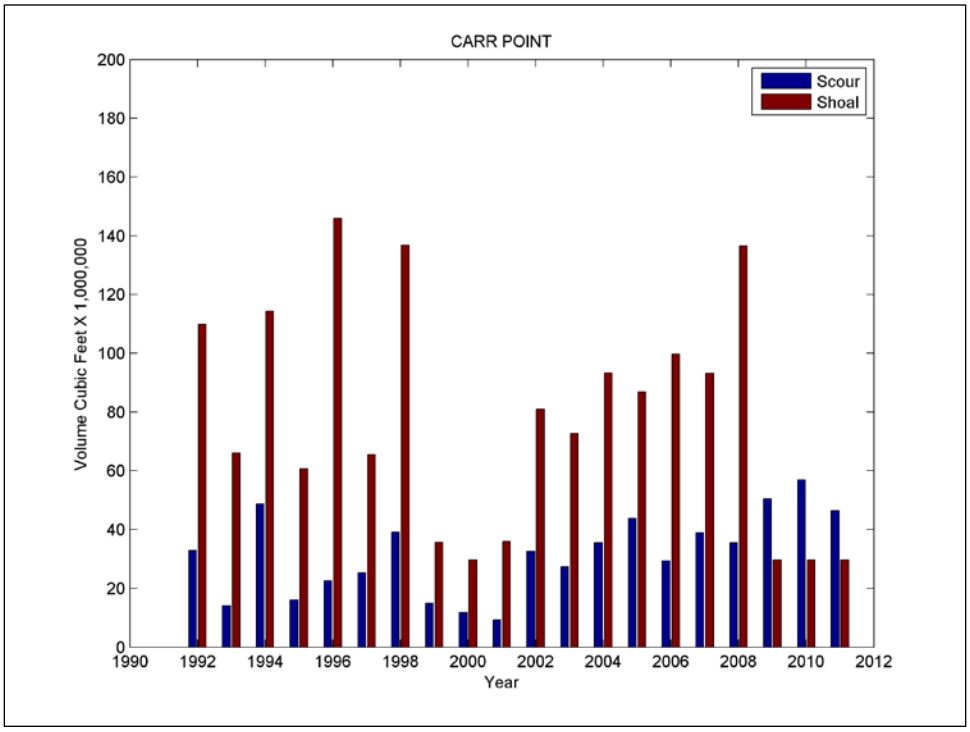

Figure 4.13. Hog Point revetment scour and shoal volumes.

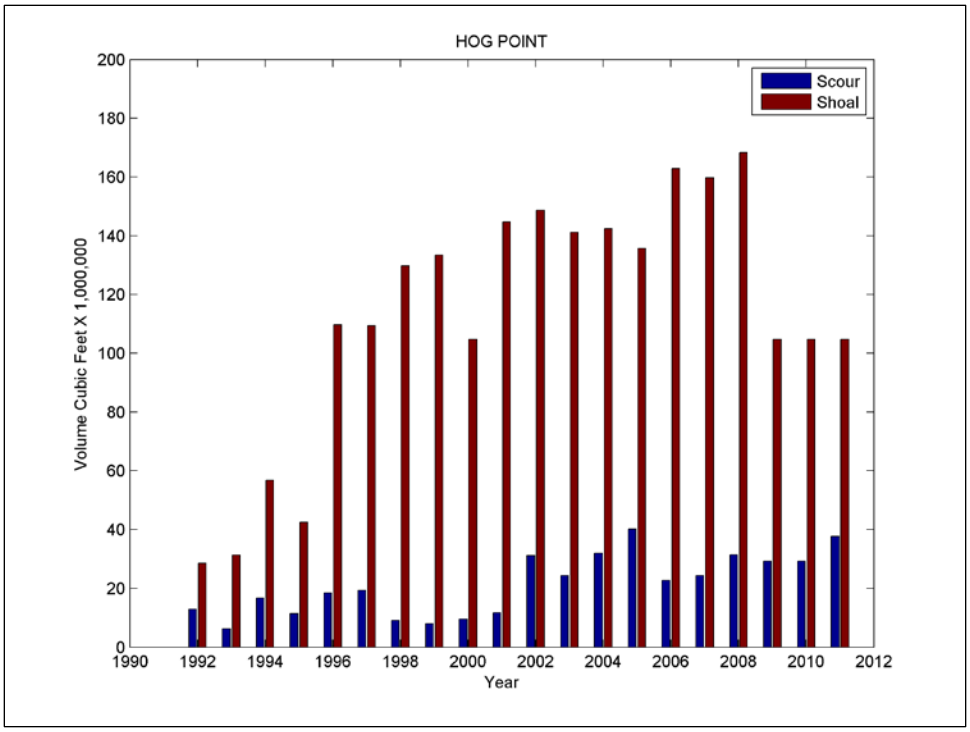

Note that scour and shoal volumes are referenced to the base year at each location and NOT differences between each year. Thus, the 2011 volumes represent the existing conditions and changes that have occurred from the base year through 2011. The revetment range surveys are performed yearly at all locations primarily to capture the elevation conditions of the specific revetment. Thus, they are not collected across the entire channel (Figure 4.14) and do not fully capture local scour and shoaling.

Although volumes are not representative of the entire channel, the computations provide quantitative estimates as well as spatial and temporal historic trends. Figure 4.15 through Figure 4.18 show the scour and shoal changes for all locations for the years 1992, 1997, 2008, and 2011. Two revetment locations in 1992 stand out with ~180 x 10^6 ft^3 of shoaling. However, 1997 was a high-water year, and two different locations show over 200 × 10^6 ft^3 of shoaling. 2008 was another high-water year with over 200 × 10^6 ft^3 of shoaling at four locations two of which are the same 1992 revetment locations. The 2011 major flood event was very close to project flood conditions, and these surveys show over ~180 × 10^6 ft^3 of shoaling at several locations (peak shoaling occurred at Plaquemine, White Castle) and also ~170 × 10^6 ft^3 of scouring at Poydras.

Figure 4.14. Representative revetment range section survey.

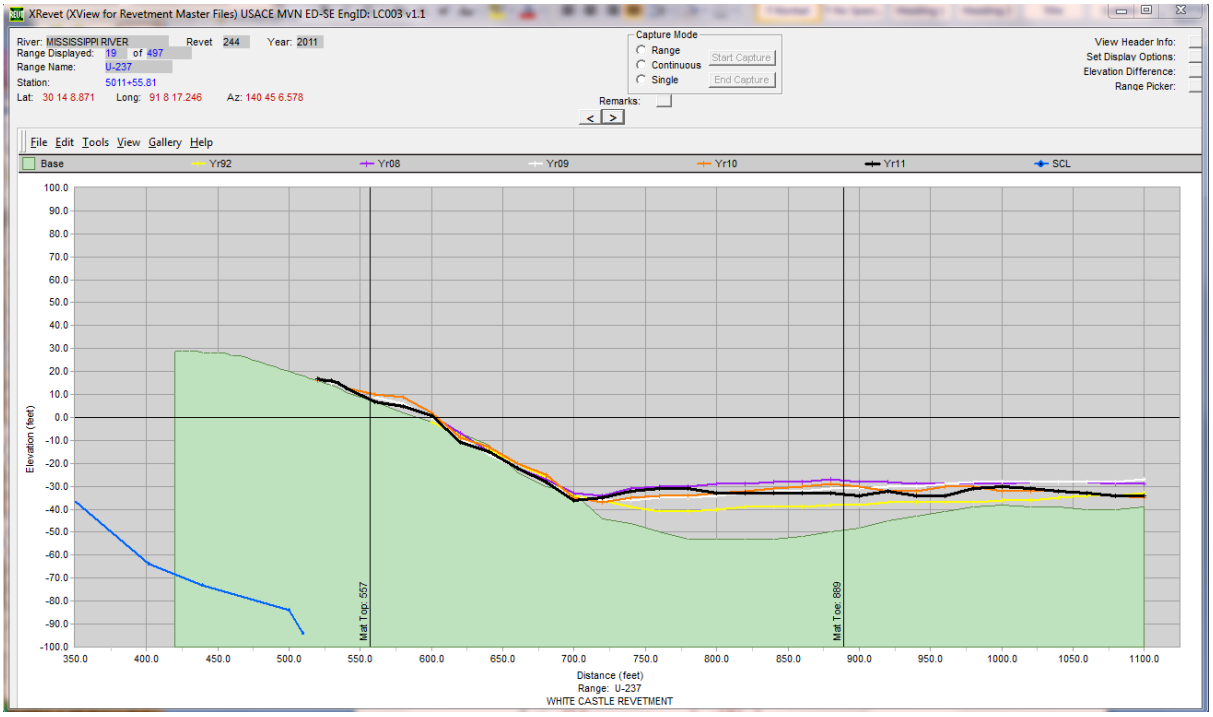

Figure 4.15. Volume change for 85 Mississippi River revetments 1992.

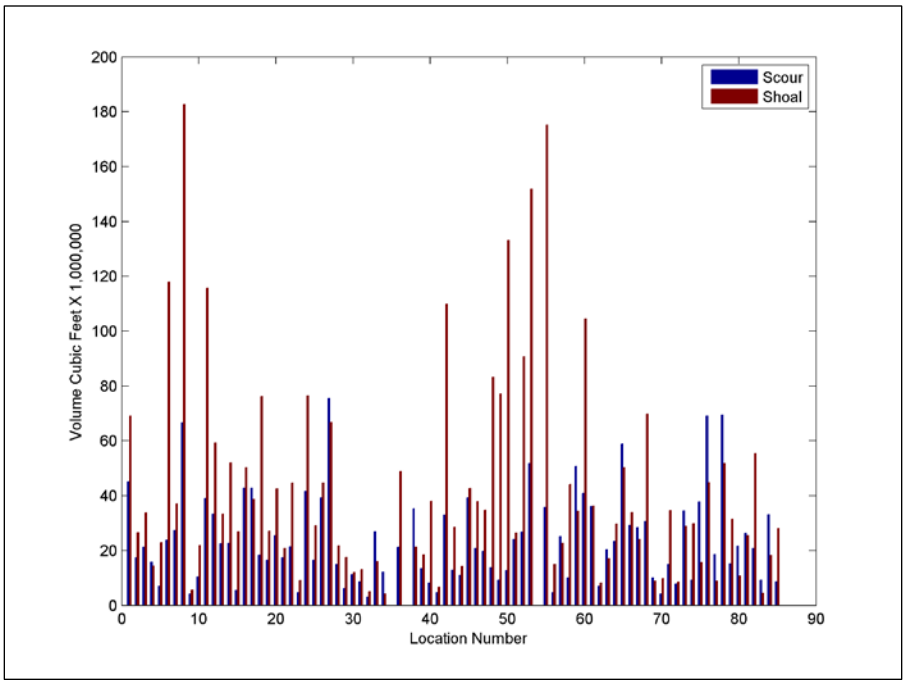

Figure 4.16. Volume change for 85 Mississippi River revetments 1997.

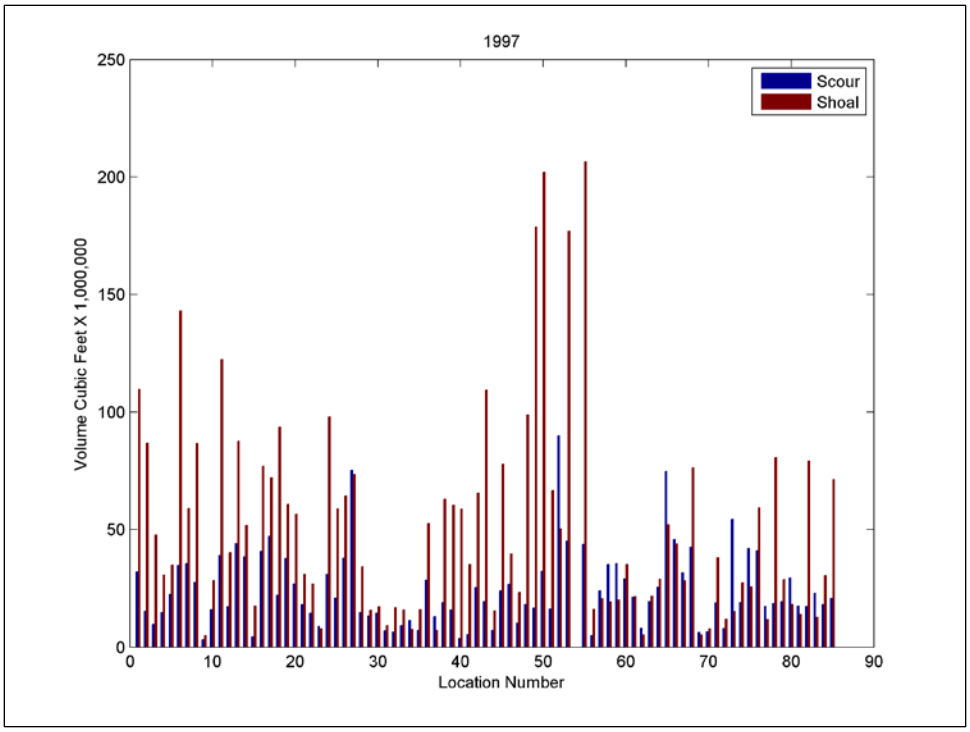

Figure 4.17. Volume change for 85 Mississippi River revetments 2008.

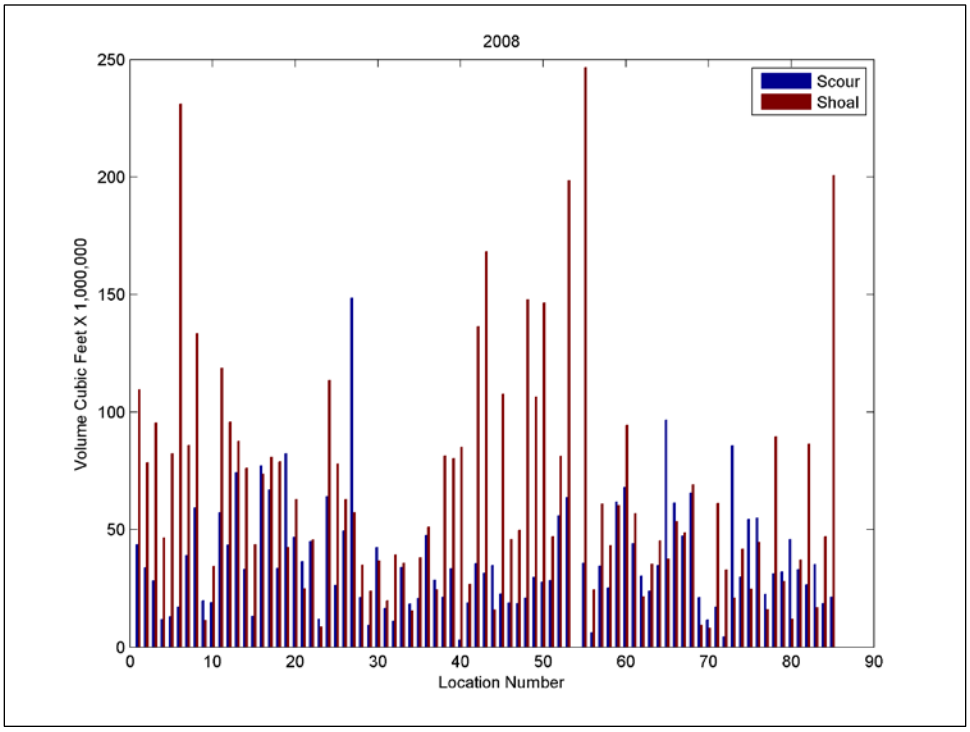

Figure 4.18. Volume change for 85 Mississippi River revetments 2011.

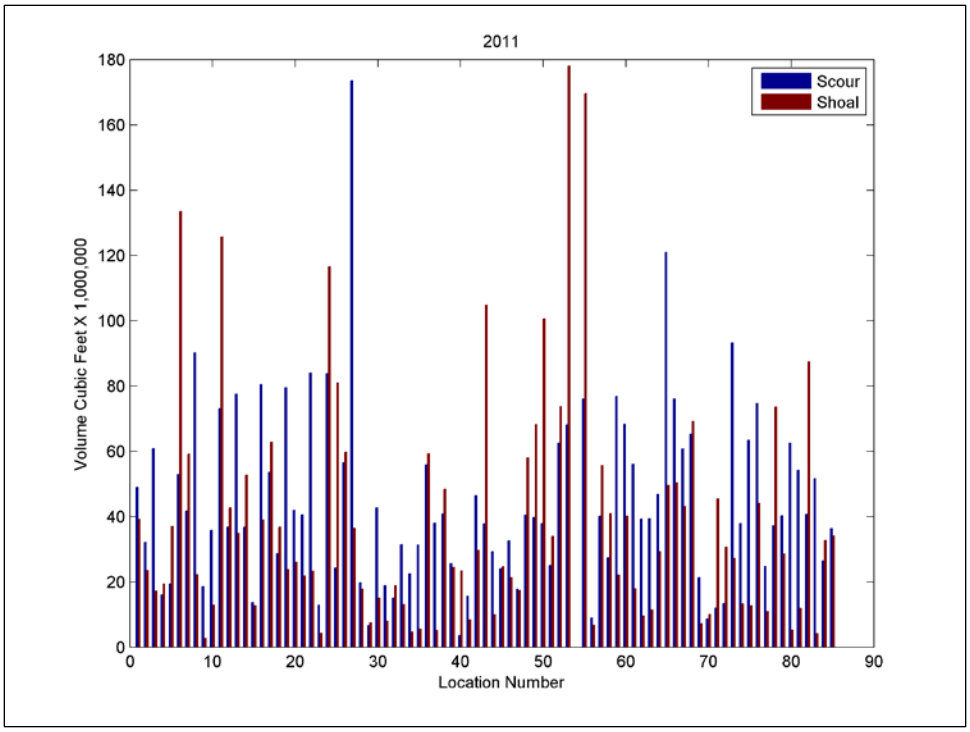

Temporal volume changes across revetment locations can be compared to identify the most significant scour and shoaling regions. Figures 4.19 through 4.21 show net volume change comparisons of revetment locations from 1992 through 2011. Several locations immediately stand out with between 150×10^6 ft^3 and 200×10^6 ft^3 of shoaling compared to base-year elevations.

Figure 4.19. Volume change for selected Mississippi River revetments 1992 to 2011.

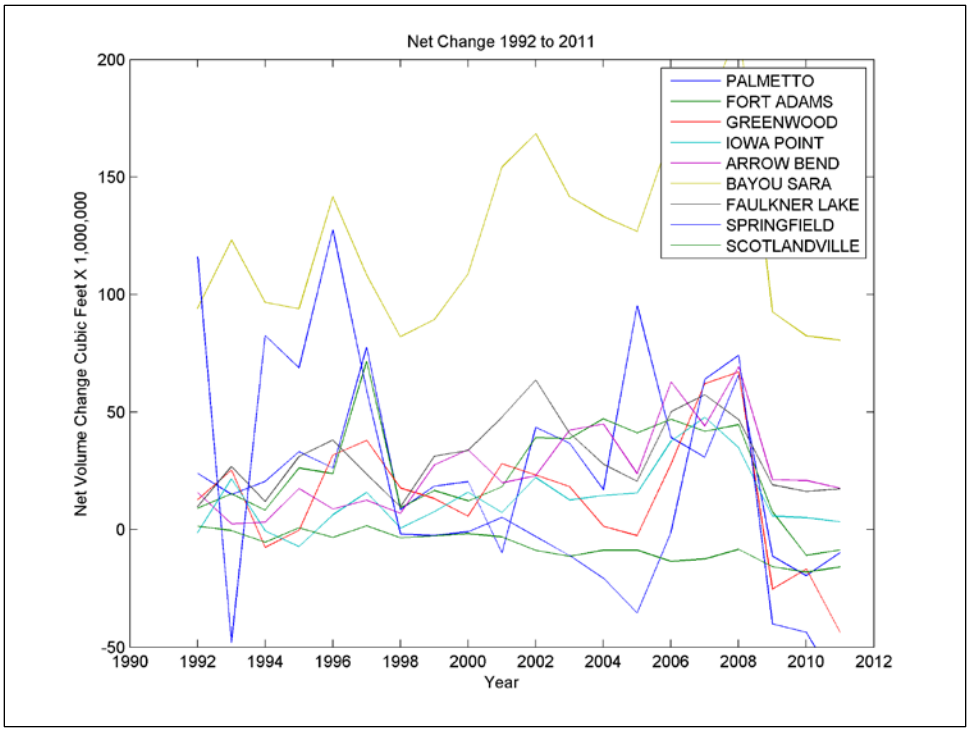

Figure 4.20. Volume change for selected Mississippi River revetments 1992 to 2011.

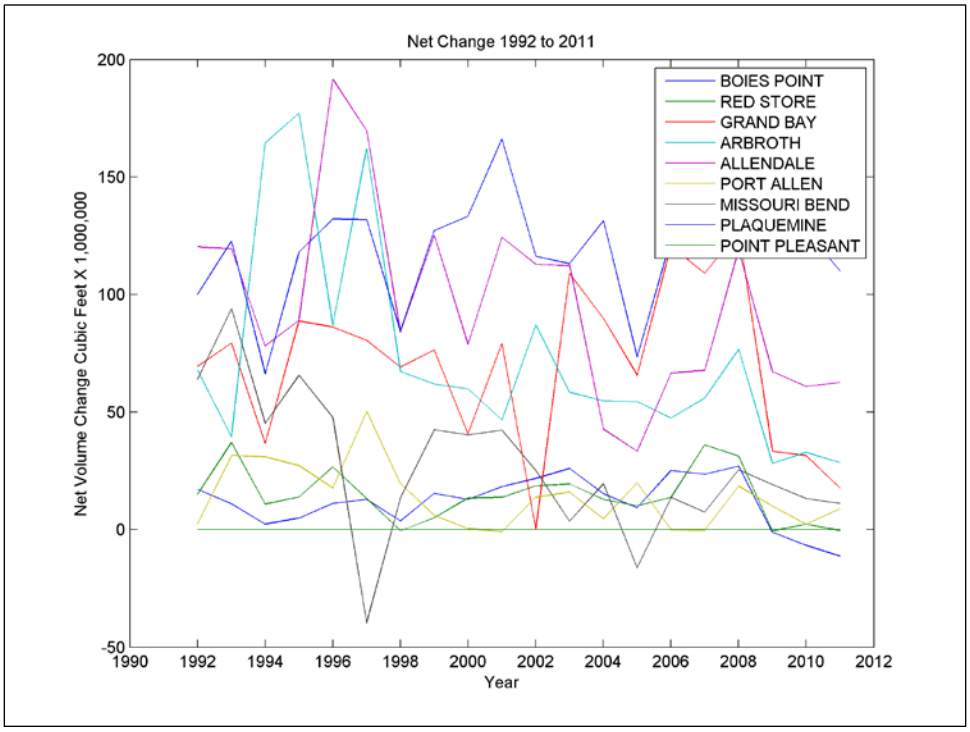

Figure 4.21. Volume change for selected Mississippi River revetments 1992 to 2011.

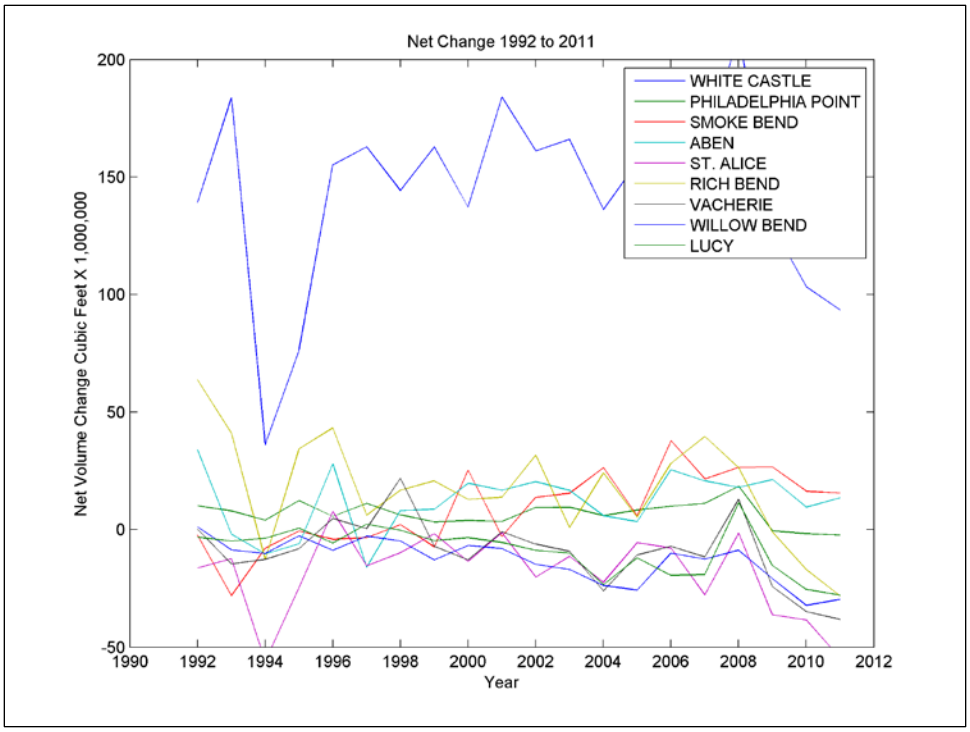

Summary and recommendations

Three methods of analyses have been performed to investigate changes in the Mississippi River that have potential to impact channel capacity. Vegetation analyses have shown significant changes in land use and land cover and over 100,000 acres of flood waters in 2011. It is recommended to extend this analysis with more recent classified satellite imagery to perform a more detailed land class change assessment within the river levee system. These results could provide more accurate acreage changes as well as up-to-date roughness coefficients for modeling efforts.

Selected section computations of channel conveyance have shown that areas of shoaling have reduced channel capacity. However, full-scale, automated computations are required in order to ascertain the historic total channel capacity changes. River channel cross section surveys are generally performed every 10 yr and have been archived by MVN although individual sections cannot readily be compared due to inconsistencies in surveys ranging from vertical and horizontal datums, traverse base lines, as well as reference bench mark locations.

Yearly cross section surveys are performed at specific range lines for all revetments. Volumetric changes computed from these surveys have

identified several regions of predominant shoaling. The highest amount of shoaling was not in revetment locations in the near vicinity of the ORCC. The Carr Point revetment is adjacent to the Auxiliary Structure, but the large sand bar in the main river channel is not captured well in the survey data. The regions of highest shoaling are all downstream of the ORCC and are potentially locations of reduced river discharge capacity. The 2011 volumes show the most shoaling at the Plaquemine and White Castle locations followed by Bayou Sara and St. Gabriel. The most scour occurred at the Poydras revetment. The yearly results demonstrate the frequency and change of the river channel. One location can experience a large amount of shoaling in one year followed by a high degree of scour the next year.

Scour and shoal quantities are based upon survey sections that do not extend bank to bank. Due to the increasing significance of the quantification of the volume of sediment transported by the river, it is recommended to capture full river channel geometry on a more frequent basis. Efforts could begin with extending the yearly range surveys across the river channel to provide a complete data set which could be analyzed for sediment volume computations. These surveys could then be used to compute scour and shoaling across the width of the river channel, provide a more accurate assessment of the river's changing capacity, and serve as essential data sets in support of water level and sediment transport modeling.

5 Multidimensional Modeling Analysis

Analytic considerations of ORCC sediment diversions

Important terms

This section provides some basic, but important, analytic considerations associated with sediment diversions in general, and the ORCC in particular. Before embarking on this discussion, however, two important terms should be defined: sediment diversion coefficient and sediment diversion efficiency.

Definition of the sediment diversion coefficient

To quantify the effects of sediment diversions, it is useful to define dimensionless parameters that characterize the rate of sediment diversion by individual diversions (or groups of diversions) and potential impacts on river channel stability downstream of the diversion. To this end, it is convenient to adopt the concept of a sediment diversion coefficient from the HEC-6 1D sedimentation modeling computer program (USACE 1991)[1]. This coefficient (δ_{SD}) is defined (Equation 5-1) as the ratio of the average sediment concentration (C) in the diverted flow to the average sediment concentration in the approaching river flow, where *Diversion* and *River* refer to reference cross sections where these quantities will be measured. For computational purposes, this coefficient may be defined in terms of water discharge (Q) and sediment load (Q_S):

$$\delta_{SD} = \frac{C_{Diversion}}{C_{River}} = \frac{\left(Q_S / Q\right)_{Diversion}}{\left(Q_S / Q\right)_{River}} \tag{5-1}$$

Thus, if the fraction of the river discharge diverted and the fraction of the sediment load diverted are equal, the sediment diversion coefficient would be 1. This is generally the case for homogenously distributed fine sediments transported as wash load. However, lower or higher coefficient values are possible for bed material loads which exhibit significant vertical

[1] The sediment diversion coefficient and closely related concepts also appear in the literature as "sediment-water ratio" and "sediment diversion (concentration) ratio."

and lateral variations within a cross section. In an HEC-6 model, the sediment diversion coefficient is defined as a function of grain size and diversion discharge. The diverted sediment load at any simulation time-step can be defined by Equation 5-2 where $\delta_Q$is the fraction of river discharge diverted. Thus, higher values of the coefficient result in greater diversions of sediment, other factors being equal.

$$\left(Q_S\right)_{Diversion} = \delta_{SD}\left(Q_S\right)_{River}\delta_Q \tag{5-2}$$

where:

$$\delta_Q = Q_{Diversion}/Q_{River}$$

The locations of the reference cross sections and the periods of measurement both influence the value of the coefficient. Typically, the reference section in the river will be located immediately upstream of the diversion, the location most appropriate for analysis of diversion behavior and 1D sedimentation modeling. For the purposes of this report, a single reference section in the Mississippi River upstream of the complex, section 26 in Figure 5.1, was selected to simplify comparison of individual diversions to each other and to the complex as a whole. Additionally, the reference sections for the diversions, sections 27, 29, and 32 in Figure 5.1, were selected as near as practical to the entrances to the inflow channels to characterize the removal of sediment from the Mississippi River. Thus, the computed coefficient accounts for both sediment stored in the inflow channels and sediment passed through to the outflow channels.

Except for the rare case of steady flow and steady sediment transport, determination of meaningful coefficient values requires averaging over time periods greater than the average transit time of sediment particles between the reference cross sections. Any scour and deposition that occurs between the reference sections will also influence the value. Additionally, stage drawdown associated with opening of a diversion may increase sediment loads at the upstream reference section in the river. In most cases, the most reliable approach to determining the coefficient value is to sum flows and sediment loads by grain size at both reference sections over moderate periods (hours to days) of nearly constant flow and divide by the period of diversion operation to determine a mean value.

Figure 5-1. Reference cross sections used in multidimensional models for computation of water and sediment fluxes. Section 26 was adopted as the primary Mississippi River reference section and compared to sections 27, 29, and 32 for computation of sediment diversion coefficients.

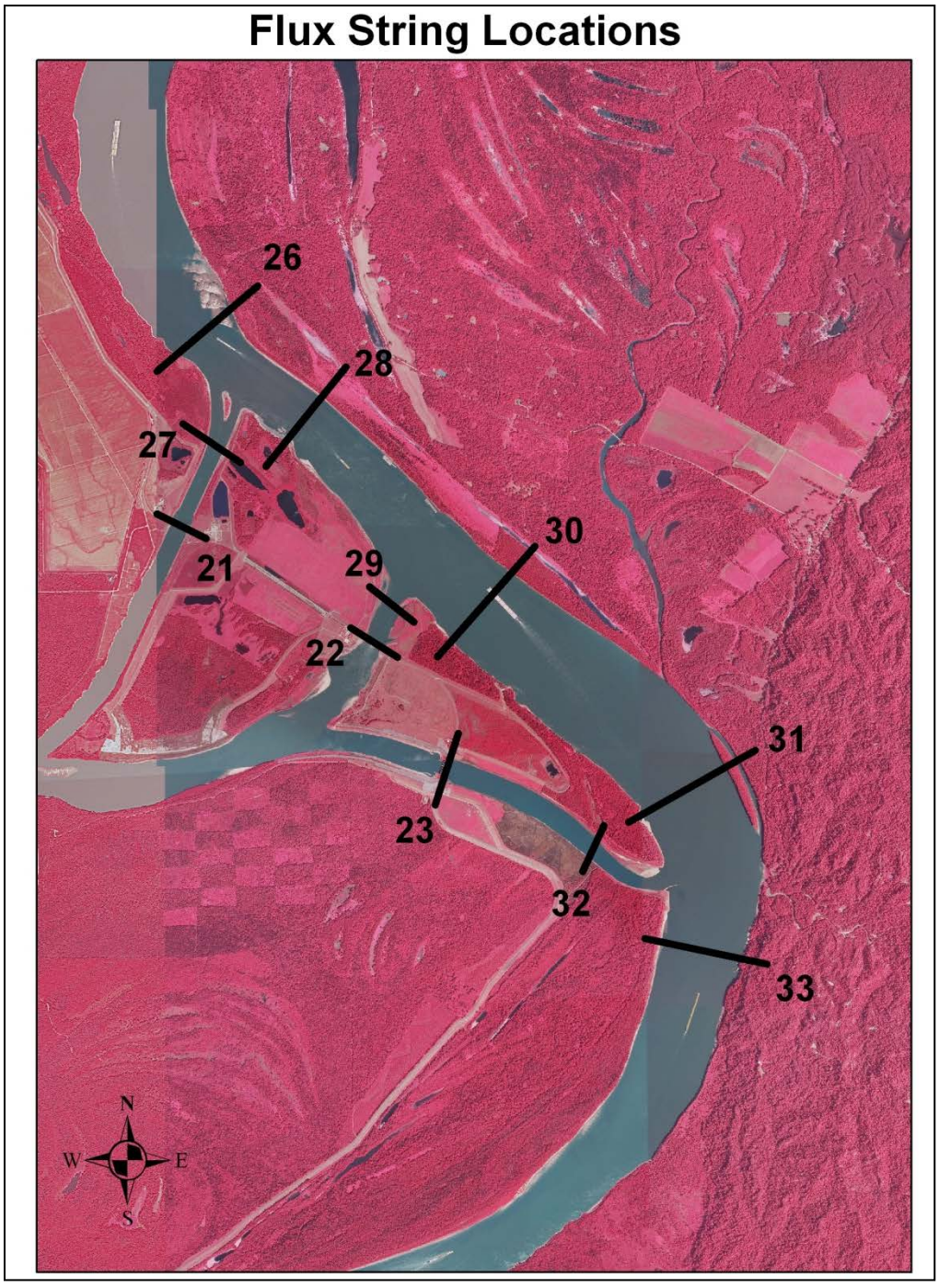

Since the complex is operated to maintain a 70%–30% flow split on a daily basis, the sediment diversion coefficient for each structure is defined by the mean daily values for each individual structure considering only days

on which the structure is diverting flow. As so defined, the coefficient is a characteristic of the structure and its associated inflow channel.

Definition of sediment diversion efficiency

By accumulating flows and sediment loads over longer periods of time, a sediment diversion efficiency (ϵ_{SD} in Equation 5-3) may be determined that incorporates the impacts of structure operations, variability of sediment supply, and other factors for the entire complex or for individual diversions. Because sediment load is a nonlinear function of water discharge, the value of this ratio may differ significantly from the sediment diversion coefficient defined above. The efficiency characterizes the effectiveness of the complex or individual structures at diverting sediment over longer periods of time (e.g., annually).

$$\epsilon_{SD} = \frac{\left(\sum Q_S \Big/ \sum Q \right)_{Diversion}}{\left(\sum Q_S \Big/ \sum Q \right)_{River}} \tag{5-3}$$

Basic description of diversion effects

In general, sediment diversions can affect river shoaling patterns by either of two different mechanisms:

- Disruption of sand load equilibrium —This results when the sediment diversion does not remove the correct amount of sand to ensure that the river downstream of the diversion can return to equilibrium without adjusting the bed elevation.
- River drawdown and momentum loss through the diversion — The presence of a diversion induces a drawdown in the main stem of the river, as well as a discrete reduction in the momentum of the main stem of the river (due to the loss of momentum to the diversion). These adjustments can result in increased scour upstream of the diversion and increased deposition downstream of the diversion.

Each of these mechanisms is discussed in greater detail below, together with their specific application to the ORCC.

Diversions and sediment equilibrium

In general, the noncohesive bed material load, typically sand and gravel, in a river is related to the capacity of the river to transport sediment (Bagnold 1966). Hence, if a diversion is placed in a river, the amount of bed material diverted with the water can have a significant influence on the aggradational or degradational trend of the river bed downstream of the diversion. If the diversion extracts too little bed material load, the amount remaining in the river will be greater than the transport capacity of the river, and downstream aggradation will occur. Conversely, if the diversion extracts too much bed material load, the amount remaining in the river will be less than the transport capacity of the river, and downstream degradation will occur.

An analytic equation has been developed by Letter et al. (2008) that provides an estimate of the sediment diversion efficiency that is required to maintain an equilibrium river bed downstream of a diversion (i.e., the equilibrium sediment diversion efficiency). The equation assumes that the river upstream of the diversion is in sediment equilibrium with the bed and that a power law relationship exists between river discharge and total sediment concentration:

$$C_{BML} = AQ^{\alpha} \tag{5-4}$$

The equilibrium sediment diversion efficiency is given as follows:

$$\epsilon_{SD.EQ} = \frac{1}{\delta_Q}\left[1-\left(1-\delta_Q\right)^{\alpha+1}\right] \tag{5-5}$$

where:

A = the coefficient in the power law bed material load equation
C_{BML} = the bed material load expressed as a the cross-section averaged concentration
$\epsilon_{SD.EQ}$ = the equilibrium sediment diversion efficiency
Q = the river discharge
α = the exponent in the power law sand concentration equation
δ_Q = the fraction of total river flow diverted.

This equation can be used to provide an estimate of the equilibrium sediment diversion efficiency required at the ORCC to ensure bed equilibrium downstream of the complex.

A sand rating curve for the Mississippi River at Vicksburg has been developed by Copeland (2009). It is given as follows:

$$C_{BML} = 0.046Q^{1.09} \tag{5-6}$$

Assuming this rating curve is representative of the Mississippi River at near equilibrium state, it is possible to approximate the equilibrium sediment diversion efficiency required at the ORCC for the sand load to remain in equilibrium with the residual flow in the river (i.e., the incoming flow minus the diverted flow).

The long-term average water withdrawal at the ORCC is approximately 23% of the incoming Mississippi River flow. Therefore, from Equation 5-5:

$$\epsilon_{SD,EQ} = \frac{1}{0.23}\left[1-\left(1-0.23\right)^{1.09+1}\right] = 1.8 \tag{5-7}$$

Hence, this simple, analytic method suggests that a sediment diversion efficiency of approximately 1.8 is required at the ORCC in order to maintain channel equilibrium downstream of the complex. This means that the average sand concentration in the diverted flow must be 80% greater than the average concentration in the river.

Brown et al. (2013) demonstrated that the above procedure underestimates sediment diversion requirements during the initial response of a channel to a new diversion. Over time, sediment diversion requirements decrease and converge on the value proposed by Letter et al. (2008). The Mississippi River has been adjusting over a period of decades to both the regulated diversion at the ORCC, and before construction of the ORCC, to the unregulated diversion through Old River. Therefore, the equilibrium sediment diversion efficiency is unlikely to be greater than 1.8.

It should be noted that measured sediment concentration data exhibit significant variability. Therefore, the sediment concentration rating curve defined by Equation 5-6 is not the only reasonable interpretation of the available data. Alternate ratings could produce slightly higher or lower

estimates of the equilibrium sediment diversion efficiency. Additionally, daily variations in the fraction of river discharge diverted by the ORCC add some uncertainty to the estimate.

River drawdown and momentum loss through the diversion

When a diversion is placed in the river, it provides an additional outlet for the flow. This effectively represents a discrete reduction in the resistance to flow, inducing a drawdown in the main stem of the river. This drawdown will tend to increase the slope of the energy grade line of the river upstream of the diversion, thereby increasing the bed shear stress. Although the maximum effect is at the cross section just upstream of the diversion, in a mild-gradient, deep river such as the Mississippi, the drawdown will influence the river many miles upstream of the diversion site.

At the diversion site, there is also a discrete loss of momentum to the diverted flow. This causes the water surface elevation just upstream of the diversion to drop slightly, relative to the downstream elevation. This effect adds to the drawdown effect.

In order to illustrate this effect in the Mississippi River at the ORCC, four steady state hydrodynamic simulations were conducted with AdH. For each simulation, the Mississippi River inflow at the upstream boundary was specified as 984,000 cfs. The first simulation had no flow diversion at ORCC. Simulations 2–4 each diverted 188,000 cfs: simulation 2 diverted the flow through the hydropower structure, simulation 3 through the low sill structure, and simulation 4 through the auxiliary structure. Figures 5.2–5.4 represent the percent increase in bed shear stress for each of the diversion simulations 2–4 relative to the no-diversion simulation. That is, the figures show the impact of the diversion on the bed shear stress in the Mississippi River.

Note that the presence of the ORCC flow diversions induces a 50% to 100% increase in the bed shear stress upstream of the ORCC. Note also that this effect persists for many miles upstream, although it begins to diminish in magnitude. This increase in bed shear stress serves to increase the transport capacity of the river above the equilibrium transport capacity. Since the diversion has been in place for many years, the River has had time to adjust to this increased shear stress by adapting the upstream morphology and/or coarsening the bed.

Figure 5.2. Percent increase in Mississippi River bed shear stress due to the diversion of flow through the hydropower structure.

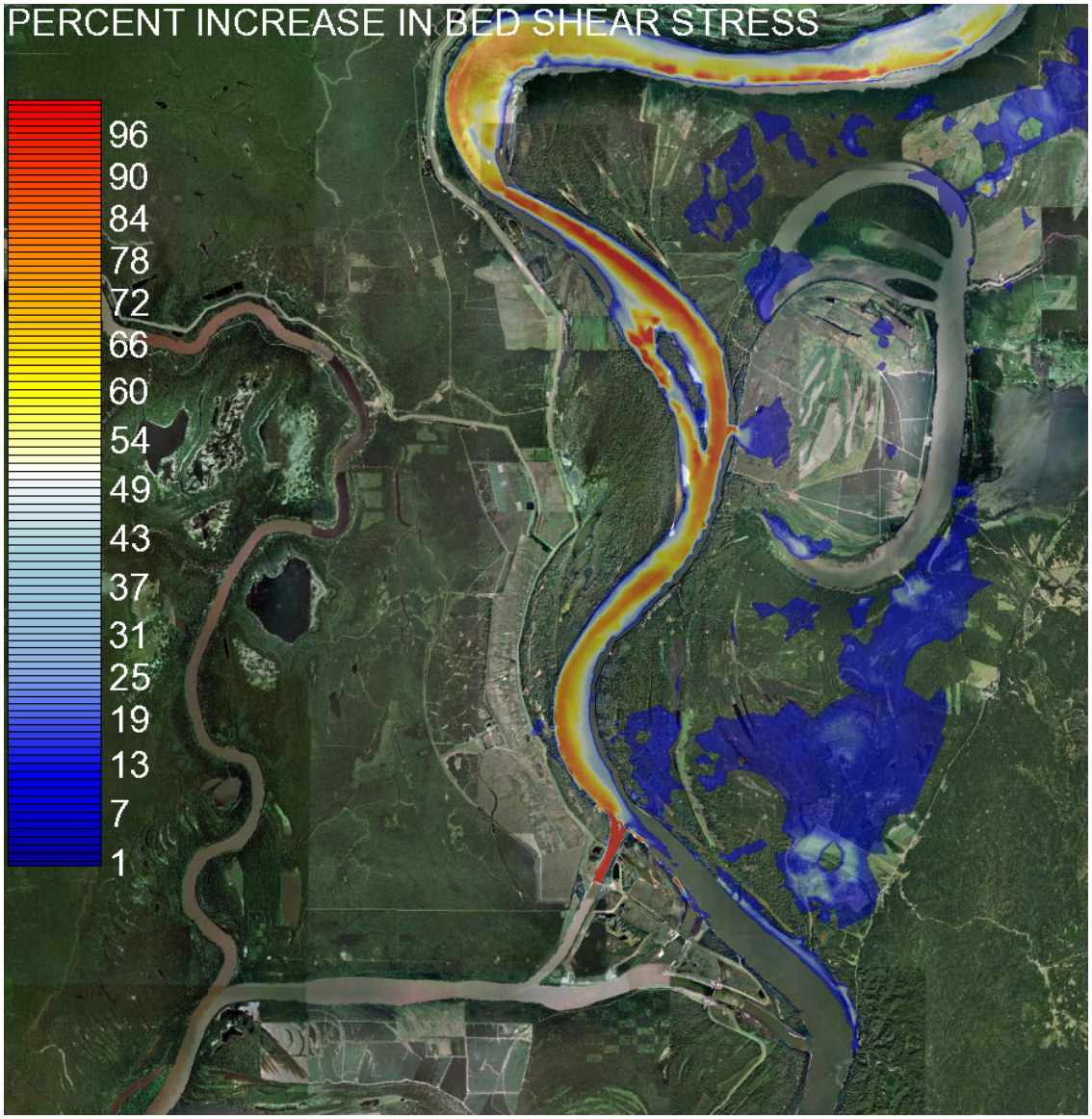

Figure 5.3. Percent increase in Mississippi River bed shear stress due to the diversion of flow through the low sill structure.

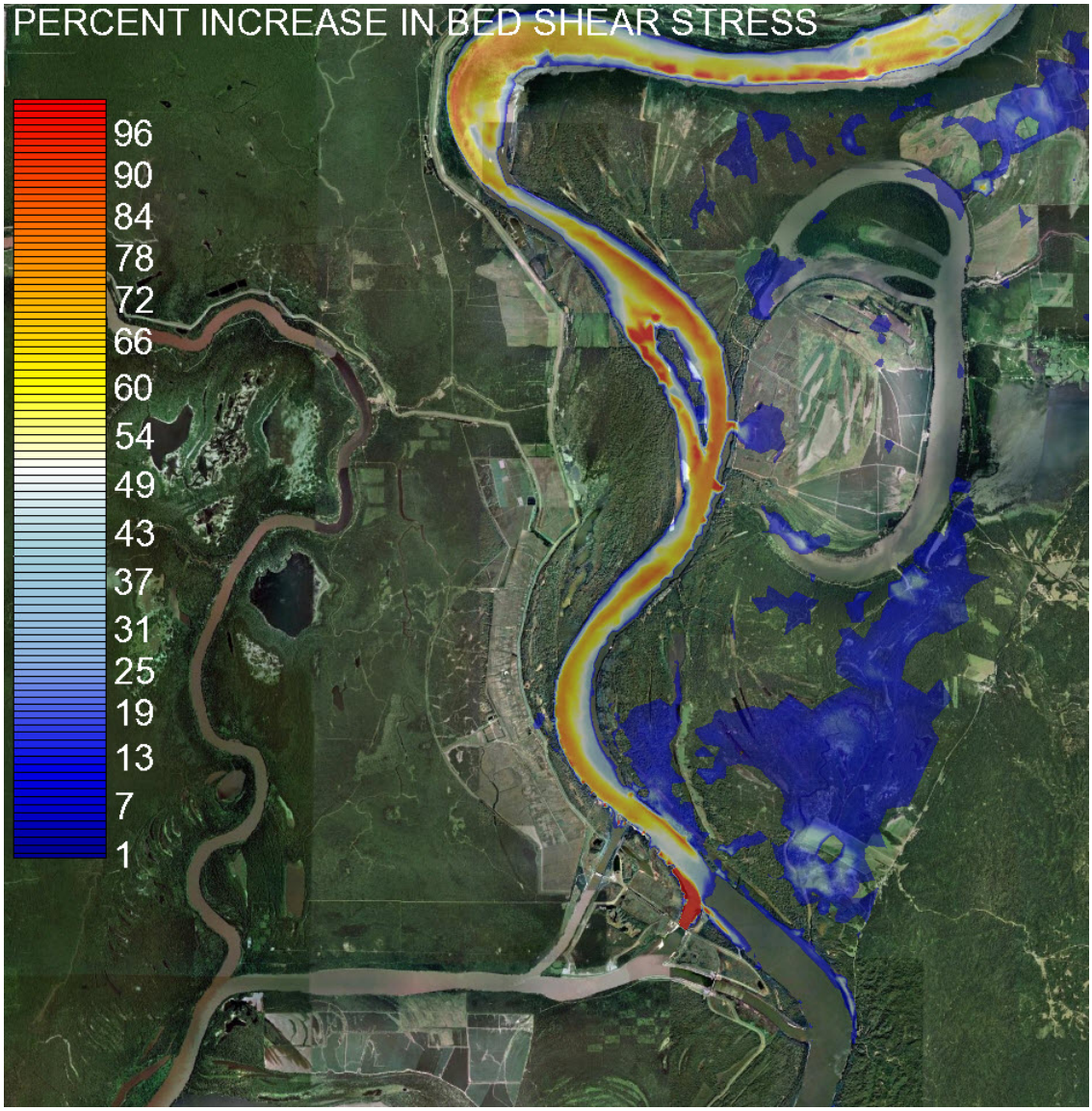

Figure 5.4. Percent increase in Mississippi River bed shear stress due to the diversion of flow through the auxiliary structure.

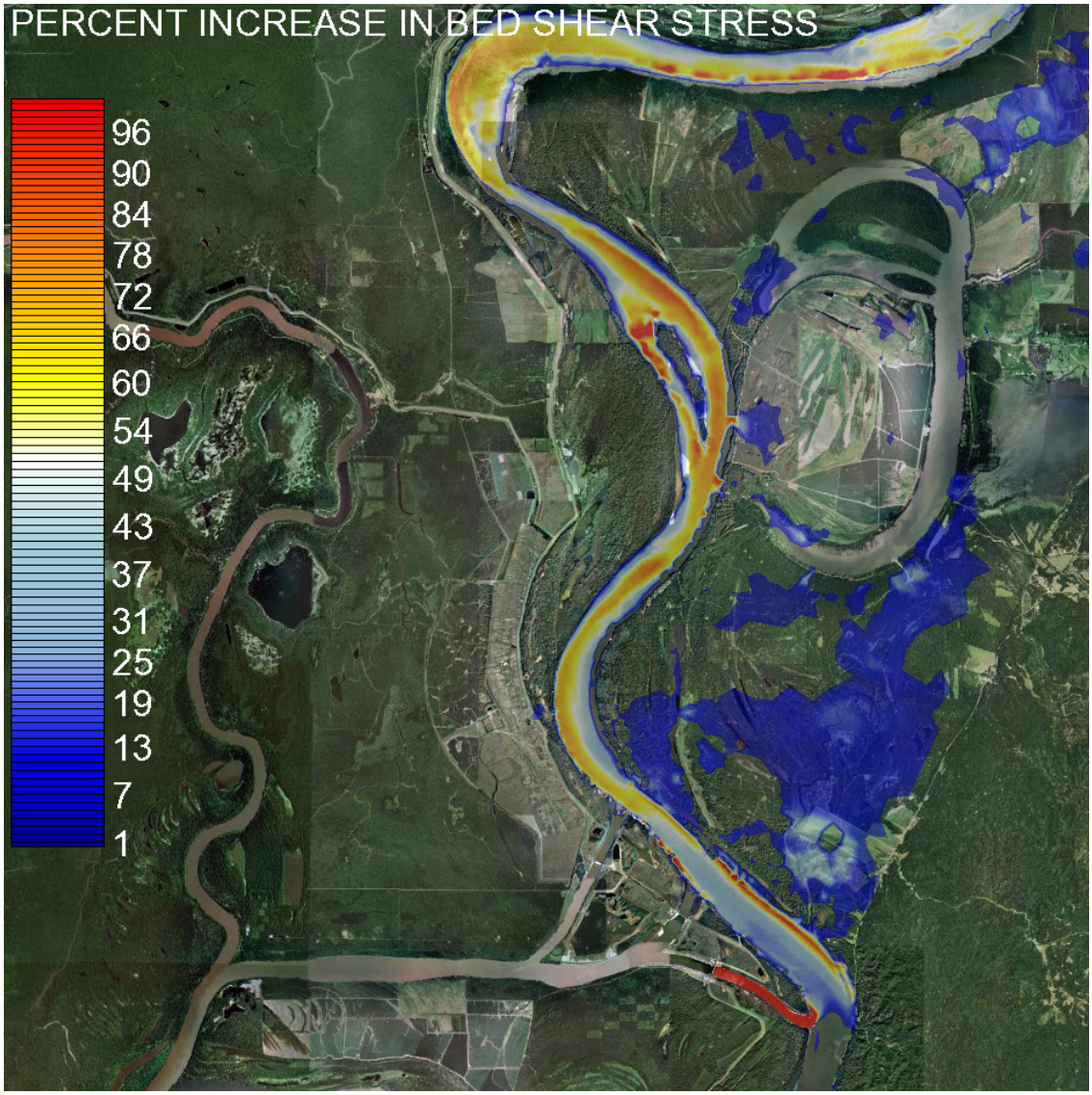

However, the presence of this increased bed shear stress also serves to alter the location where the river stores sediment during the falling limb of the hydrograph. Some of the sediment that would otherwise be stored upstream of the diversion is passed to the downstream side of the diversion. This is likely a significant contributor to the shoal that is observed to form in the river just downstream of the low sill structure.

Figures 5.5 and 5.6 illustrate the local effect on the bed shear stress due to flow passing though each of the structures. Note that these plots indicate that the operation of the auxiliary structure tends to increase the bed shear stress over the observed shoaling site; this implies that the auxiliary structure can be used to scour this site.

Figure 5.5. Percent increase in bed shear stress due to the diversion of flow through the auxiliary structure relative to diversion through the hydropower structure.

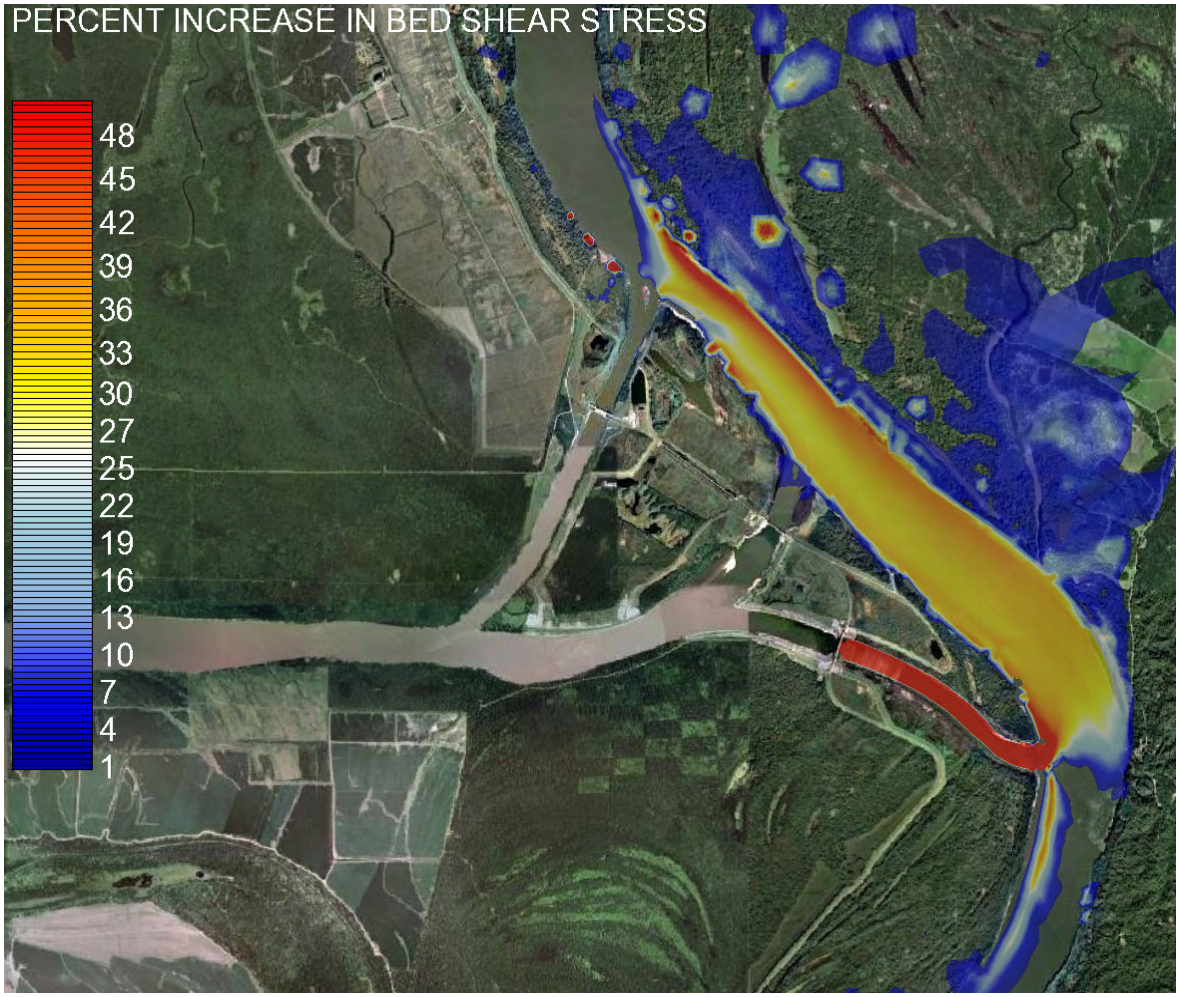

Figure 5.6. Percent increase in bed shear stress due to the diversion of flow through the auxiliary structure relative to diversion through the low sill structure.

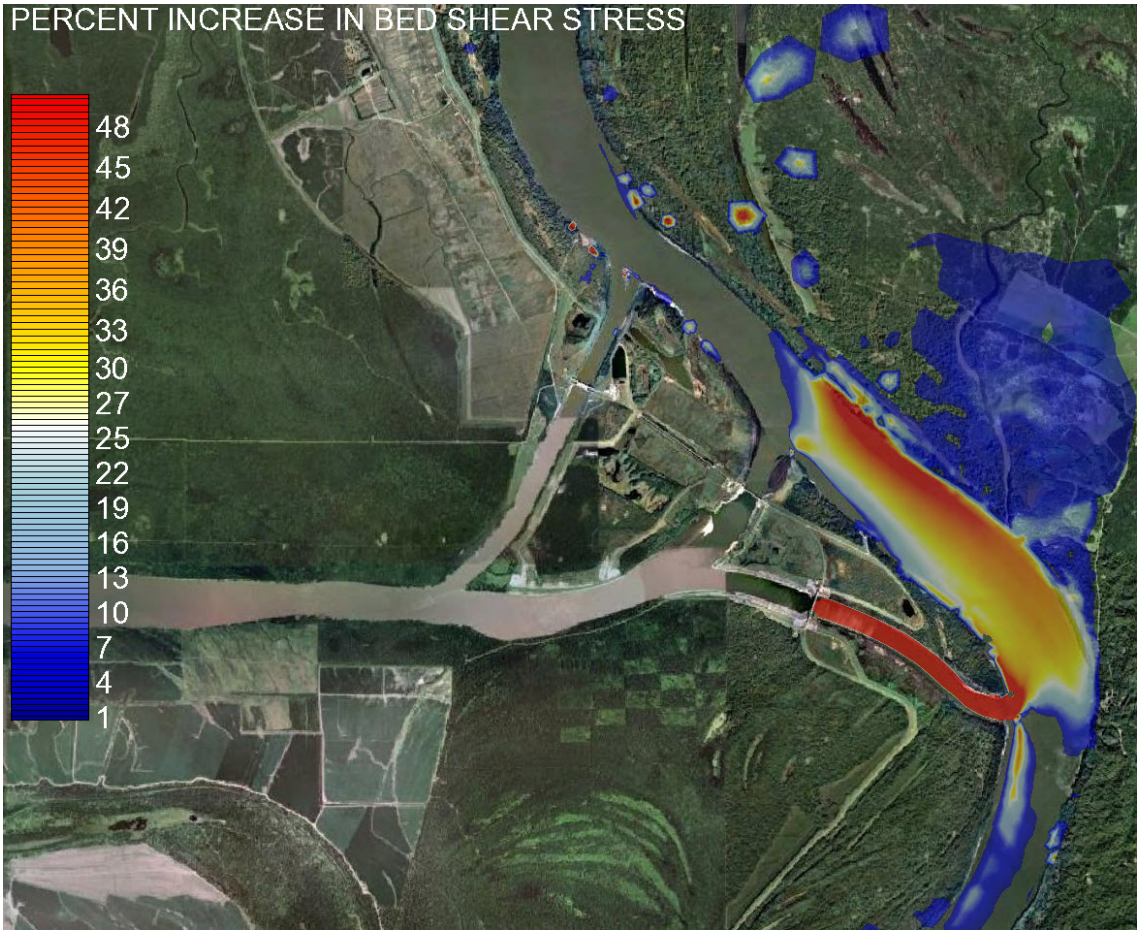

Multidimensional modeling Approach

In general, sediment diversions are multidimensional phenomena. Horizontal and vertical variations in both velocities and sediment concentrations can have a significant impact on the performance of the diversion. In addition, erosion and deposition patterns in the main stem also tend to be spatially variable.

For this study, The AdH 2D model, linked to the SEDLIB sediment model, was applied in depth-averaged mode to analyze the impacts of ORCC operations on sediment transport and morphology in the Mississippi River. The Adh/SEDLIB model is equipped with quasi-3D capabilities that represent the effects of the vertical variation of velocity and sediment in a river with approximate, semianalytic methods.

The Ch3D fully 3D model was also applied (Chapman et al. 1996), but only in a very limited sense. The CH3D model was used to verify that no significant 3D effects are observed in the study area that violate the simplifying assumptions employed in the quasi-3D logic employed in AdH/SEDLIB.

Adaptive Hydraulics modeling

Model description

AdH is a finite element model that is capable of simulating 3D Navier Stokes equations, 2D and 3D shallow water equations, and groundwater equations. It can be used in a serial or multiprocessor mode on personal computers or parallel, high-performance computing systems. The uniqueness of AdH is its ability to dynamically refine the domain mesh in areas where more resolution is needed at certain times due to changes in the flow conditions. AdH can simulate the transport of conservative constituents, such as salt or dye clouds, as well as sediment transport that is coupled to bed and hydrodynamic changes. The ability of AdH to allow the domain to wet and dry as the river stage changes is important for simulating floodplain dynamics within the river system. This tool was developed at the ERDC and has been used to model sediment transport in sections of the Mississippi River, tidal conditions in southern California, and vessel traffic in the Houston Ship Channel, among others.

SEDLIB is a sediment transport library developed at ERDC (Brown et al. 2012). The fundamental architecture of the sediment transport algorithms in SEDLIB are taken from the Ch3D model (Spasojevic and Holly 1994). This architecture is extended in SEDLIB to a more generalized sediment computational engine. It is capable of solving problems consisting of multiple grain sizes, cohesive and cohesionless sediment types, and multiple layers. It calculates erosion and deposition processes simultaneously and simulates such bed processes as armoring, consolidation, and discrete depositional strata evolution.

The SEDLIB library system is designed to link to any appropriate hydrodynamic code. The hydrodynamic code must be capable of performing advection diffusion calculations for a constituent. SEDLIB interacts with the parent code by providing sources and sinks to the advection diffusion solver in the parent code. The solver is then used to calculate both bed load and suspended load transport, for each grain class.

The sources and sinks are passed to the parent code via a fractional step modification of the time-derivative term.

The AdH /SEDLIB sediment model contributes several capabilities to the ORCC analysis:

- Quasi-3D flow and transport formulations, which use analytical and semiempirical methods to approximate the 3D character of the flow and sediment transport phenomena.These include the ability to model the effects of helical flow through a river bendway on the suspended and bed load sediment transport, by utilizing the bendway vorticity transport algorithm given by Bernard (1992).
- Simulation of multigrain class suspended load and bed load sediment transport phenomena. It is also equipped to handle generalized multigrain class bed processes, including armoring, sorting, erosion to a solid boundary, and the storage of discrete depositional strata.
- An unstructured model mesh that permits very high resolution in areas of interest and high fidelity resolution of shoreline geometry only where needed.
- The ability to extend the boundaries sufficiently far from the project area so as not to prescribe the answer, ensuring that the results are not biased by judgments concerning boundary conditions.

Mesh development

The mesh was developed using the Surface-water Modeling System (SMS), a graphical user interface developed by ERDC for increasing the modeling productivity for a variety of U.S. Army Corps of Engineers (USACE) numerical models, including AdH. The model mesh is depicted in Figure 5.7. The base mesh consists of 14,964 base nodes and 29,232 base elements, although more are added by AdH at run time due to dynamic mesh adaption. The model extends from Red River Landing (9 miles downstream of the Auxiliary Entrance Channel) to (24 miles upstream of the Hydropower Entrance Channel). The model extends across the width of the floodplain, measuring 12 miles at its widest point. The mesh includes all of the known river training structures and bank protection measures in the river, including the dike just downstream of the Auxiliary Channel entrance. The horizontal datum for the mesh is NAD83 State Plane Louisiana South. The vertical datum is NAVD88. The bathymetry used to define the model mesh was taken from a composite of survey data from 2006, 2008, and 2010; hence, it does not represent a historical snapshot of the condition of the river.

Figure 5.7. Finite element mesh for AdH/SEDLIB model of the ORCC.

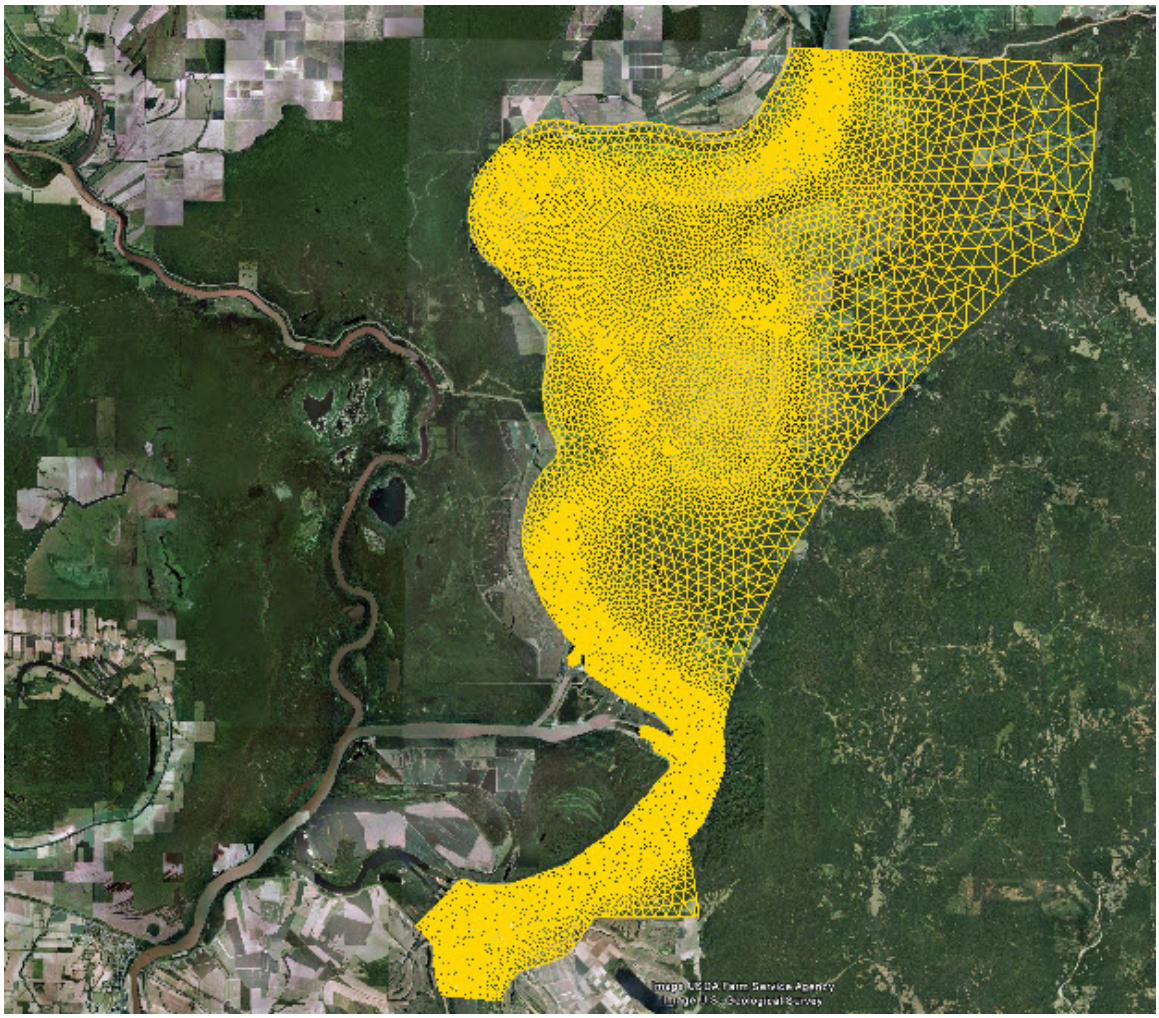

Hydrodynamic boundary condition development

The model was run using observed boundary conditions for January–September of 2010. This corresponds with the ERDC data collection period. The downstream stage boundary is taken from the gage at Red River Landing. The diversion structure water withdrawals at each structure are taken from observed data at the ORCC. The upstream Mississippi River discharge boundary condition is calculated by taking the measured data at Tarbert Landing (near the downstream boundary) and adding back the water withdrawals at the ORCC. The model boundary conditions are given in Figures 5.8 and 5.9.

Figure 5.8. The applied river boundary conditions for January–September 2010.

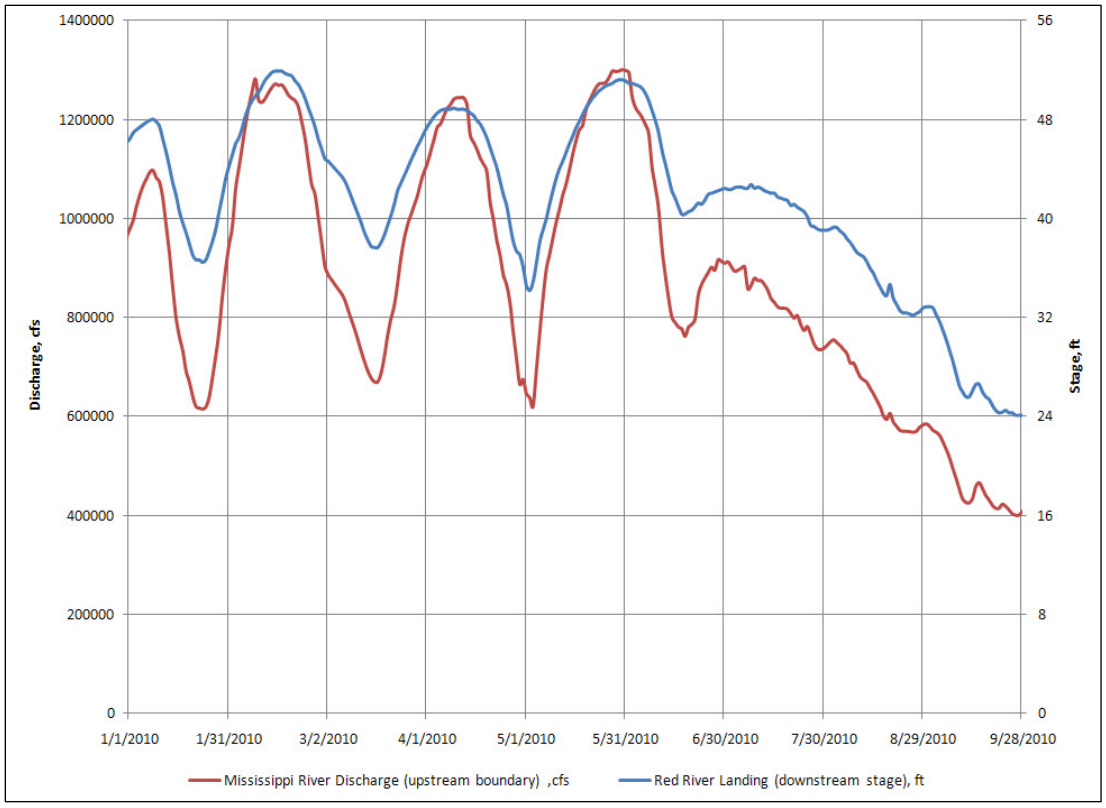

Figure 5.9. The applied structure discharges for January–September 2010.

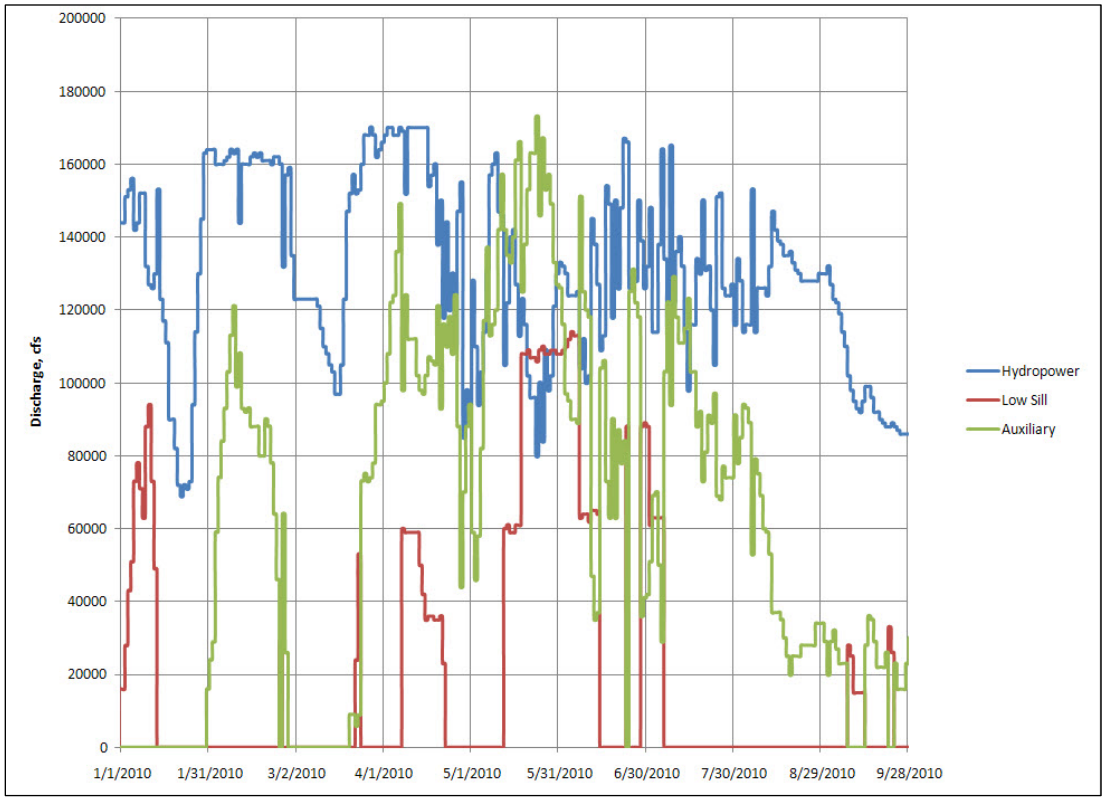

The model bed roughness is given by two different methods: Manning's *n* and an unsubmerged, rigid vegetation loss equation. The bed roughness in the river is approximated with a Manning's *n* value of 0.025, and the roughness of submerged structures or rock outcrops is given with a Manning's *n* of 0.035. (Note that AdH is equipped with a friction algorithm that automatically adjusts the friction for variations in water depth).

The friction loss in the flood plains is given by an algorithm that is appropriate for the estimation of loss due to unsubmerged, rigid vegetation (Walton and Christensen 1980). The algorithm yields the appropriate functional relationship between friction loss and depth for flow through a vegetated floodplain, and hence is more appropriate than Manning's *n* for characterizing this roughness (the relationship between friction loss and depth in Manning's equation is only appropriate for roughness elements that are much smaller than the depth of flow). For the ORCC mesh, the parameterization of this loss is given by the following coefficients:

- Equivalent roughness height of undergrowth = 0.05 m
- Average trunk diameter = 1.0 m
- Average tree density = 0.02 trees/m^2.

Sediment boundary condition and initial condition development

In an alluvial river, the transport of sediment is tied very closely to the reservoir of sediment available in the sediment bed. Therefore, the characterization of the sediment bed is of primary importance.

Analysis of the bed samples shows a wide range of sand classes present in the bed, and some gravel classes. Based on this data, and on some experimental simulations to investigate the behavior of the sediment bed, the following sediment classes and initial bed characteristics were chosen for the ORCC simulation (Table 5.1). Grain size classes were defined according to the American Geophysical Union (AGU) scale (Lane 1947). The specific gravity of all sediment classes was set to 2.65 (typical value for quartz sands), and the in situ porosity of the sediment bed was set to 0.35.

Table 5.1. AdH/SEDLIB ORCC sediment properties.

AGU Grain Size Class	Geometric Mean Grain Size (mm)	Bed Fraction (top 5 m bed thickness)	Bed Fraction (below 5 m bed thickness)
Very fine sand (VFS)	.088	.01	.08
Fine sand (FS)	.177	.01	.08
Medium sand (MS)	.354	.63	.58
Coarse sand (CS)	.707	.14	.13
Very coarse sand (VCS)	1.41	.01	.03
Very fine gravel (VFG)	2.83	.01	.01
Fine gravel (FG)	5.66	.01	.09

The inflowing sediment boundary was given as the local equilibrium value. That is, the model computes an equilibrium concentration for each grain class at the model boundary, and that value is used as the boundary condition for that time step.

The sediment bed was initialized by running the model through the entire January–September 2010 hydrograph, without allowing the bed elevation to change. This adjusted the grain size distribution to vary spatially in a manner consistent with the local bed shear stress regime. This adjusted bed grain class distribution was then used as the initial condition for all subsequent simulations; during these simulations, the bed elevation was permitted to change in the study area so that the changing morphology would interact with the flow field.

Model verification

Suspended sediment flux and bed load flux verification

The suspended sediment load and bed load were measured in the model at several cross sections in the river. These cross sections, presented in Figure 5.1, were selected to correspond with flux observation cross sections used by the field data collection crew. The numbering convention is associated with internal AdH numbering protocols. Table 5.2 relates these cross section numbers to identifying descriptions.

Table 5.2. Names of AdH flux observation cross sections.

Cross Section Number	Description
21	Hydropower Structure
22	Low Sill Structure
23	Auxiliary Structure
26	Mississippi River Upstream of Hydropower
27	Hydropower Channel Entrance
28	Mississippi River Downstream of Hydropower
29	Low Sill Channel Entrance
30	Mississippi River Downstream of Low Sill
31	Mississippi River Upstream of Auxiliary
32	Auxiliary Channel Entrance
33	Mississippi River Downstream of Auxiliary

Figures 5.10–5.15 show comparisons of the modeled and observed suspended load and bed load at cross sections 26, 27, 28, 29, 32, and 33.

Figure 5.10. Modeled and observed fluxes in the Mississippi River upstream of hydropower.

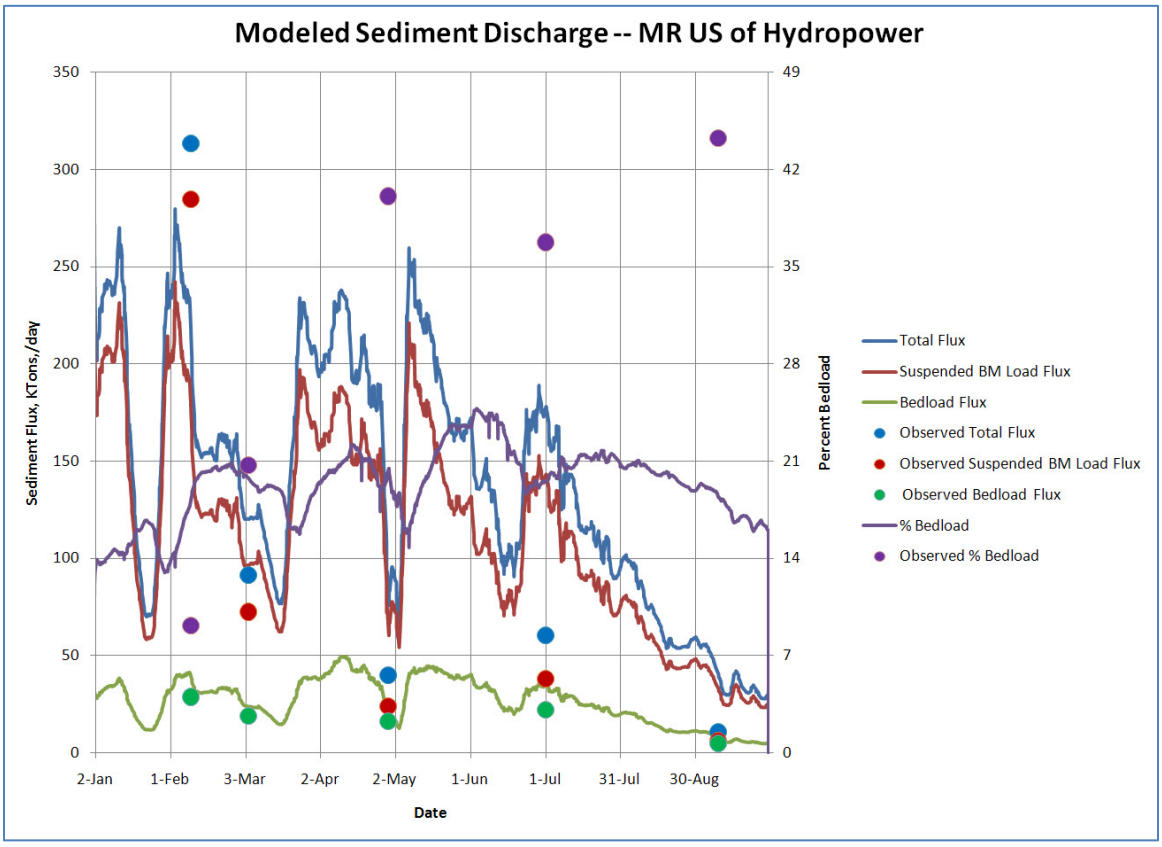

Figure 5.11. Modeled and observed fluxes in the hydropower channel entrance.

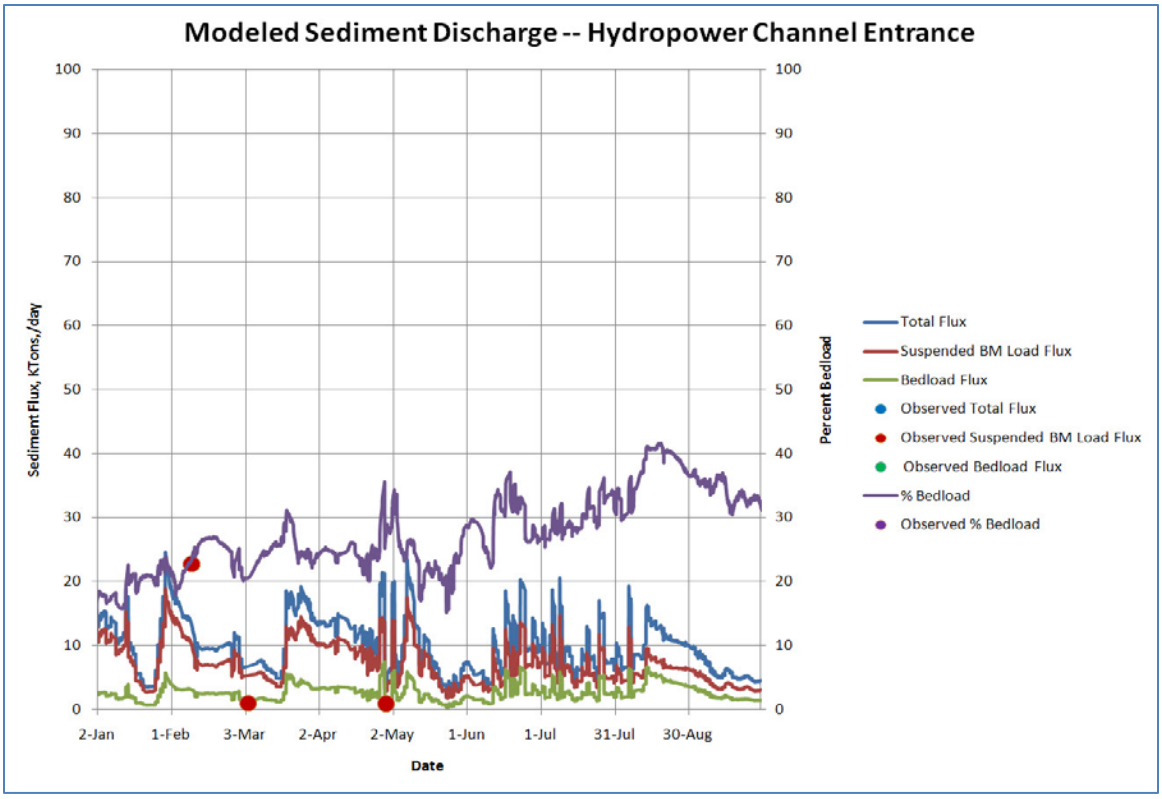

Figure 5.12. Modeled and observed fluxes in the Mississippi River downstream of hydropower.

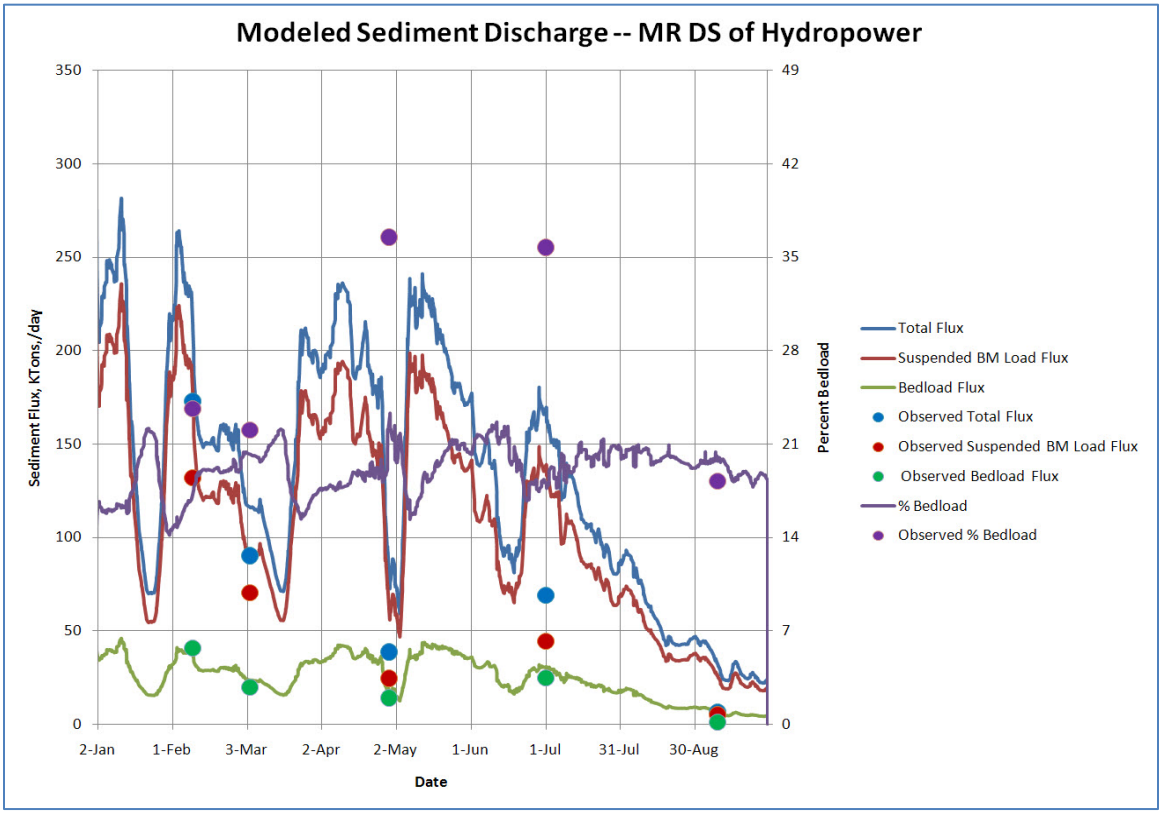

Figure 5.13. Modeled and observed fluxes in the low sill channel entrance.

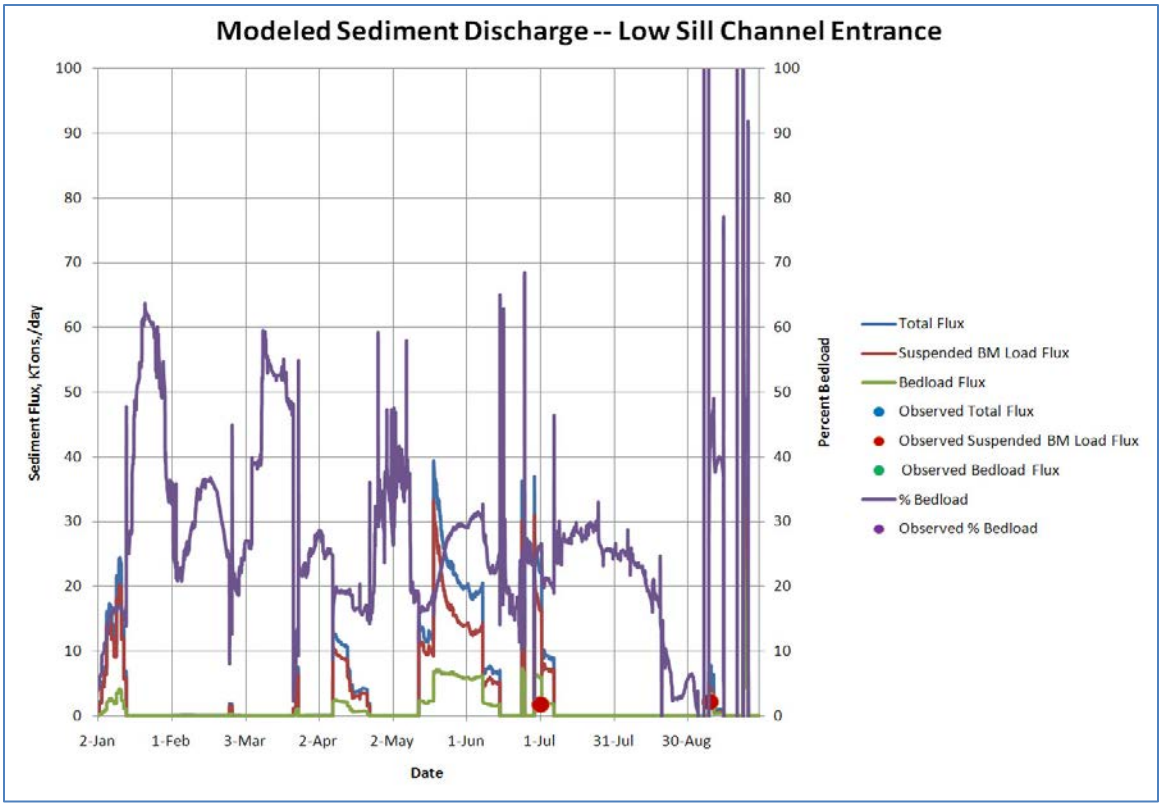

Figure 5.14. Modeled and observed fluxes in the auxiliary channel entrance.

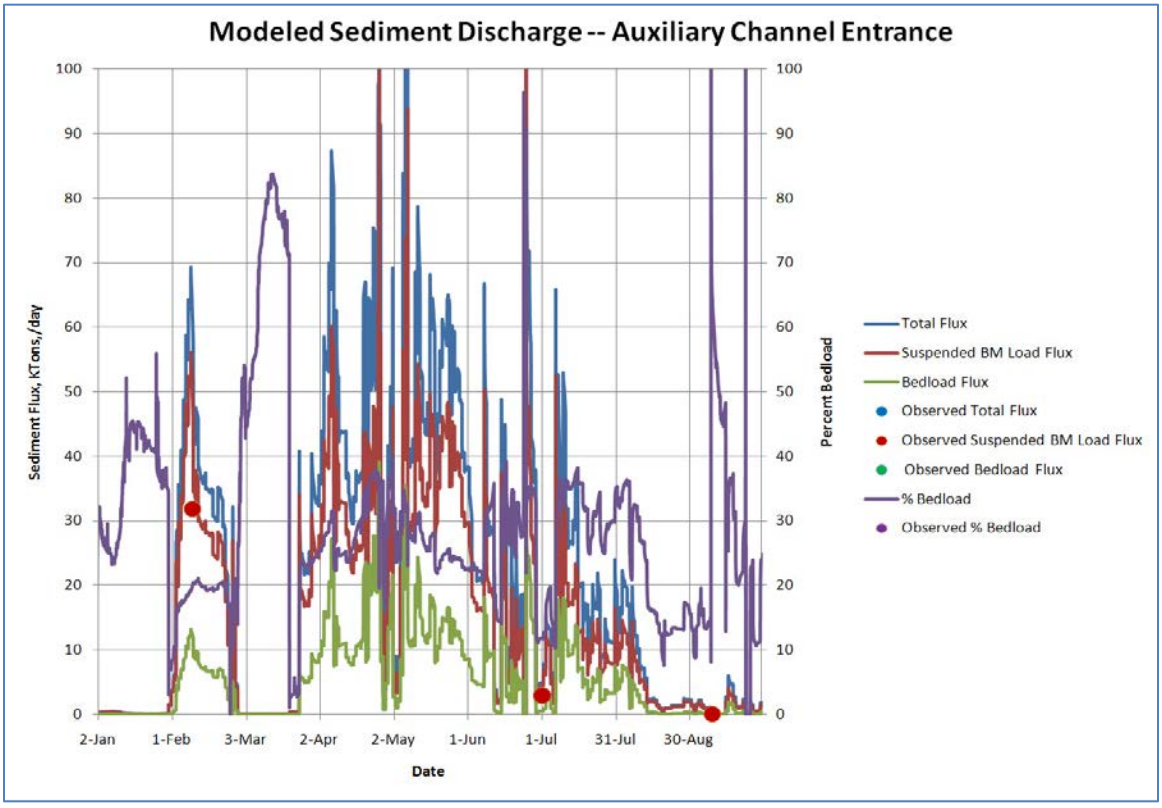

Figure 5.15. Modeled and observed fluxes in the Mississippi River downstream of auxiliary.

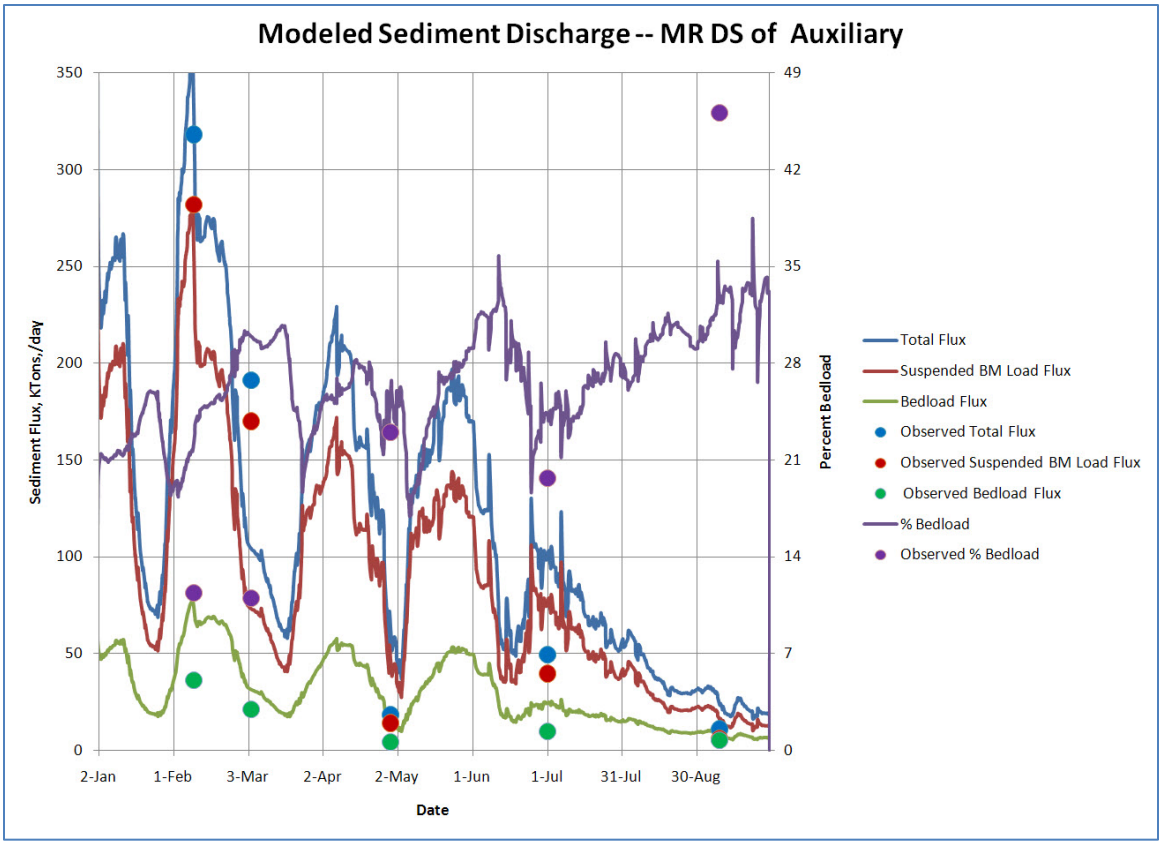

The model results show good agreement with the bed load measurements at the Mississippi River ranges. The results show agreement with the trends of the suspended sediment flux measurements, but the quantitative comparison sometimes differs by as much as 100,000 TPD. Note, however, the good agreement between both model and field data for the 1 February data collection event, at both the downstream of hydropower Mississippi River range, and the auxiliary channel entrance range. This indicates that the auxiliary channel is extracting sediment from the river in the same proportion as the prototype. Also, the total modeled flux of sediment passing the upstream of hydropower Mississippi River range for the January–September 2010 hydrograph is 37.4 million tons, and the total flux predicted by the rating curve given in Equation 5-6 for the January–September of 2010 is 40.6 million tons.

Without better knowledge of the prior bed state of the river, and without better measurement of sediment inflow, it is not likely that better meaningful agreement between model and field measurements than the ones depicted here can be achieved. For example, inflowing sediment and the bed gradation could be carefully calibrated to match the data better,

but the resulting model would have no greater predictive skill than the one give here; it would merely be better tuned to match a specific data set. Instead, what is needed is a model that displays the kinds of behavior seen in the river and responds properly to forcing (i.e., that reacts to forcing the way the river does). This model meets the requirements and is appropriate for base and plan comparisons.

General observations

Figures 5.16 and 5.17 show the modeled bed elevation in the study area for 1 January and 1 October of 2010. Note that, because the initial model bathymetry was derived from a composite of several surveys, the initial state of the bed in the model is not identical to that observed at the beginning of 2010. For this simulation, some scour of the channel downstream of hydropower and the shoal between the low sill and auxiliary channels has occurred, and some infilling of the thalweg just upstream of the auxiliary channel entrance and shoaling of the bar on the right descending bank downstream of the auxiliary channel is evident.

Figures 5.18 and 5.19 show the d_{50} of sand at the bed surface. Figure 5.18 depicts the bed condition on the rising limb of the hydrograph at approximately 1 million cfs river discharge. Figure 5.19 shows the bed condition on the falling limb of the hydrograph at approximately 1 million cfs discharges. Note the additional bed armoring in the falling limb condition. This is related to the hysteresis of the sediment flux through a hydrograph. The richer sediment on the rising limb correlates to a generally finer d_{50} in the surface bed material; the coarser d_{50} on the falling limb indicates bed armoring.

Figures 5.20 and 5.21 show the modeled typical spatial distribution of the suspended sediment and bed load sediment concentrations, respectively. Note that both concentration fields respond to the curvature of the channel by focusing the highest concentrations at the inside bank of the meander bends. This phenomenon is the primary reason for the difference in the diversion efficiencies of the three ORCC structures.

Figure 5.16. Modeled bed elevation at the beginning of the simulation (1 January 2010).

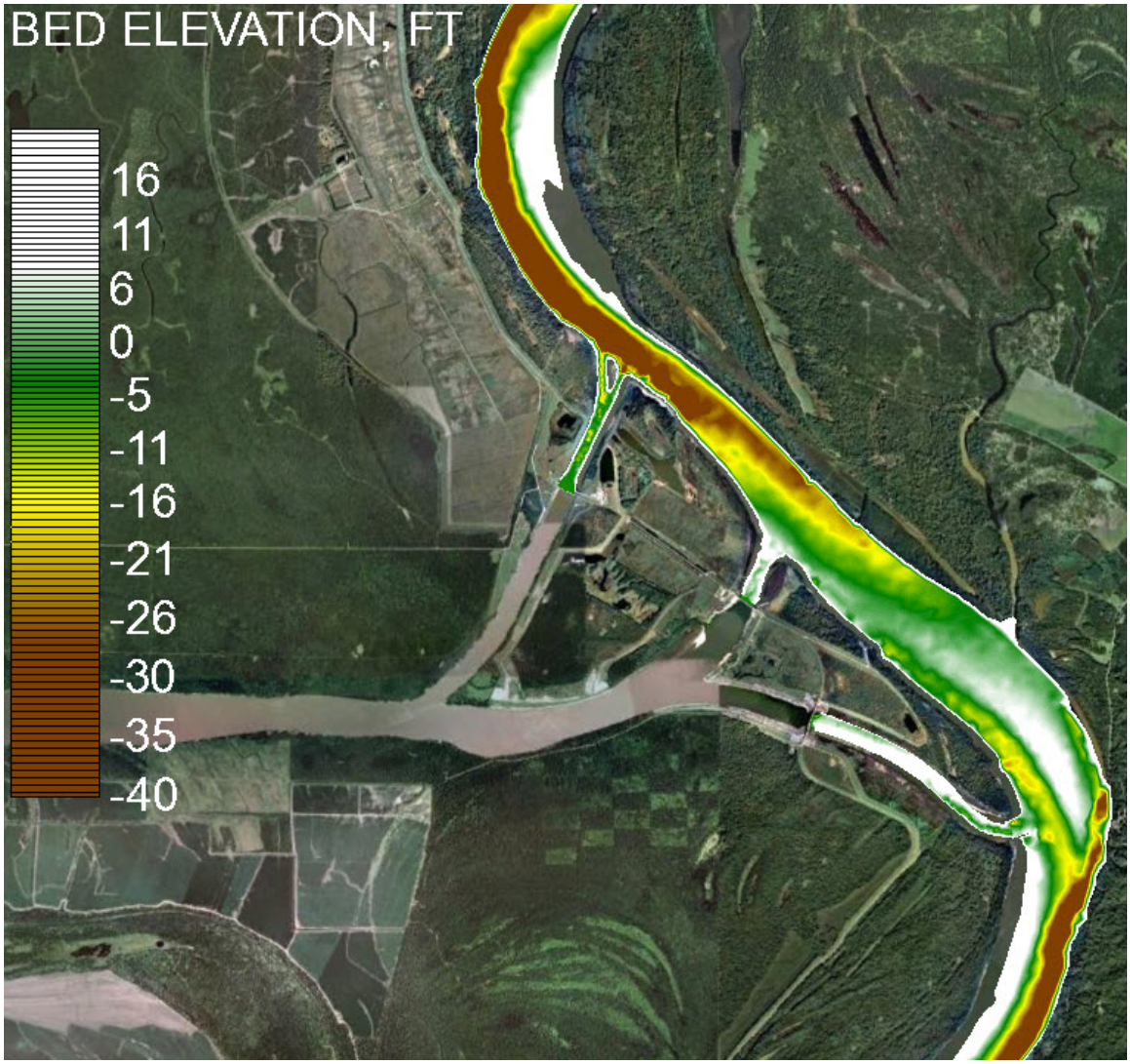

Figure 5.17. Modeled Bed elevation at the end of the simulation (1 October 2010).

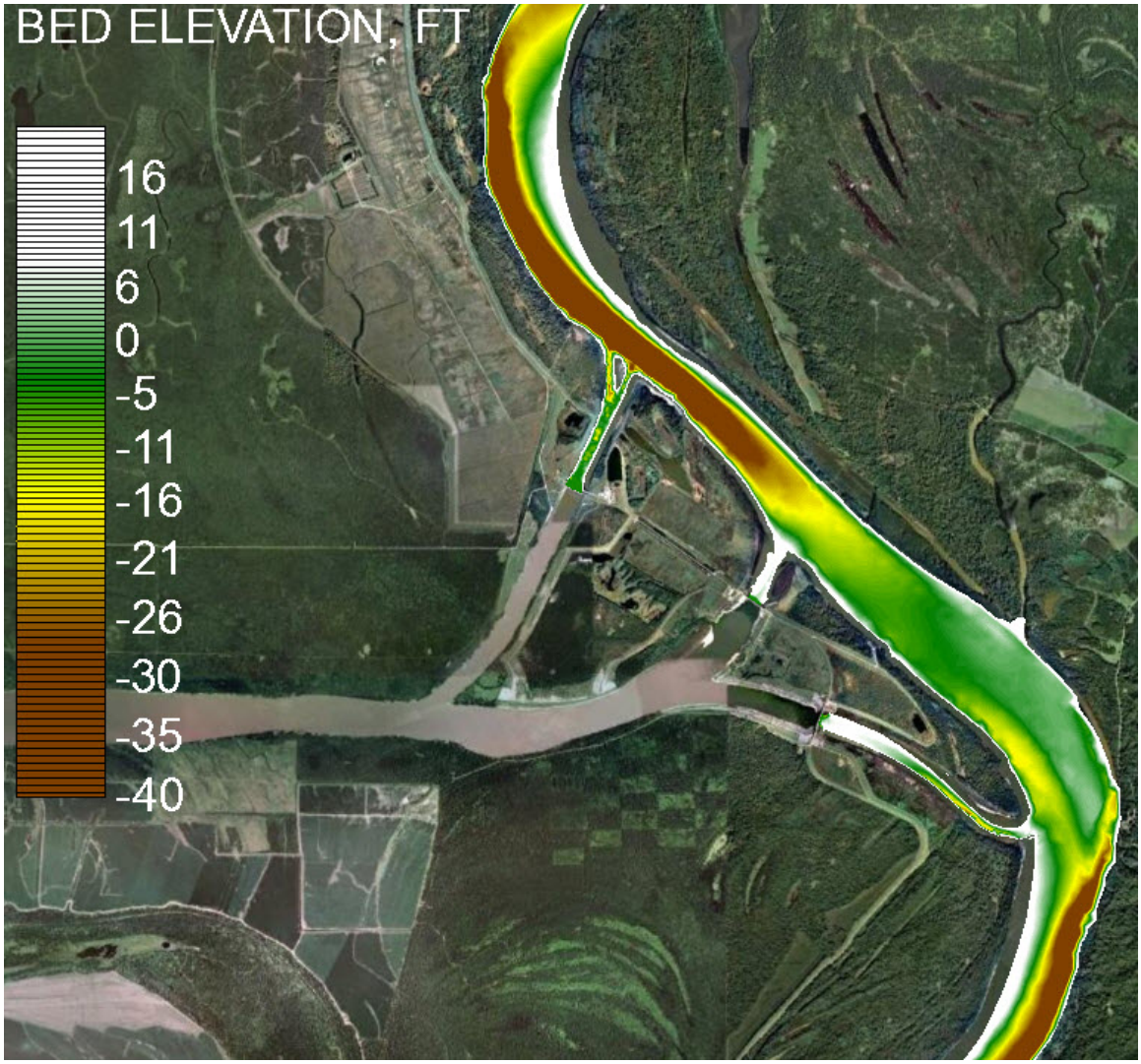

Figure 5.18. Modeled d_{50} of bed surface on the rising limb of a hydrograph.

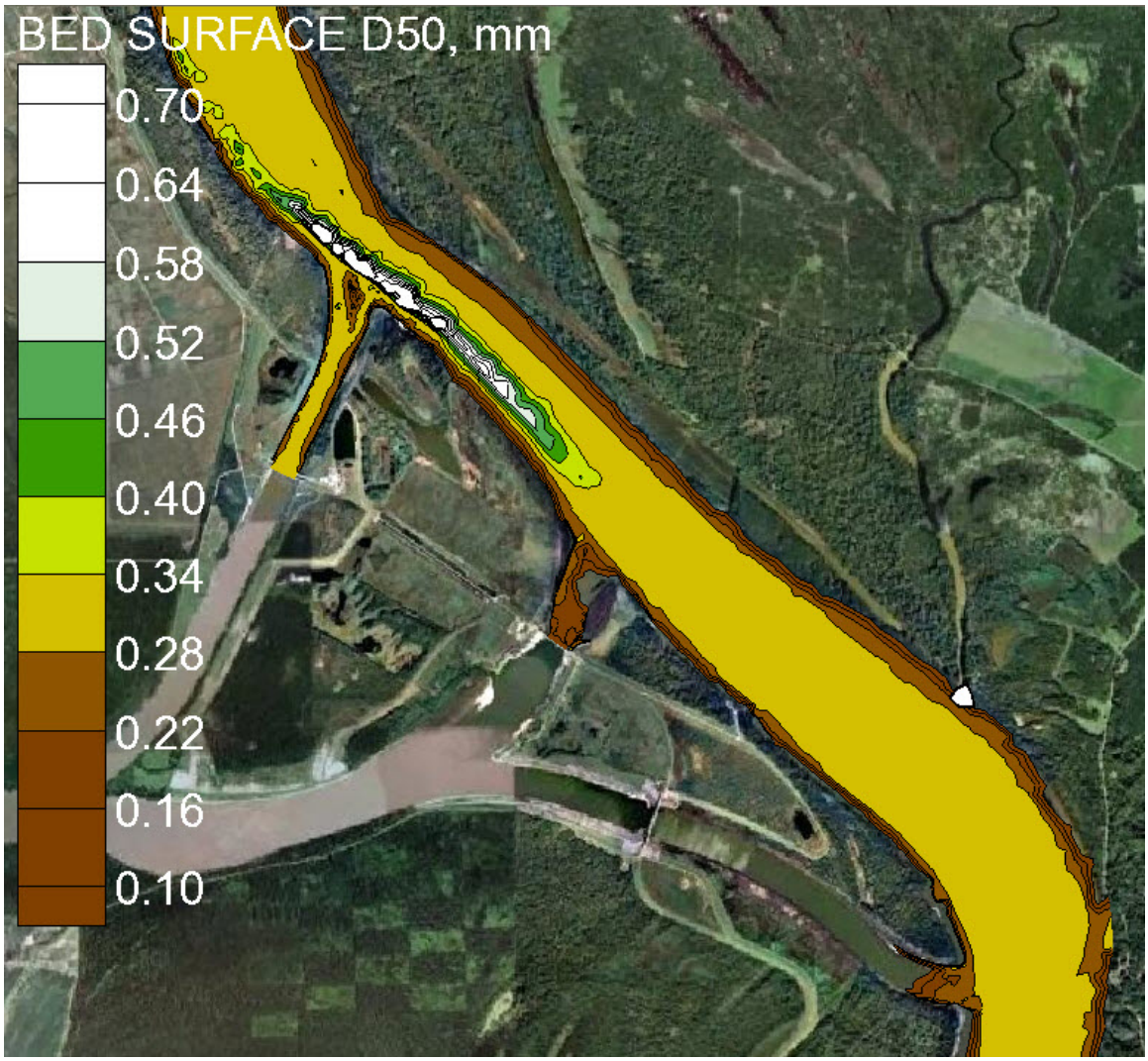

Figure 5.19. Modeled d_{50} of bed surface on the falling limb of a hydrograph.

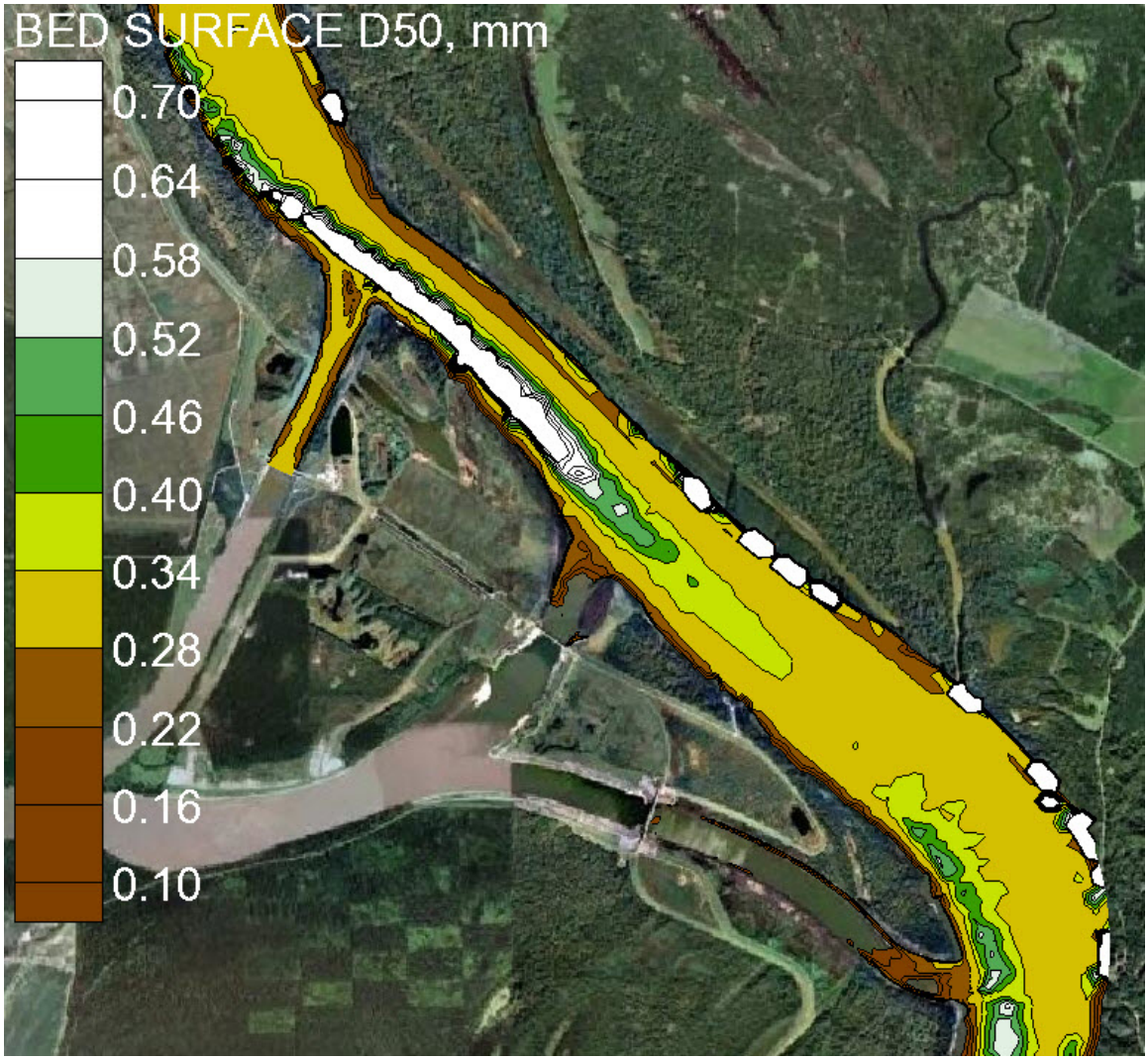

Figure 5.20. Typical modeled suspended sediment concentration distribution.

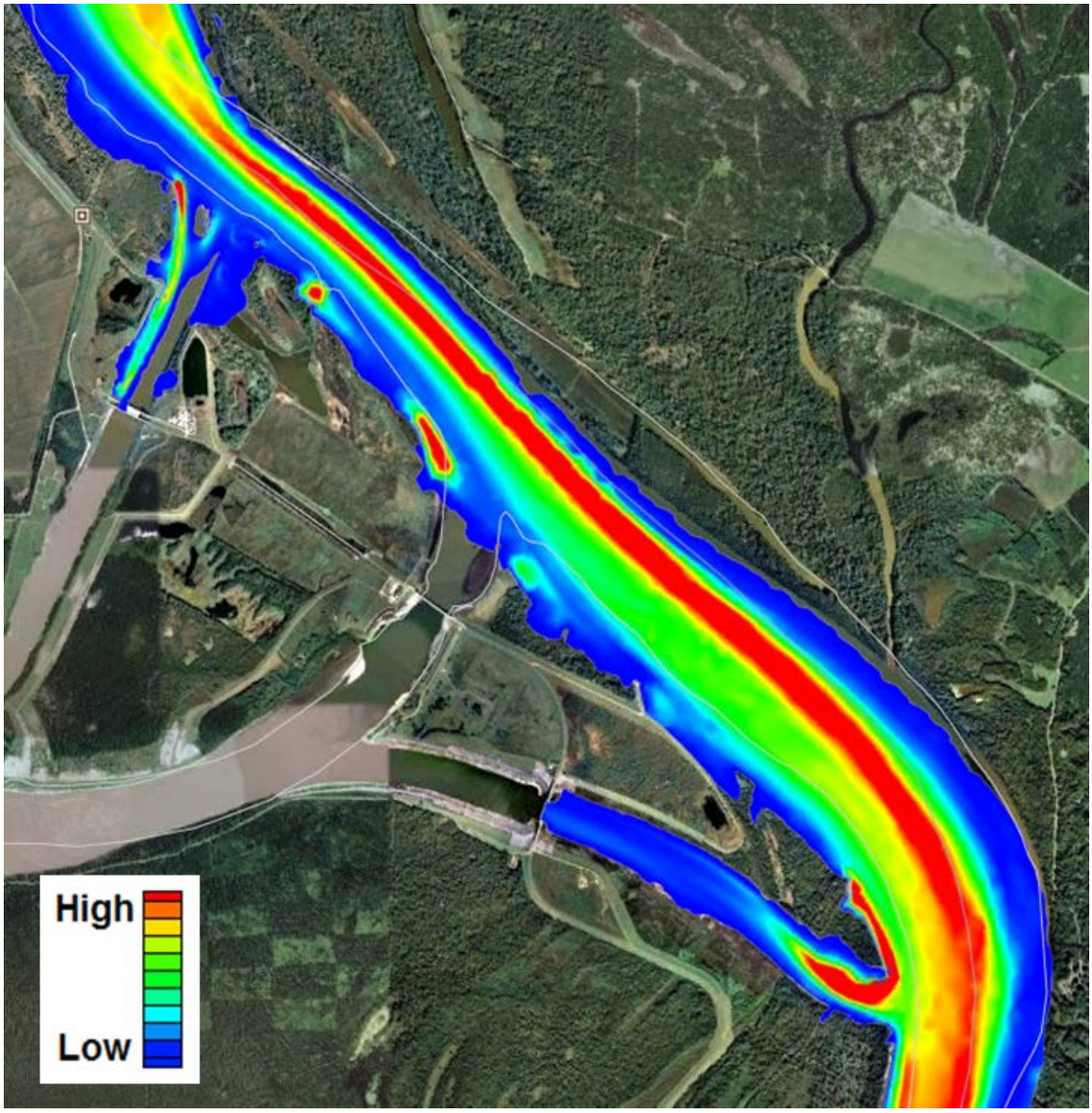

Figure 5.21. Typical modeled bed load sediment concentration distribution.

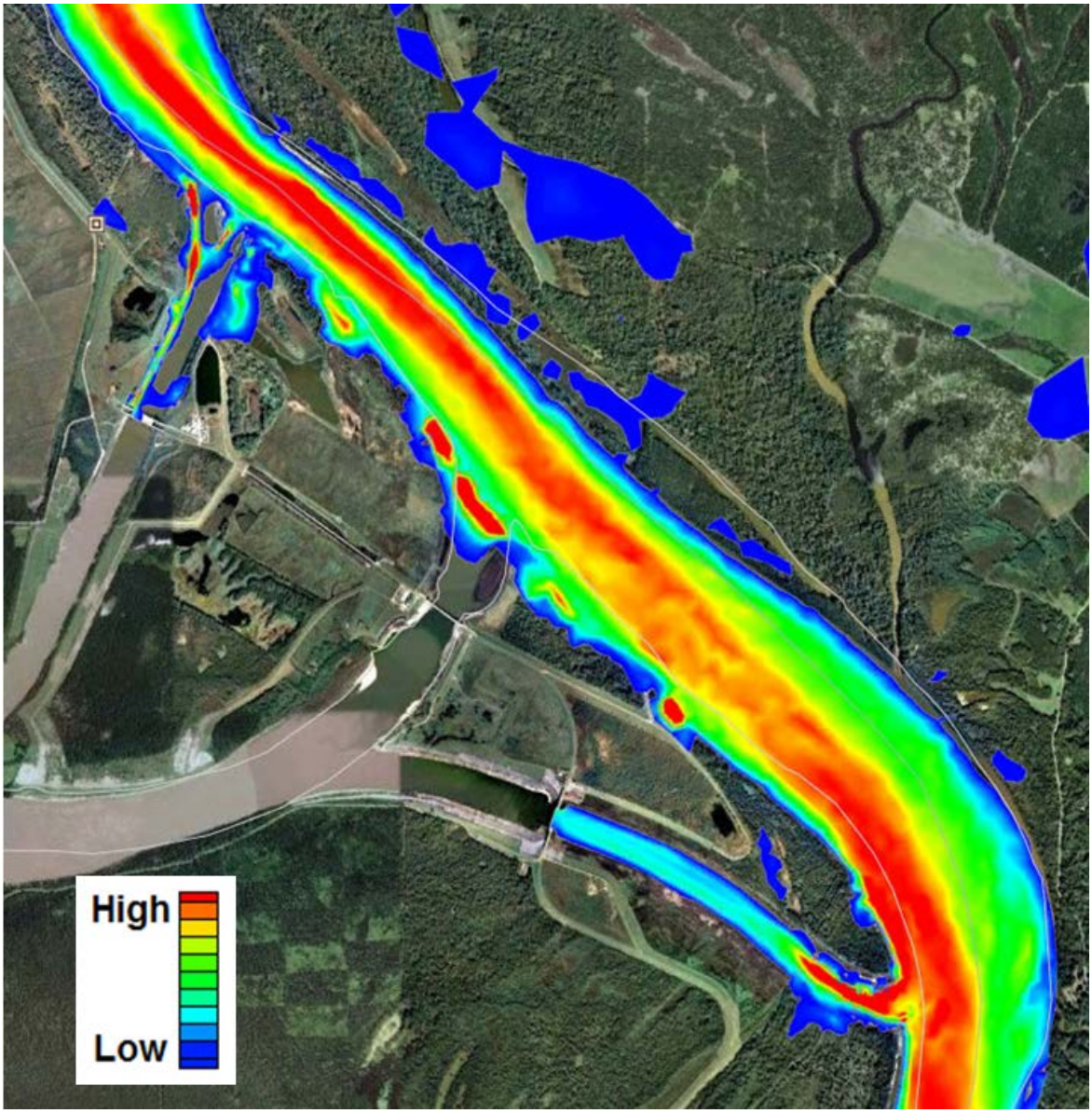

Figure 5.22 shows the estimated sediment diversion coefficients for each of the three diversion entrance channels (i.e., a measure of the ability of the individual diversion to remove sediment from the river; it can then either be passed through the structure or stored in the entrance channel). Note that the auxiliary diversion is the most efficient, followed by low sill and hydropower. Note also that the auxiliary structure is more efficient for coarser sediment classes, the low sill diversion diverts all classes at approximately equal efficiency, and the hydropower diversion is more efficient for the finer classes. All of these results are primarily due to the position of the diversions relative to river bend ways; the hydropower

diversion is on the outside bank of the upstream bend, the low sill diversion is in a crossing, and the auxiliary diversion is on the inside bank of a bend way.

Figure 5.22. Estimated sediment diversion coefficients of individual ORCC diversions by grain size class as determined from mean daily values.

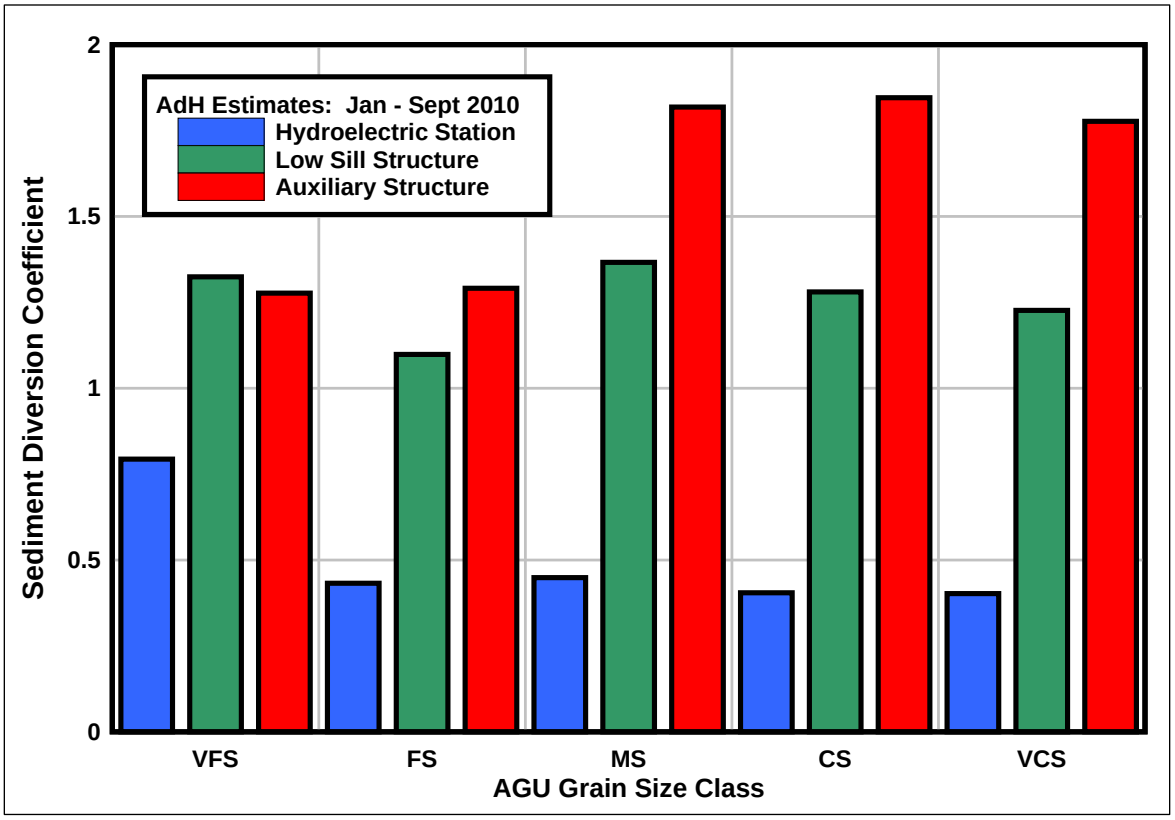

Table 5.3 lists the sediment diversion efficiencies for sand for each of the diversion channels and for the entire ORCC. Note that the observed sediment diversion efficiency for the ORCC of 1.0 is much less than the analytic approximation of the value required to maintain channel equilibrium of 1.8 (see Equation 5-7).

Table 5.3. AdH estimate of ORCC sediment diversion efficiency.

ORCC structure inflow channel	Sediment Diversion Efficiency, total sand load
	Jan-Sep-2010
Hydropower	0.5
Low Sill	1.3
Auxiliary	2.0
ORCC	1.0

The auxiliary channel often has sufficient energy to divert sediment but insufficient energy to pass the sediment through to the structure. Hence, sediment trapping is a concern in the auxiliary channel because of the current method of operation. Figure 5.23 depicts the modeled sediment trap efficiency as a function of time for the 2010 hydrograph. [1] Note that the model suggests that the sediment trapped in the channel can be mobilized but only under falling limb conditions when the sediment load in the river is reduced and only when sufficient flow is diverted though the auxiliary channel to erode the shoaled sediments.

Figure 5.23. Auxiliary channel trapping efficiency.

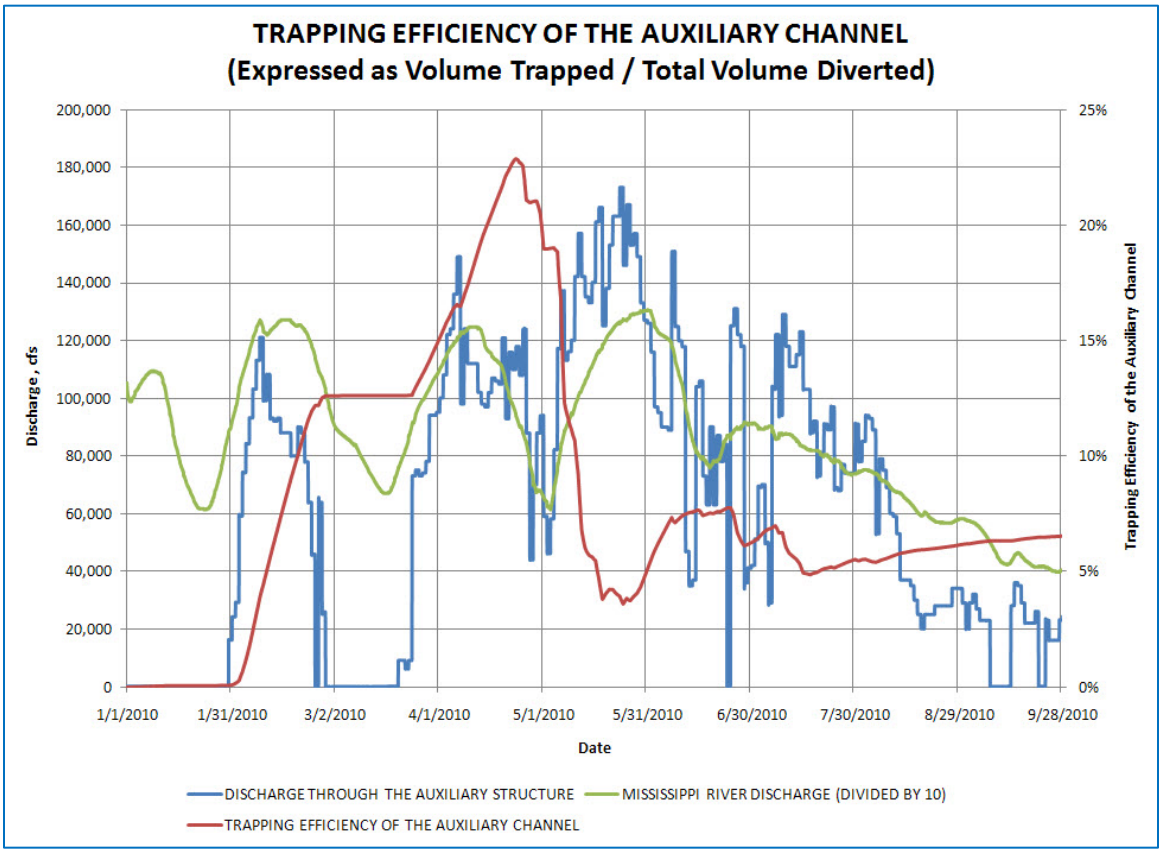

Scenario simulation

Several issues that require a solution have been identified as a result of the model simulations:

- The complex is diverting less sediment that the amount required to maintain downstream equilibrium.

[1] Trap efficiency is the percentage of the bed material sediment inflow retained in the channel.

- This deficit exists even when the most efficient diversion (the auxiliary channel) is used frequently.
- Therefore, the only way to divert more sediment is to reduce the allocation to the hydropower channel.
- Although the auxiliary diversion diverts the most sediment, it has a tendency to shoal, and under certain conditions can shoal severely.

In order to determine whether there are any courses of action that can be taken to address these issues, a series of scenarios for changes in ORCC operations were developed and run over the January–September 2010 hydrograph. These scenarios are given below:

Observed Operations – This is the base condition, with operations as the occurred in the prototype in 2010.

Hydrograph Optimization Operations – This scenario is designed to address the issues while minimizing impacts to hydropower diversion requirements. The operational changes to the observed 2010 operations are given below:

- During the rising limb of a hydrograph, the hydropower diversion is limited to a minimal flow. The remaining diversion is passed through the low sill structure. This is designed to capture the high sand concentration associated with the rising limb.
- During the falling limb of the hydrograph, the hydropower diversion is restored to full capacity, and the remaining diversion flow is passed through the auxiliary channel. This is designed to pass relatively sediment-poor flow through the auxiliary channel, thereby mitigating any sediment trapping in the channel.

Low Sill Only Operations – This scenario passes all flow though the low sill structure. It is designed to give an indication of the ORCC performance before the introduction of the auxiliary structure.

Ratio 1 Operations – This scenario operated the low sill and auxiliary structures according to Ratio 1 protocol defined in Figure 1.2. This is designed to give an indication of the ORCC performance before the introduction of the hydropower structure.

The cumulative structure hydrographs for each scenario are given in Figures 5.24–5.26.

Figure 5.24. Cumulative water volume diverted for each model scenario at the hydropower diversion. Note that no flow passes through the Hydropower diversion for low sill only and Ratio 1 operations.

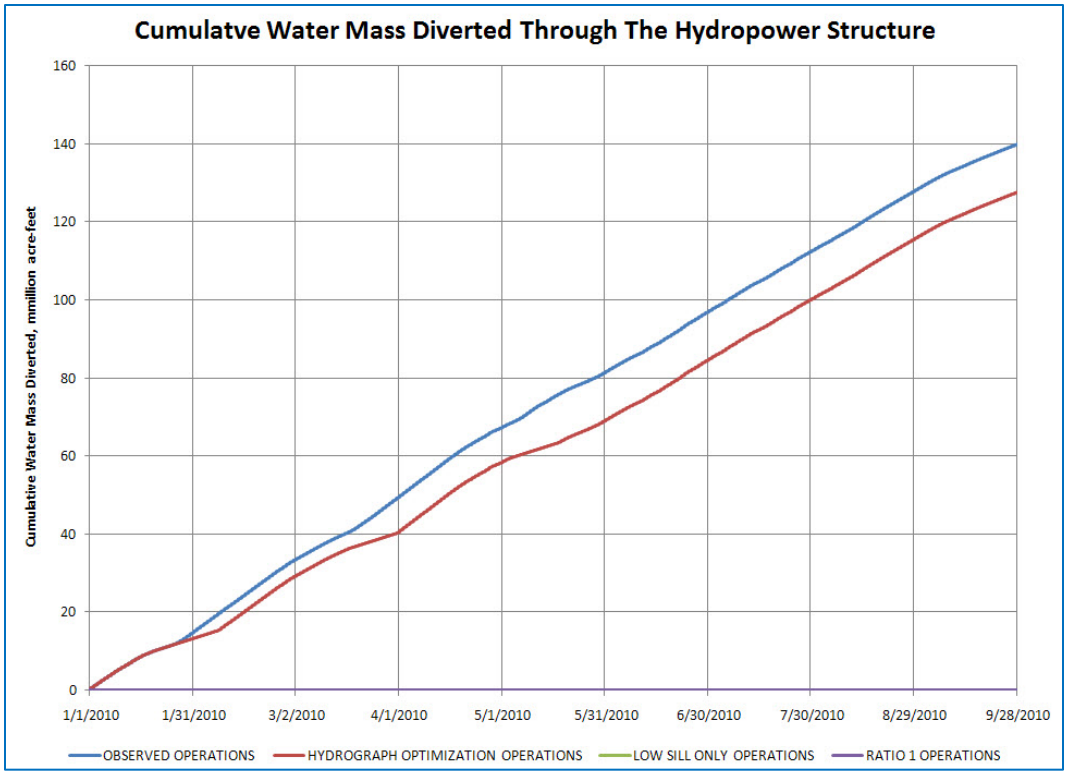

Figure 5.25. Cumulative water volume diverted for each scenario at the low sill diversion.

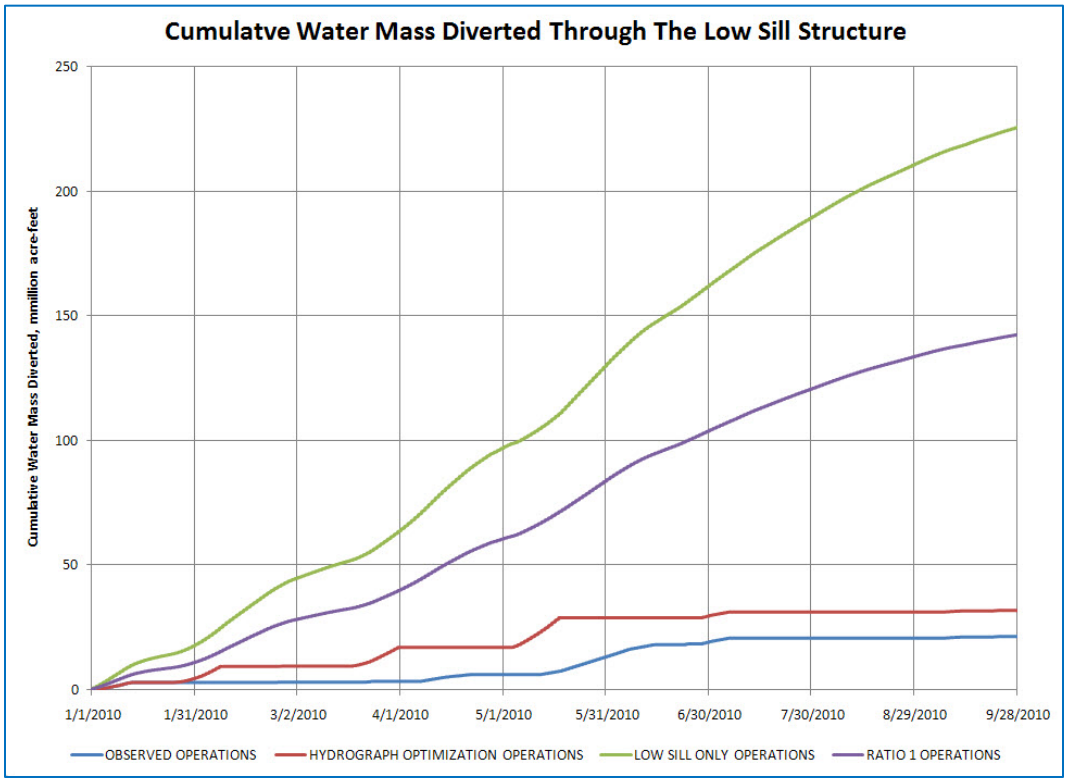

Figure 5.26. Cumulative water volume diverted for each scenario at the auxiliary diversion.

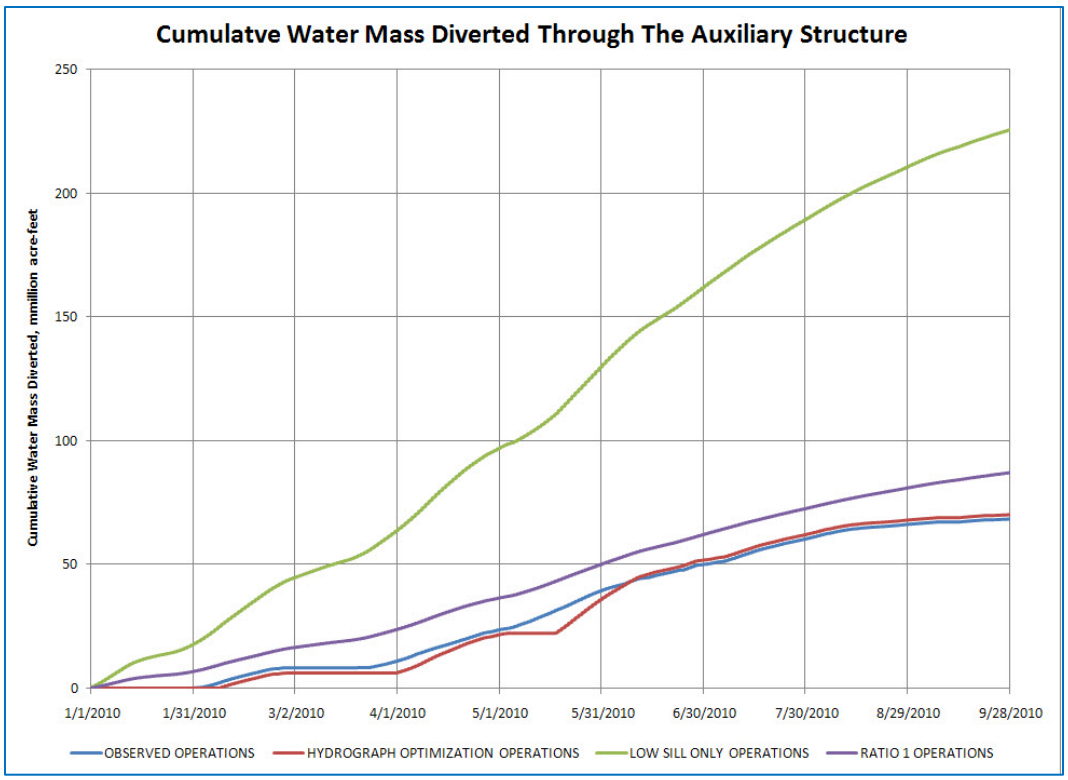

Figure 5.27 shows the results in terms of the sediment diversion efficiencies for each of the diversion channels. The target approximation of the equilibrium efficiency is included for reference. Note that none of the scenarios exceed the equilibrium estimate for the entire ORCC. This may be an indication that the equilibrium estimate is too conservative and that the sediment diversion efficiency associated with the Ratio 1 operations may be a more realistic target value.

Note also that the hydrograph optimization scenario does improve the complex efficiency by 20%.

Figure 5.28 depicts the same results in terms of the amount of excess sediment passed downstream, assuming the equilibrium target value is valid. Note that the excess value estimated for the current operations is 7.5 million tons, which is somewhat greater than the 5.1 million tons estimated from a MVN study of suspended sand flux records.[1] This is further evidence that the target value selected for the equilibrium (1.8) is a good estimate, but likely a conservative estimate.

[1] Don Rawson, MVN, personal communication, 30 December 2010.

Figure 5.27. Sediment diversion efficiencies for each of the operational scenarios.

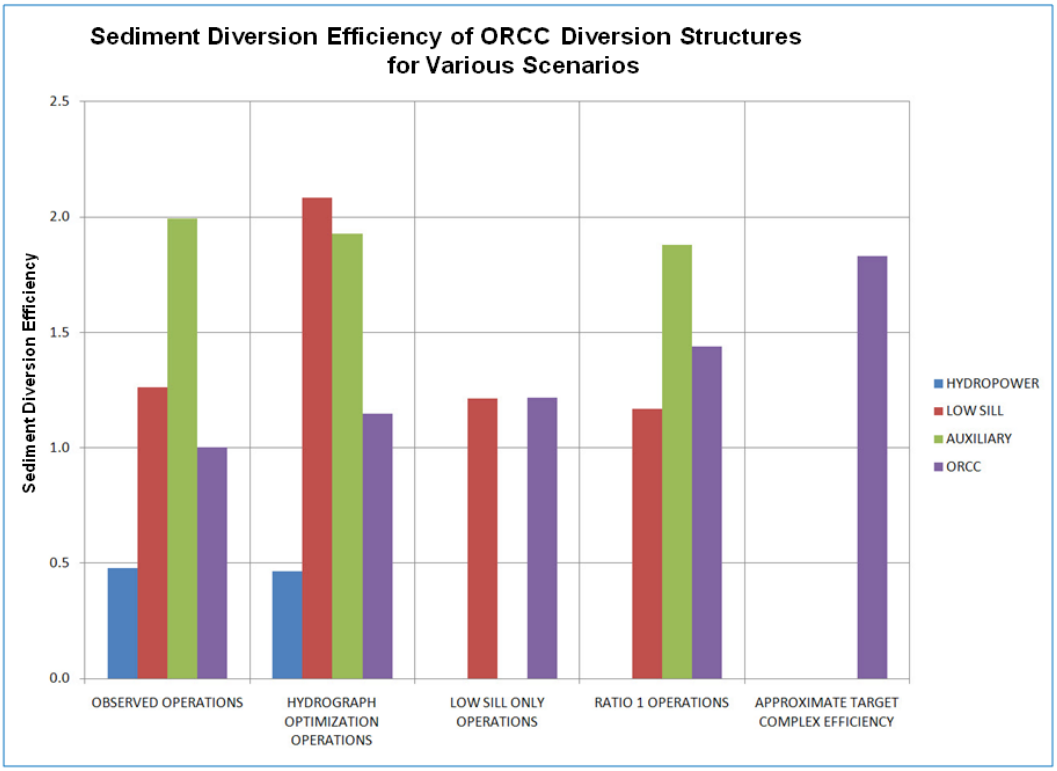

Figure 5.28. Excess bed material load remaining in the Mississippi River downstream of the ORCC for each operational scenario.

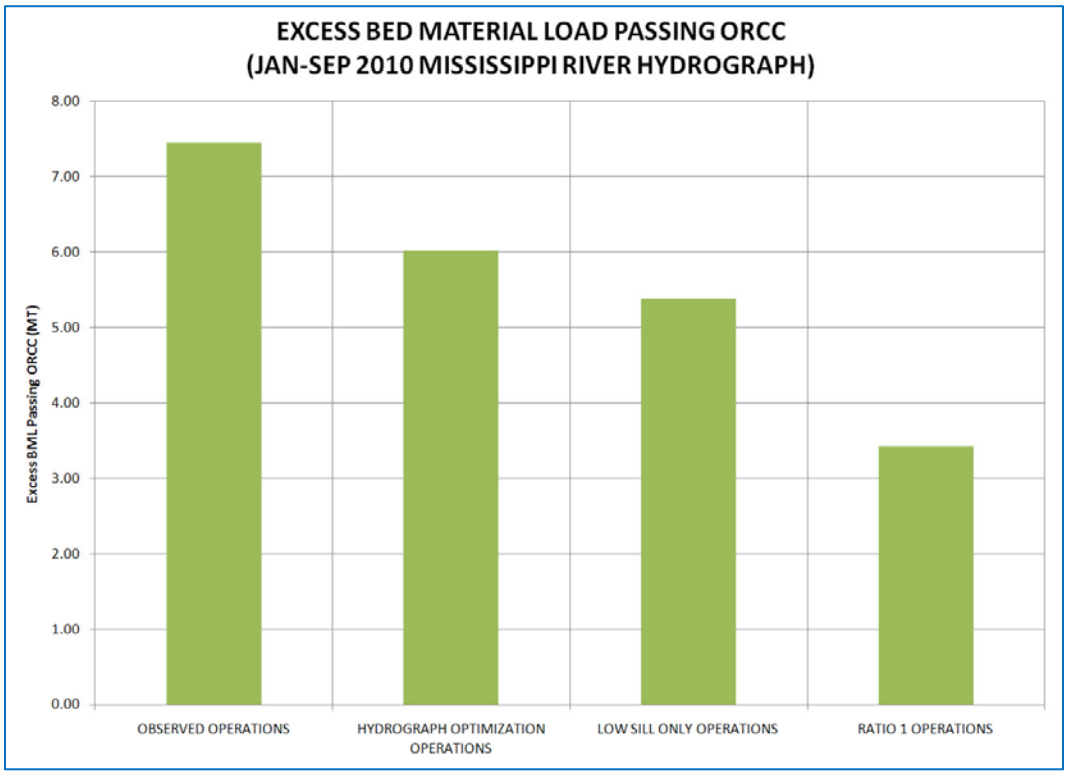

Figure 5.29 shows the improvement in the auxiliary channel trap efficiency associated with implementing the hydrograph optimization operations. For the new operations, the channel actually experiences net erosion during the simulation.

Figure 5.29. Improvement in sediment trapping efficiency for the auxiliary channel due to the implementation of hydrograph optimization operations.

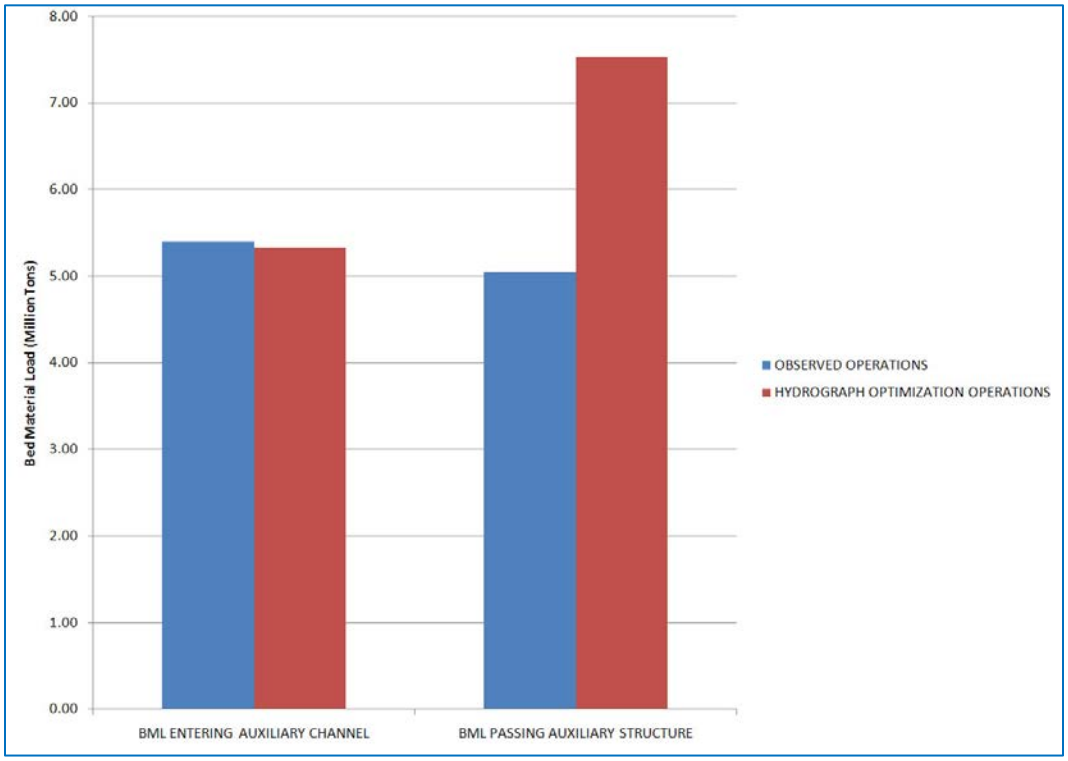

Screening tool

In order to allow water control personnel to apply the results of this study to practical operational decisions, a spreadsheet application screening tool has been developed whereby the results of the numerical analysis can be used to estimate the impact of changes in the ORCC operations on bed material (sand) diversions. Long-term estimates of the sediment diversion efficiency of individual ORCC structures and the entire complex for historical operations are shown listed in Table 5.4. The estimated sediment diversion coefficients (mean daily values) were derived from AdH model simulations of the January–September 2010 hydrograph. For each structure, Equation 5-8 was used to estimate the daily sand load diverted from the Mississippi River for historical operations.[1] The average

[1] This equation is a modified form of Equation 5-2 where 0.0027 is a conversion factor for concentration in mg/L, flow in cfs, and load in TPD.

sand concentration in the river was estimated from a rating curve. Historical diversion flows at each structure were used to compute the values shown in Table 5.4, but may be modified to evaluate operational changes. This procedure considers both historical structure operations and the nonlinear response of sediment transport rates to flow variations.

$$\left(Q_S\right)_{Diversion} = 0.0027 \delta_{SD} C_{River} Q_{Diversion} \tag{5-8}$$

Table 5.4. Long-term estimates of ORCC efficiency for diversion of total sand load.

ORCC Structure Inflow Channel	Total Sand Load	
	Sediment Diversion Coefficient	Sediment Diversion Efficiency Water years 1991–2010
Hydropower	0.5	0.5
Low Sill	1.3	1.9
Auxiliary	1.7	1.8
Old River Control Complex		0.9

Since hydropower production accounted for most of the ORCC diversion during low-flow periods when sand loads are relatively low, its estimated average annual efficiency was slightly, but not significantly, lower than its estimated sediment diversion coefficient. Since the largest flow diversions at the low sill and auxiliary structures were experienced when sediment loads were relatively high, their average annual efficiency is notably higher. This procedure provides a relatively simple method for estimating how operational changes would affect the diversion of sand from the Mississippi River.

Using the screening tool, the potential impact of flow regulation on sediment diversion is demonstrated for a hypothetical scenario in Table 5.5 where all flow was diverted through the low sill and auxiliary control structures according to the Ratio 1 operation plan. This scenario results in the diversion of an additional 7 million tons of sand per year as compared to historical operations described in Table 5.4.

Table 5.5. Long-term estimates of ORCC efficiency for diversion of total sand load for hypothetical Ratio 1 operations.

ORCC Structure Inflow Channel	Total Sand Load	
	Sediment Diversion Coefficient	Sediment Diversion Efficiency Water years 1991–2010
Low Sill	1.3	1.2
Auxiliary	1.7	1.7
Old River Control Complex		1.5

In the screening tool, the sediment diversion coefficient is held constant. Results from AdH simulations suggest the sediment diversion coefficient increases with increasing diversion discharge; however, efforts to date to develop statistically valid descriptions of a relationship have not been successful. Additionally, the AdH estimates of variability for the low sill and auxiliary structures are much greater than for the hydroelectric station. It is considered that the values in Table 5.5 probably represent a conservative estimate of the potential increase in efficiency as compared to historical operations.

The screening tool does not account for scour or deposition of Mississippi River bed material in the river reaches between ORCC inflow channels which influence ambient sediment concentrations immediately upstream of individual inflow channels. A 1D sedimentation model, such as the regional HEC-6T model of the Lower Mississippi River developed by the Mississippi Valley Division, can address this process and estimate the long-term stability of downstream reaches of the Mississippi River for decades. Neither approach fully accounts for temporal variability of diversion efficiency. Currently, the AdH 2D sedimentation model developed for this study provides the best available estimates of diversion efficiency but extends downstream only to Red River Landing and has been successfully applied only to annual simulations as of the conclusion of this study in 2012. For all sedimentation models, estimating both seasonal and long-term variations in sediment inflows from the Mississippi River and long-term response of the river bed remains a challenging scientific and technical issue.

6 Conclusions

The overall assessment based on the limited geomorphic analysis is that the local reach of the Mississippi River in the vicinity of the ORCC has experienced a reduction in overall depth due to channel filling. Specific gage analysis also indicates a long-term trend of increased stages for the Mississippi River stations at Vicksburg, Natchez, Red River Landing, Bayou Sara, and Baton Rouge. As much as 5 to 10 ft of stage increase was noted for the long-term periods of record for these stations. However, for the post-1973 flood period, there were no significant trends observed for these stations, with the exception of Natchez where the stage trend was still increasing and Vicksburg and Red River Landing where trends were more uncertain.

Interpretation of the results of the specific gage analysis with the findings of the geometric data analysis suggests that most of the changes on the Mississippi River in the ORCC reach are likely local responses to changes in operation of the ORCC with the addition of the hydropower and auxiliary structures. The reach has experienced a long-term, system-wide increase in stage; therefore, the overall changes are likely a combination of a systematic adjustment of this reach of the Mississippi River as well as local responses at the ORCC structures. Due to the spatial limitations of the geomorphic assessment the potential impacts of these changes on Mississippi River reach-scale morphology is uncertain, as well as the possible effects on flood stages.

Overbank vegetation change analyses have shown significant changes in land use and land cover. Over 100,000 overbank acres were flooded in 2011. Selected section computations of channel conveyance have shown that areas of shoaling have reduced channel capacity. Volumetric changes computed from surveys have identified several regions of predominant shoaling although the highest amounts of shoaling were not in revetment locations in the near vicinity of the ORCC. The regions of highest shoaling are all downstream of the ORCC and are potentially locations of reduced river discharge capacity. The 2011 volumes show the most shoaling at the Plaquemine and White Castle locations followed by Bayou Sara and St. Gabriel. The most scour occurred at the Poydras revetment. The yearly results demonstrate the frequency and change of the river channel. One

location can have a large amount of shoaling in one year followed by a high degree of scour the next year.

Of the three ORCC diversions, the auxiliary diversion is the most efficient at diverting sediment from the Mississippi River, followed by low sill diversion and the hydropower diversion. Also, the auxiliary diversion is more efficient for coarser sediment classes, the low sill diversion diverts all classes at approximately equal efficiency, and the hydropower diversion is more efficient for the finer classes. All of these results are primarily due to the position of the diversions relative to river bend ways: the hydropower diversion is on the outside bank of the upstream bend, the low sill diversion is in a crossing, and the auxiliary diversion is on the inside bank of a bend way.

Based on an approximate analytical analysis, the ORCC complex is diverting less sediment than the amount required to maintain downstream equilibrium. This deficit exists even when the most efficient diversion (the auxiliary channel) is used frequently, as was the case in January–September of 2010. Therefore, the only way to divert more sediment through the ORCC as a whole is to reduce the allocation to the hydropower diversion and increase diversion through the remaining structures.

While the hydropower and low sill structures tend to pass nearly all of the sand diverted from the Mississippi River, the entrance channel to the auxiliary structure traps a significant portion of the diverted sediment load, particularly during Mississippi River floods. This behavior was also documented in the physical model report that also describes flushing operations in which flow was diverted exclusively through the auxiliary structure for up to 7 weeks at low-to-moderate Mississippi River stages to remove the deposits. Consequently, the low sill structure is more efficient at delivering bed material to the Atchafalaya River side of the ORCC than the other structures as currently operated. This behavior was observed during field measurements of bed load transport in the combined outflow channel, which consistently showed the largest transport rates occurring when the low sill structure was in operation.

One potential operational change that could increase the efficiency of the ORCC is optimized diversion of sediment during the rising limb of the hydrograph. During the rising limb, the hydropower structure diversion can be limited to a minimal flow. The remaining diversion can be passed

through the low sill structure. This is designed to capture the high sand concentration associated with the rising limb. During the falling limb of the hydrograph, the hydropower diversion can be restored to full capacity, and the remaining diversion flow can be passed through the auxiliary structure. This is designed to pass relatively sediment-poor flow into the auxiliary entrance channel, thereby mitigating any sediment trapping in the channel.

In order to allow water control personnel to apply the results of this study to practical operational decisions, a spreadsheet application has been developed whereby the results of the numerical analysis can be used to estimate the impact of changes in the ORCC operations on bed material diversions.

To enhance the operation of the ORCC, development of a complete bed-material-load and flow measurement scheme, coordinated with structure operations, is recommended.

References

Abraham, D., R. Kuhnle, and A. J. Odgaard. 2011. Validation of bed load transport measurements with time sequenced bathymetric data. *ASCE Journal of Hydraulic Engineering* 137(7):723–728.

Bagnold, R. A. 1966. *An approach to the sediment transport problem from general physics*. Prof. Paper 422-1. Reston, VA: U.S. Geological Survey.

Bernard, R. 1992. *Depth-average numerical modeling for curved channels*. Technical Report HL-92-9. Vicksburg, MS: U.S. Army Engineer Research and Development Center.

Brown, G. L., J. N. Tate, and G. Savant. 2012. *SEDLIB multiple grain sized mixed sediment library: Technical manual*. Coastal and Hydraulics Laboratory (CHL). Vicksburg, MS: U.S. Army Engineer Research and Development Center.

Brown, G. L., J. V. Letter, Jr., R. E. Heath, R. M., L. L. Wehmeyer, and B. L. Gunkel. 2013. *A simplified analytical investigation of the riverside effects of sediment diversions*. ERDC/CHL CHETN-VII-13. Vicksburg, MS: U.S. Army Engineer Research and Development Center.

Chapman, R. S., B. H. Johnson, and S. R. Vemulakonda. 1996. *Users guide for the sigma stretched version of CH3D-WES; A three-dimensional numerical hydrodynamic, salinity, and temperature model*. Technical Report HL-96-21. Vicksburg, MS: U.S. Army Engineer Waterways Experiment Station.

Chien, N., and Z. Wan. 1999. *Mechanics of sediment transport*. Sec. 6.6, Table 6.5. Reston, VA: American Society of Civil Engineers Press. ISBN-0-7844-0400-3.

Copeland, R. R., and L. Lombard. 2009. *Numerical sedimentation investigation, Mississippi River Vicksburg to Pilots Station*. U.S. Army Corps of Engineers.

Graf, W. 1984. *Hydraulics of sediment transport*. Sec 11.1.2.1. USA/Canada: Water Resources Publications. ISBN-0-918334-56-3.

Lane, E. W. 1947. Report on the subcommittee on sediment terminology. *Transactions, American Geophysical Union*. 28(6):936–938.

Letter, Jr., J. V., C. F. Pinkard, Jr., and N. K. Raphelt. 2008. *River diversions and shoaling*. ERDC/CHL CHETN-VII-9. Vicksburg, MS: U.S. Army Engineer Research and Development Center. http://chl.erdc.usace.army.mil/library/publications/chetn/pdf/chetn-vii-9.pdf

Spasojevic, M., and F. Holly, Jr. 1994. *Three-dimensional numerical simulation of mobile-bed hydrodynamics*. Technical Report HL-94-2. Vicksburg, MS: U.S. Army Engineer Waterways Experiment Station.

U.S. Army Corps of Engineers (USACE). 1980. *Old River Control, Mississippi River and tributaries, Louisiana; Design memorandum no.17, hydraulic design, auxiliary structure; Appendix d, moveable bed model report.* New Orleans, LA: U.S. Army Corps of Engineers, New Orleans District.

———. 1993. *HEC-6 scour and deposition in rivers and reservoirs user's manual.* Davis, CA: Hydrologic Engineering Center. http://www.hec.usace.army.mil/software/legacysoftware/hec6/hec6-documentation.htm

———. 1998. *Mississippi River mainline levees enlargement and seepage control; Supplement no: 1 to the final environmental impact statement Mississippi River and tributaries project Mississippi River levees and channel improvement.* Vicksburg, MS: U.S. Army Corps of Engineers, Vicksburg District.

U.S. Department of Agriculture (USDA). 1965. *Misc. Publication No. 970.* June 1965, 275–276. Washington, DC.

Vogelmann, J. E., S. M. Howard, L. Yang, C. R. Larson, B. K. Wylie, and J. N. Van Driel. 2001. Completion of the 1990's national land cover data set for the conterminous United States. *Photogrammetric Engineering and Remote Sensing* 67:650–662.

Walton, R., and B. A. Christensen. 1980. Friction factors in storm surges over inland areas. *Journal Waterway Port Coastal Ocean Division, ASCE* 106:261–271.

REPORT DOCUMENTATION PAGE

Form Approved
OMB No. 0704-0188

1. REPORT DATE	2. REPORT TYPE	3. DATES COVERED *(From - To)*
June 2015	Technical Report	

4. TITLE AND SUBTITLE

Old River Control Complex Sedimentation Investigation

5a. CONTRACT NUMBER

5b. GRANT NUMBER

5c. PROGRAM ELEMENT NUMBER

6. AUTHOR(S)
Ronald E. Heath, Gary L. Brown, Charles D. Little, Thad C. Pratt, Jay J. Ratcliff, David D. Abraham, David Perkey, Naveen B. Ganesh, Keith Martin, and David P. May

5d. PROJECT NUMBER

5e. TASK NUMBER

5f. WORK UNIT NUMBER

7. PERFORMING ORGANIZATION NAME(S) AND ADDRESS(ES)
Coastal and Hydraulics Laboratory
U.S. Army Engineer Research and Development Center
3909 Halls Ferry Road
Vicksburg, MS 39180-6199

8. PERFORMING ORGANIZATION REPORT NUMBER

ERDC/CHL TR-15-8

9. SPONSORING/MONITORING AGENCY NAME(S) AND ADDRESS(ES)

U.S. Army Corps of Engineers
Washington, DC 20314-100

10. SPONSOR/MONITOR'S ACRONYM(S)

11. SPONSOR/MONITOR'S REPORT NUMBER(S)

12. DISTRIBUTION/AVAILABILITY STATEMENT

Approved for public release; distribution is unlimited.

13. SUPPLEMENTARY NOTES

14. ABSTRACT

This report documents an investigation of sediment diversions at the Old River Control Complex (ORCC) conducted for the U. S. Army Engineer District, New Orleans. The investigation was conducted via a combination of field data collection and laboratory analysis, geomorphic assessments, and numerical modeling. The objectives were to determine current rates of sediment diversion, evaluate potential impacts on the stability of the Mississippi River, and identify options to increase sediment diversion rates. As operated since the early 1990s, sediment diversion at the ORCC probably is less efficient than required to maintain channel stability in the Mississippi River downstream of the ORCC. While there is clear evidence of significant channel aggradation in the vicinity of the ORCC, the impacts of ORCC operations on regional sedimentation remain uncertain. Operational alternatives were analyzed that potentially could increase the long-term sediment diversion efficiency at the ORCC. In particular, the investigation found, via a synthesis of field investigations and numerical modeling, that while the auxiliary control structure is the most efficient at diverting bed material from the Mississippi River, the low sill structure is more efficient at delivering bed material to the outfall channel leading to the Atchafalaya River.

15. SUBJECT TERMS
Diversion
Mississippi river
Sediment
Shoaling
Numerical modeling
Field data collection
Geomorphic assessment

16. SECURITY CLASSIFICATION OF:			17. LIMITATION OF ABSTRACT	18. NUMBER OF PAGES	19a. NAME OF RESPONSIBLE PERSON
a. REPORT	b. ABSTRACT	c. THIS PAGE			Ty V. Wamsley
Unlimited	Unlimited	Unlimited	SAR	149	19b. TELEPHONE NUMBER *(Include area code)* 610-634-2099